RCHS-35: Configuration Dynamics, Refinement Geometry and Record-Conditioned Curvature Response in VERSF

Primitive temporal tests, source-stopped current response, commitment progress, unit Fact response and common-carrier gauge normalization

Keith Taylor
VERSF Standard-Model Derivation Programme
RCHS-35-R15 • 19 September 2026

General-reader summary

This paper asks how a physical change follows from a commitment in VERSF, and how that change could determine the strengths of the forces. A Fold describes relational structure; a Fact is a completed, retained distinction. The task is to connect that description to a rule that predicts what the surrounding fields do.

On the scalar-field model written in Fact-Momentum, one retained Fact supplies one unit of source. We calculate the resulting impulse and the field response on a stated seven-site model. The graph shows how the same impulse produces different later responses when the field's resistance to disturbance changes. Every width, sign and normalization needed to reproduce this example is specified.

The calculations also distinguish reversible interaction, information gained by a neighbour, and a permanently retained record. An interaction can reduce coherence without producing a readable record. Fresh contacts can accumulate progress, while repeated reversible contact can undo unfinished progress. A fixed completed bit can therefore coexist with variable progress per opportunity. Physical time enters through the admitted effective description; an elementary tick is not assigned an assumed duration.

The remaining gauge-normalisation task is now more sharply typed. A charge-carrying event fixes the conjugate gauge-flux impulse on the common compact link, and the common-carrier and Wilson conventions remove two apparent normalization freedoms. The scalar K7 admission 7/960 remains a structural probability: on the strict closure-projection branch its saturated 14/15 throughput is field-rigid, so it cannot supply the physical gauge stiffness by differentiation. The strength-bearing object must instead come from the positive source-response or complete physical Hessian. The later D36 source work fixes a conditional pre-Fact endpoint generator and source-stopped current occupation, leaving its physical same-event attachment and the action scale as the live release gates.

Opposite histories can give opposite mixed responses yet the same stiffness correction. The broader corpus already supplies conditional phase assignment, connection reconstruction and record-operation laws. Matching fixed-field probabilities does not preserve all their comparison data. The remaining task is to connect those existing constructions on the same physical event carrier; this calculation has not selected a recording phase or gauge coupling.

The paper closes with a calculable connection between the specified recording operation and field momentum. Earlier probability-based lower bounds survive field-independent completion in the outcome ensemble. The native operation now also gives an explicit mean impulse, second moment and positive additional-variance operator, evaluated for the archived weak and hypercharge probes. Its occurrence law adds a separate variance contribution. These are completed response calculations on their stated preparations and carriers. They provide concrete data for physical work matching; they do not yet determine the energetic gauge metric or unique force strengths. The existing scalar response, current-link identities and conditional coupling results are retained.

Abstract

This paper develops the connection between retained records and field response in VERSF. Its endpoint is an explicit calculation of how a specified native recording operation changes conjugate field momentum. The operation's normalized derivatives determine the mean impulse, second moment and positive additional-variance operator. Evaluation on the archived weak and hypercharge probes gives nonzero response coefficients, and the selected-edge occurrence law supplies a separate Bernoulli variance contribution. These results provide concrete source-response data for energetic matching.

The construction combines exact reconstruction and reduction results with finite numerical witnesses. An admitted reversible generator determines a conservative kinetic reference and relative raw potential; paired derivatives with an independently work-normalized source recover the action Hessian. The six-defect differential includes independent currents, records, completion and moving support. A spectral divided-difference formula corrects the printed support-projector derivative, with an explicit counterexample. Whole-history contraction recovers the prescribed endpoint energy in the Gaussian class, while ordered-record and completion tests identify which observations retain curvature information.

On the declared compact gauge carrier, a charge-conserving event fixes the conjugate flux impulse without a separate source gain. The shared-carrier identification and Wilson continuum map fix their respective normalization freedoms under the stated premises. The saturated K7 support trace is field-rigid on the strict closure-projection branch and therefore cannot supply Maxwell stiffness. The electroweak analysis separates source covectors from relaxed field responses and corrects the weak–hypercharge ordering threshold. Existing phase-assignment and record-operation theorems constrain the admissible comparison data. The scalar branch independently yields a unit-Fact impulse and a verified six-mode response.

The claim ledger distinguishes derived mathematical results, executed numerical witnesses, conditional physical identifications and external calibrations. No source-selected physical transverse weight or endogenous Standard Model gauge coefficient is obtained. One remaining physical matching problem joins the calculated response to the complete energetic action or an independently calibrated susceptibility on the same carrier. It includes responding auxiliaries, matter and record sectors, physical preparation, event grain, operational scale, curvature embedding and continuum/regulator matching. The paper supplies the response calculation and its verification; energetic matching is the starting point of the next calculation.

Claim grades

Four labels distinguish what each result establishes. They classify the evidence and physical attachment; they are not a confidence ranking. A theorem remains subject to its stated hypotheses, and numerical agreement does not by itself establish a physical identification.

Grade	Result type	Scope
D	Derived mathematical result	An identity, theorem or counterexample proved under its stated hypotheses. Established mathematical tools are distinguished from source-specific applications.
N	Executed numerical witness	A finite calculation with declared inputs, preparation, tolerances and checks. It establishes the reported witness, not a universal theorem or measured physical value.
P	Conditional physical identification	A mathematical or numerical object is attached to a physical carrier, source, clock or action only under the named identification premises.
E	External calibration	A measured quantity supplies a scale or reference. The resulting value is calibrated rather than an endogenous prediction.

Labels are used in the scientific status, corrections table and consolidated claim ledger. Local equations retain all assumptions needed for validity. Repeated general cautions are centralized here; a new carrier, preparation, clock or action identification is stated where it enters.

Scientific status

Result family	Grade	Established result and location
Reconstruction and response	D / N	Generator reconstruction, calibrated susceptibility and finite checks; Parts I–II.
Complete defect differential	D / N	Six-family differential, moving-support correction and derivative witnesses; Part III.
History and refinement	D / N	Gaussian history contraction and ordered-holonomy geometry under the specified metrics; Parts IV–V.
Retained-record information	D / N	Prepared-input laws, ordered-record rank and completion-filing witnesses; Part VI.
Electroweak response	D / N / E	Source maps and corrected hierarchy; measured-alpha and PDG-based effective calibration; Part VII.
Gauge impulse and normalization	D / P	Charge-normalized compact-link impulse; degree-one common-carrier bridge; fixed Wilson map; VII.19–VII.23.
Current and temporal laws	D / N / P	Source-stopped current, reciprocity and portal conditions; temporal support and finite-history tests; VII.24–IX.6.
Commitment and scalar response	D / N / P	Contact progress, unit-Fact impulse and six-mode benchmark response; Parts X–XI.
Native momentum response	D / N	Flux moments, positive additional variance, completion identities and selected-edge occurrence term; XII.8–XII.11.
Physical coupling matching	P — open	Complete energetic/source-response identification remains required. No source-selected transverse weight or endogenous Standard Model gauge coefficient is issued.

The detailed status inventory and original objective-by-objective ledger are preserved in Technical Supplement S1 and S5. The main paper's closing ledger states the remaining physical matching requirements.

Corrections and advances in R15

This register brings together the corrected inferences and completed response results. It identifies what is superseded while retaining the scope of the surviving claims.

Result and grade	Correction or advance	Consequence and location
Support-projector derivative D / N	Spectral divided differences replace the cutoff-dependent resolvent formula. A rotating rank-one example has off-diagonal derivative 1 where the printed formula gives 6/5, 3/2 or 3.	Corrects moving-support differentiation; fixed-full-support results survive. III.5–III.7A; [A3; P4].
Weak/hypercharge threshold D / N	The final integer-hypercharge/weak coefficient ratio must exceed 36. The threshold 140 belongs to the internal norm convention.	Removes an erroneous ordering rejection; physical source attachment is a separate P claim. VII.15–VII.16; [A29].
Score-feedback proposal D / N	The added score-dependent field displacement fails the affinity required of a fixed quantum instrument on incoming mixtures.	Rejects physical promotion of that proposal. The inherited Born instrument survives; its imposed-model ratios are retained only at N grade. VII.7; [A23–A24].
BCN normalization proof D / P	The reviewed proof imposes its reliability floor and selects an upper bound as a minimum. In the specified logistic experiment, ln 2 requires the independently chosen error tolerance 1/3.	Retains BCN as conditional calibration and corrects this proof route. It neither withdraws the binary primitive nor proves programme-wide nonuniqueness. XII.12; [A46].
K7 electromagnetic typing D / E	The admission 7/960 is structural; the saturated 14/15 support trace has zero field curvature on the strict closure-projection branch.	Removes that trace as a Maxwell-stiffness source. Charge-normalized impulses and external electromagnetic calibration remain. VII.19–VII.23; [P51–P56].
Phase-source reconciliation D / P	Existing holonomy, connection and record-operation constructions constrain the comparison kernel. Equal fixed-field probabilities need not preserve complete comparison data.	Supersedes a reading of the phase diagnostic as a full-corpus nonuniqueness result. Joint physical evaluation remains open. XII.7; [A43; P64–P67].
Native momentum response D / N	The recording operation supplies exact flux moments and positive additional variance, with weak/Y coefficients and an occurrence contribution on the specified preparation.	Provides the constructive endpoint for physical work matching. The pure endpoint preparation remains distinct from the earlier neutral-input tensor. XII.8–XII.12; [A44–A46].

Contents

Section, equation and theorem labels are part-qualified. Citations such as [P5, §9K] point to a source document; technical-supplement references are stated explicitly.

Scope, source basis and the action-object ledger

The retained scientific question

The physical target is the quadratic response to curvature-changing gauge links on the complete Hessian-connected carrier. The problem is not settled by a positive finite response, a complete derivative engine, or recovery of deliberately inserted numerical prices. A physical return must identify the common action and its source-derived weights, or supply an independently work-calibrated response of that same action. The known endpoint subsystem is useful source content, but it does not provide independent link and record evolution. [A2, §§2, 12; A3, §§2, 12]

The paper additionally consumes the Fact-to-gauge event bridge, the supplied U(1) geometric-closure calculation, the finite-distinguishability/interface-bridge pair, the Wilson-normalization audit, the later K7/PFDMI source retyping, and the RCHS-25–28 / RCHS-6–7 source-stopped current and current-link continuation. They are used only for the claims they support: exact compact-link source transport, a conditional common-carrier identification, exact Wilson continuum normalization, closure-projection rigidity, the source-native D36 matter-generator shape, source-stopped E_2 current occupation, exact current-link reciprocity and the conditional single-U(1)-portal fingerprints. None is used to insert a measured gauge coupling or to identify current covariance with action stiffness. [P51–P62]

Source basis

The source-by-source audit and coverage limits are in Technical Supplement S2. The archive-to-section map and verification inventory are in S3; execution details are in S4. The original citation keys are retained in both documents. The action-object ledger below distinguishes the mathematical objects used in the physical argument.

Different action and response objects

Object	Where used	Interpretation and non-identification
$v = V - E_0$ and $D^2 v$	Part I	Relative scalar potential of a specified ground-state-transformed generator; not automatically a free-energy or gauge-action Hessian
$F_{\text{end}} = F_{\text{diff}} + \mathcal{G}$	Parts II–III	Conditional integration of the known endpoint gradient equation; $\mathcal{G}$ remains endpoint independent and unselected
$\Gamma_D = 1/2\,\langle d, Wd\rangle$	Part III	Declared six-defect residual functional; its differential is explicit for supplied W
$H = -R^{-1}B$ and $K_f = \chi^{-1}$	Part II	Calibrated same-action quadratic response, conditional on the actual work source and complete coupled tangent
$\mathcal{A}[u, j]$	Part IV	Quadratic expression associated with a specifically normalized Gaussian history construction
I_T and βF	Part IV	Endpoint-dependent boundary cost; obtained by history contraction, not by setting $\dot{u} = 0$
W_{prim} and physical Z_3, Z_2, Z_q	Physical handoff	Unreturned physical source and continuum quantities; no diagnostic value substitutes for them
g_n and the refinement coarse maps	Part V	Operational refinement metric and coarse-map geometry; relative link scaling is derived, but the absolute physical metric and the full completion/bath refinement remain unreturned

Object	Where used	Interpretation and non-identification
Ordered probabilities and efficient Fisher information	Part VI	Conditional observational law and nuisance-profiled response; neither is the physical action Hessian or the full background-averaged law
Contact distinguishability and amplification	Part X	Receiver coherence, readable neighbour information and irreversible record retention are distinct
TPB and physical time	Part X	Opportunity count, local proper time, external time and completed-bit count require explicit conversion

Local symbols retain their meanings from the corresponding calculation. The susceptibility is χ in Parts II, III and VII. The configuration phase is $\vartheta(z)$; torus characters are $\mathcal{E}_n(\theta)$; elementary-kick Fourier coefficients are η_m; and the receiver coherence factor is ζ. The subscript ch labels the chiral candidates A_{ch} and C_{ch}. These are distinct quantities. The symbol R denotes a conjugate-force derivative in Part II and an endpoint residual projection in Part IV; W in Part IV is a Gaussian residual precision, not an established full physical W_{prim}. The native instrument's occupied 49-dimensional support, the 50-dimensional derivative fixture and the low-dimensional history tests remain distinct from the complete MASD/CAR/Fock carrier.

Part I: Configuration-generator reconstruction

I.1. Reconstruction scope and source position

This part retains the calculation of RCHS-35-R0 [A1]. RCHS-34's finite split inverse required a known kinetic reference. The narrower continuous-time reconstruction below determines that reference from an admitted conservative reversible generator, together with its relative raw potential. The required physical rates or moment fields are not supplied by the theorem. HMGBC's distinction between the allowed-move catalogue and its continuous amplitude law remains controlling. [P2, §§2–4; P3, §11A.1]

The compact smooth result, proved in §I.6, is

$$v = \frac{1}{2}\mathrm{div}_\nu c + \frac{1}{4}c^T A^{-1} c, \qquad H_0 = -\Delta_{\nu,A} + v. \tag{I.1}$$

It assumes the specified reference density, ellipticity, global exactness and domain conditions. The generator inverse, finite-step obstructions and nonlinear raw-potential calculations below retain those conditions. Part II subsequently distinguishes this raw-potential response from a calibrated stationary-action response on the unchanged diagnostic cost.

I.2. Three objects that must remain distinct

Let z denote a complete admitted configuration, including changing gauge links. The full intended carrier is schematically $(\rho, U, J, \Phi; \psi, \bar{\psi}; q_{\mathrm{bath}})$. The probability and operator constructions below apply directly only to a classical bosonic carrier or to a separately justified positive representation. They do not supply a positive probability density on Grassmann variables, a CAR/Fock reduction or the missing fermionic positivity certificate. [P3, §§56A.1–56A.3]

There are three different levels:

$$T_a = M_V Q_a M_V, \qquad Q_a = e^{-aL_0}, \qquad (M_V)_{zz} = e^{-aV(z)/2}. \tag{I.2}$$

This is the finite-step split used in RCHS-34 and HMGBC. It is not generally equal to $e^{-a(L_0+V)}$. Products of the split converge to that continuous operator only under the corresponding product-formula assumptions and a limiting procedure. A primitive finite event must not be replaced by such a limit merely because it is convenient.

A different admitted object is the continuous raw semigroup

$$T_t = e^{-tH}, \qquad H = L_0 + V, \qquad Hh = E_0 h, \quad h > 0. \tag{I.3}$$

Its normalized ground-state transform is

$$K_t = e^{tE_0}\mathrm{diag}(h)^{-1} T_t \mathrm{diag}(h), \qquad \mathcal{L} = \mathrm{diag}(h)^{-1}(-H + E_0)\mathrm{diag}(h). \tag{I.4}$$

The third object is a physical quadratic field action obtained from the correctly admitted raw source, its embeddings and the full coupled-field reduction. Neither D^2V, $-\log\pi$, an information matrix nor $-\log K_t$ is automatically that action. The existing RCHS-24 and HMGBC distinctions remain controlling. [P3, §56A.3; P5, §§9H–9L]

I.2.1. Additional reconstruction class

The inverse assumes a known reference measure and clock, a connected conservative Markov generator, reversibility, and a raw split into **conservative symmetric kinetic operator plus multiplication by a scalar potential**. "Conservative kinetic" means $L_0\mathbf{1} = 0$ in its reference representation. Allowing an arbitrary killing term to move between L_0 and V would destroy uniqueness of that split.

Ground-state/Doob transformations and reversible diffusion decompositions are established mathematics. [M1, M2] The contribution here is their explicit source-identification application, the sharp comparison with the predecessor's fixed-step inverse, and the executed nonlinear VERSF-shaped tests. No priority claim is made for the general transformation.

I.3. Finite generator reconstruction without a supplied kinetic reference

Theorem I.1: conservative generator inverse. Let $\mathcal{L}$ be an irreducible continuous-time Markov generator on a finite connected state set, in counting measure. Write

$$(\mathcal{L}f)_i = \sum_{j\neq i} r_{ij}\,(f_j - f_i), \qquad r_{ij} \geq 0.$$

Assume detailed balance with positive stationary masses π_i. Then

$$c_{ij} = \sqrt{r_{ij}r_{ji}}, \quad (L_c f)_i = \sum_{j\neq i} c_{ij}\,(f_i - f_j), \quad v_i = \sum_{j\neq i}(r_{ij} - c_{ij}) \tag{I.5}$$

reconstructs $H_0 = L_c + \mathrm{diag}v$. Its ground energy is zero and its positive ground vector is $h_i = \sqrt{\pi_i}$. The kinetic reference $Q_t = e^{-tL_c}$ is an output. Any other operator in this same conservative symmetric-kinetic plus scalar class with the same normalized generator differs from H_0 by a constant multiple of the identity.

Proof. Detailed balance gives $\pi_i r_{ij} = \pi_j r_{ji}$. Hence

$$(H_0)_{ij} = -\sqrt{\pi_i}\,r_{ij}/\sqrt{\pi_j} = -c_{ij} \quad (i\neq j), \qquad (H_0)_{ii} = \sum_{j\neq i} r_{ij}. \tag{I.6}$$

Thus $H_0 = -\mathrm{diag}(\sqrt{\pi})\mathcal{L}\mathrm{diag}(\pi^{-1/2})$. Its off-diagonal entries fix c, and conservation fixes the kinetic diagonal. The remaining diagonal is exactly (I.5). The transformed Dirichlet identity is

$$\langle f, H_0 f\rangle = \frac{1}{2}\sum_{i,j} \pi_i\, r_{ij}\left|\frac{f_i}{\sqrt{\pi_i}} - \frac{f_j}{\sqrt{\pi_j}}\right|^2 \geq 0. \tag{I.7}$$

The connected graph makes the zero vector space one-dimensional, spanned by $\sqrt{\pi}$. A different positive ground-state transform with the same rates has the same stationary masses and hence the same ground-vector ratios. Only $E_0 I$ remains. This proves existence, positivity and uniqueness within the class. ▫

I.3.1. Reference measure is not erased

For known nonuniform reference masses w_i, the ground function is $\sqrt{\pi_i/w_i}$. The conservative kinetic rates in the function representation are

$$c_{ij}^{(w)} = \sqrt{r_{ij}r_{ji}}\sqrt{w_j/w_i}, \qquad v_i^{(w)} = \sum_{j\neq i}\left(r_{ij} - c_{ij}^{(w)}\right). \tag{I.8}$$

They obey $w_i c_{ij}^{(w)} = w_j c_{ji}^{(w)}$. The theorem has not inferred the reference volume, action unit or physical time from normalization. These remain source data. The exact finite inverse is not a theorem that an arbitrary physical configuration law is reversible.

I.4. Exact reconstruction test and the fixed-step obstruction

I.4.1. A four-state inverse with no input Q

The primary calculation constructs symmetric kinetic weights $c_{12} = 1$, $c_{13} = 1/2$, $c_{23} = 2/3$, $c_{24} = 3/2$, $c_{34} = 1$, with $c_{14} = 0$, and a positive vector $h = (1,2,3,4)^T$. These are deliberately supplied diagnostic data. It exports the rates $r_{ij} = c_{ij}h_j/h_i$:

$$\mathcal{L} = \begin{pmatrix} -7/2 & 2 & 3/2 & 0 \\ 1/2 & -9/2 & 1 & 3 \\ 1/6 & 4/9 & -35/18 & 4/3 \\ 0 & 3/4 & 3/4 & -3/2 \end{pmatrix}. \tag{I.9}$$

The separate inverse reads these rates only, solves stationarity and reconstructs

$$\pi = (1,4,9,16)/30, \qquad v = (2,4/3,-2/9,-1)^T. \tag{I.10}$$

Conductance recovery, detailed balance and $H_0h = 0$ pass in exact rational arithmetic. Direct finite-time matrix exponentiation at $t = 0.3$ recovers the same Hamiltonian to relative error 9.24×10^{-16}. This validates the inverse; it does not turn the inserted rates into a primitive VERSF result. Negative entries of v are compatible with a nonnegative full operator.

I.4.2. Positive spectrum is not continuous-time embeddability

Consider the symmetric, entrywise-positive, stochastic matrix

$$K = \begin{pmatrix} 117/200 & 17/200 & 33/100 \\ 17/200 & 117/200 & 33/100 \\ 33/100 & 33/100 & 17/50 \end{pmatrix}.$$

Its eigenvalues are $1, 1/2, 1/100$. Its only possible real generator logarithm at unit time has

$$(\log K)_{12} = -\frac{1}{2}\log(1/2) + \frac{1}{6}\log(1/100) = -0.42095477405136 < 0. \tag{I.11}$$

A Markov generator cannot have this off-diagonal sign. Distinct positive real eigenvalues force a real logarithm to preserve the one-dimensional real eigenspaces, so alternative logarithm branches cannot repair this example. Thus the finite kernel passes positivity and reversibility but fails the continuous-time test.

The same issue can occur **inside** the split architecture (I.2). On the three-state path Laplacian, choose $a = 0.5$ and $V = (0,1,3)$. The split transfer has positive entries and spectrum. Nevertheless the distant entry of $-a^{-1}\log T_a$ is approximately $+0.01877570158$, and the corresponding Doob logarithmic generator has rate $r_{13} \approx -0.00226362010$. This is a numerical countercheck of that finite split, not an exact-decimal proof or a failure of HMGBC's declared discrete construction. The continuous-time inverse requires continuous-time admission rather than imposing it retrospectively.

I.5. From small updates to a local configuration generator

The continuous field problem need not require a separately selected full finite-step amplitude distribution **if** the source establishes a diffusion limit. This conditional reduction must not be confused with deriving that limit from VERSF.

On a fixed smooth configuration chart define, for a family of small updates δx at duration τ,

$$b^i(x) = \lim_{\tau \downarrow 0} \frac{\mathbb{E}[\delta x^i \mid x]}{\tau}, \qquad A^{ij}(x) = \lim_{\tau \downarrow 0} \frac{\mathbb{E}[\delta x^i \delta x^j \mid x]}{2\tau}. \tag{I.12}$$

Assume uniform local convergence of these moments, smooth coefficients, positive definite A, and, for bounded third derivatives of the test functions,

$$\lim_{\tau \downarrow 0} \tau^{-1} \mathbb{E}[\| \delta x \|^3 \mid x] = 0. \tag{I.13}$$

This convenient sufficient remainder condition excludes finite jumps of order-one size occurring with probability proportional to τ. More general Lindeberg hypotheses are possible; they are not needed for the tests performed here.

Proposition I.2: moment closure. For every such smooth local observable,

$$\lim_{\tau \downarrow 0} \frac{\mathbb{E}[f(x + \delta x) - f(x) \mid x]}{\tau} = b^i \partial_i f + A^{ij} \partial_{ij} f =: \mathcal{L} f. \tag{I.14}$$

Proof. Taylor-expand to second order. The expectation of the linear term returns b, the quadratic term returns A, and (I.13) bounds the remainder divided by τ by a quantity tending to zero. If the limiting martingale problem is well posed, this generator fixes the limiting Markov diffusion. The result identifies a generator under those assumptions; it does not prove tightness, global uniqueness or physical admission for an arbitrary VERSF update family. ▫

I.5.1. What has been reduced

Different small-update distributions with the same two moment **fields** can have the same limiting dynamics. This is stronger than specifying only the support or total spread of a move, but weaker than specifying every finite-step amplitude probability. The fields must be known throughout the relevant configuration patch, including their needed spatial derivatives. Two numbers at the reference point are not enough.

The operational frame, transport convention and reference clock must accompany (I.12). In curved coordinates the drift is an Itô-coordinate object; the invariant statement is the resulting differential operator. If the full source has jumps, memory after projection, deterministic constraints or a primitive finite event that cannot be made infinitesimal, the reduction cannot simply be assumed.

I.6. Smooth kinetic and potential reconstruction

Let the configuration carrier be a connected compact smooth manifold without boundary, with a specified positive reference density $d\nu = w(x)dx$. Work in compatible local charts. Assume a smooth, uniformly elliptic diffusion generator (I.14). Define

$$\Delta_{\nu,A} f = w^{-1}\partial_i\big(wA^{ij}\partial_j f\big), \quad d^j = w^{-1}\partial_i\big(wA^{ij}\big), \quad c = b - d, \quad \alpha = A^{-1}c. \tag{I.15}$$

The expression α is a one-form. Local closedness alone is not enough on a carrier with noncontractible loops.

Theorem I.3: smooth conservative-kinetic inverse. A positive scalar ground-state representation

$$\mathcal{L}f = h^{-1}(-H + E_0)(hf), \qquad H = -\Delta_{\nu,A} + V \tag{I.16}$$

exists in this class precisely when α is globally exact. Then

$$\nabla \log h = \frac{1}{2}\alpha, \qquad V - E_0 = v = \frac{\Delta_{\nu,A} h}{h} = \frac{1}{2}\mathrm{div}_\nu c + \frac{1}{4}c^T A^{-1} c. \tag{I.17}$$

The normalized stationary density relative to ν is $h^2/\int h^2 d\nu$. The kinetic reference $e^{t\Delta_{\nu,A}}$ is determined by the same recovered principal symbol and reference measure. Only the common energy origin is lost.

Proof. Product differentiation gives

$$h^{-1}\Delta_{\nu,A}(hf) = \Delta_{\nu,A} f + 2(A\nabla\log h)\cdot\nabla f + f\,\Delta_{\nu,A}h/h.$$

Equation (I.16) therefore forces $c = 2A\nabla\log h$, which is the necessity of global exactness. Conversely, integrating $\alpha/2$ supplies a positive h up to a constant. Choosing V by (I.17) cancels the zero-order term and returns the original drift and principal symbol. Integration by parts yields

$$\langle f, (H - E_0)f\rangle_\nu = \int h^2 \left[\nabla(\bar{f}/h)\right]^T A\nabla(f/h)\, d\nu \geq 0. \tag{I.18}$$

Compactness gives normalisability; ellipticity and connectedness give the unique positive ground state. If two reconstructions share b, A, w, their $\log h$ gradients agree and their relative potentials coincide. ▫

On noncompact carriers or in the presence of boundaries, domains, boundary conditions, normalisability and the ground-state claim require separate hypotheses. The formal differential cancellation is not a universal ground-state existence theorem. This is the same distinction retained in the RCHS-29 discussion [P1].

I.7. Integrability, stationary currents and the derivative order

I.7.1. Two explicit reversibility tests

On the unit circle with $A = 1, w = 1$ and constant drift $b = 1$, the one-form is $\alpha = dx$. It is locally closed but

$$\oint \alpha = 2\pi \neq 0. \tag{I.19}$$

There is no periodic positive h with $\partial_x \log h = 1/2$. The stationary density is uniform, yet the process carries a circulation and fails Theorem I.3. Stationarity cannot replace detailed balance.

For constant A and a smooth periodic stationary cost S, consider

$$b_\Omega = -A\nabla S + \Omega\nabla S, \qquad \Omega^T = -\Omega. \tag{I.20}$$

The same density e^{-S} remains stationary: $\mathrm{tr}(\Omega D^2 S) = 0$ and $(\Omega\nabla S)\cdot\nabla S = 0$ make the added probability current divergence free. It is generally nonzero. A stationary density therefore cannot determine or remove the irreversible part. [M2] In the 24-coordinate test below the antisymmetric derivative of $A^{-1}b_\Omega$ at zero has Frobenius norm approximately 5.01327, rejecting the reversible scalar class directly.

I.7.2. The raw potential requires more than a linear restoring slope

For flat reference volume and constant A, (I.17) becomes

$$v = \frac{1}{2}\partial_k b^k + \frac{1}{4} b^T A^{-1} b.$$

At a zero-drift background,

$$(D^2 v)_{ij} = \frac{1}{2}\sum_k \partial_i \partial_j \partial_k b^k + \frac{1}{2}[(Db)^T A^{-1}(Db)]_{ij}. \qquad \text{(I.21)}$$

This follows by twice differentiating the two terms, with all terms proportional to b vanishing at the reference. Field-dependent A or w requires differentiating the full formula (I.17); those derivatives may not be discarded.

An exact one-dimensional test uses $S(x) = kx^2/2 + \lambda x^4/4$, $A = a > 0$, and $b = -aS'$. Then

$$b'(0) = -ak, \qquad v''(0) = \frac{ak^2}{2} - 3a\lambda. \qquad \text{(I.22)}$$

At $a = k = 1$, the confining cases $\lambda = 0$ and $\lambda = 1$ have the same diffusion and drift slope but give raw potential curvatures $1/2$ and $-5/2$. Both full ground-state-transformed operators are nonnegative. Thus neither a known drift Jacobian nor operator positivity alone determines a positive raw-potential Hessian. This does not contradict RCHS-24's $H_F = -M^{-1}Db$ for a separately specified gradient **free energy**; it distinguishes that quantity from the raw scalar potential in (I.16). [P5]

I.8. Does gauge covariance select the missing moment tensor?

The source audit motivates testing the strongest available symmetry constraint before declaring the moment fields selected. At a gauge-symmetric reference, transport local link increments to one endpoint frame. Their Lie-algebra tangent is

$$\mathfrak{g} = \mathfrak{su}(3) \oplus \mathfrak{su}(2) \oplus \mathfrak{u}(1).$$

Proposition I.4: invariant covariance freedom. For one adjoint gauge copy, a symmetric covariance commuting with the gauge adjoint action is

$$A = a_3 I_8 \oplus a_2 I_3 \oplus a_q I_1. \qquad \text{(I.23)}$$

For one independent link–record pair it has the form

$$A = S_3 \otimes I_8 \oplus S_2 \otimes I_3 \oplus S_q \otimes I_1, \qquad S_A \in \mathrm{Sym}_2. \qquad \text{(I.24)}$$

Positive-definiteness restricts these matrices to positive cones; it does not select their values. There are three real symmetric coefficients in (I.23) and nine in (I.24), before further source constraints.

Proof. The two compact simple adjoint representations are irreducible real representations, inequivalent to one another and to the trivial Abelian representation. A commuting self-adjoint form is scalar on each single irreducible factor, with no intertwiner between inequivalent factors. With two identical copies, the scalar becomes a symmetric bilinear form on the two-dimensional multiplicity space. This gives (I.23)–(I.24). An explicit basis comprises three factor projectors, tensored in the paired case with the three symmetric 2×2 matrix units. ▫

The computation constructs the adjoint matrices from the archived represented generators and solves the linear invariance equations. With one copy, 78 symmetric unknowns have constraint rank 75. With two copies, 300 unknowns have constraint rank 291. The resulting nullities are three and nine. A separate verifier constructs all nine invariant basis tensors and checks both their independence and invariance. The largest invariance residual is approximately 1.11×10^{-15}; the exact dimensions follow from the proof, not a singular-value threshold.

The 24-dimensional example in this section is one edge with two complete gauge copies. The later 24-coordinate benchmark instead uses twelve edges with two hypercharge phases each; the equal dimensions do not identify those carriers.

This is not a claim that nine new physical coupling constants exist, that all these tensors satisfy every VERSF axiom, or that the full physical carrier has only two copies. More spatial or field multiplicities require their own analysis. It demonstrates that **gauge covariance and positivity alone do not supply the requested continuous amplitude law**. UMP fixes probability assignment for supplied operational states; no source result audited here identifies its amplitude measure with a unique diffusion tensor on this complete link–record tangent. [P3, §11A.1; P8, §7]

I.9. An explicit nonlinear changing-link configuration test

This section tests the inverse and its quadratic derivative order on a fully stated mathematical model. It is **not** offered as a physical replacement for the missing source.

Use the inherited seven-vertex wheel, twelve oriented edges and six faces. Let D be vertex-to-edge incidence, C face incidence, $L = C^T C$, $F = CC^T$ and $T_C = C^T F^{-1}$. Then $CD = 0$ and spec$F = \{1,2,2,4,4,5\}$. The variables are independent compact hypercharge link and record angles:

$$x = (\theta, \varphi) \in \mathbb{T}^{24}, \qquad U_e = e^{i\theta_e q}, \quad \mathrm{Pol}\Phi_e = e^{i\varphi_e q}. \tag{I.25}$$

Record stretches, non-Abelian rotations, currents, matter and completion fields are not integrated or declared quadratic spectators. The canonical signed census is read from the preserved archive:

$$q = (1,4,-2,-3,-6,0,3), \quad d = (18,9,9,6,3,2,2),$$
$$M_2 = \sum_r d_r\, q_r^2 = 378, \qquad M_4 = \sum_r d_r\, q_r^4 = 7002. \tag{I.26}$$

The direct archived generator check has zero discrepancy. The cubic source diagnostic is -234; it is not an anomaly calculation.

Define the periodic character cost

$$f_q(y) = 49 - \mathrm{ReTr}e^{iyq} = \sum_r d_r\,[1 - \cos(q_r y)].$$

The specified stationary log-density cost is

$$S(x) = \lambda_C \sum_p f_q\left((C\theta)_p\right) + \lambda_R \sum_p f_q\left((C\varphi)_p\right) + \lambda_B \sum_e f_q\,(\varphi_e - \theta_e). \tag{I.27}$$

The record and bond character shapes follow the unit-stretch residuals in RCHS-33. **The periodic closure term is an additional diagnostic completion:** it agrees quadratically with the inherited logarithmic closure norm, but is not its exact finite-phase functional. That difference is deliberately retained because fourth derivatives affect (I.21). [P1, §19D; P2, §5]

Use product Haar volume and the frozen inputs

$$(\lambda_C, \lambda_R, \lambda_B) = (1.2,0.9,1.4)/378, \quad A = \begin{pmatrix} 0.7 & 0.2 \\ 0.2 & 1.1 \end{pmatrix} \otimes I_{12}. \tag{I.28}$$

The denominator is the inherited trace convention, not physical action normalization. The numbers are test inputs. Nonzero link–record cross diffusion is not dropped. The generator is $\mathcal{L}f = -A\nabla S \cdot \nabla f + A{:}\,D^2 f$. On the compact torus it is an elliptic reversible process with $h = e^{-S/2}$. Its finite transitions are defined by its semigroup; this calculation does not tabulate a 24-dimensional transition density.

I.10. Complete raw-potential two-jet of the test

Write all 24 scalar residual rows in one matrix,

$$\mathsf{R} = \begin{pmatrix} C & 0 \\ 0 & C \\ -I_{12} & I_{12} \end{pmatrix}, \quad \mathsf{w} = (\lambda_C \mathbf{1}_6, \lambda_R \mathbf{1}_6, \lambda_B \mathbf{1}_{12}).$$

Thus $S(x) = \sum_m w_m\, f_q(\mathsf{R}_m x)$. The exact gradient and Hessian at arbitrary angles are

$$\nabla S = \mathsf{R}^T \{w_m f_q{}'(\mathsf{R}_m x)\}, \qquad D^2 S = \mathsf{R}^T \mathrm{diag}\left[w_m f_q{}''(\mathsf{R}_m x)\right]\mathsf{R}. \tag{I.29}$$

The reconstructed raw potential is

$$v(x) = \frac{1}{4}(\nabla S)^T A \nabla S - \frac{1}{2}\mathrm{tr}(AD^2 S). \quad (I.30)$$

At $x = 0$, set $\mathsf{S} = M_2 \mathsf{R}^T \mathrm{diag}(w)\mathsf{R}$. Since $f_q{}'(0) = f_q{}'''(0) = 0$, $f_q{}''(0) = M_2$ and $f_q{}''''(0) = -M_4$, direct differentiation gives

$$\boxed{B_v := D^2 v(0) = \frac{1}{2}\mathsf{S}A\mathsf{S} + \frac{M_4}{2}\sum_m w_m \left(\mathsf{R}_m A \mathsf{R}_m^T\right)\mathsf{R}_m^T \mathsf{R}_m.} \quad (I.31)$$

Every mixed derivative is included. The second term is the divergence contribution that would be missed by retaining only the linearized drift. The alternative route (I.21), with $b = -A\nabla S$, gives the identical result.

Proposition I.5: exact diagnostic rank. For positive prices and positive definite A, B_v is positive semidefinite with kernel exactly $\ker\mathsf{R}$. On the wheel, that kernel is the six-dimensional set $(D\xi, D\xi)$, so the 24-coordinate parent has rank 18.

Proof. Both terms in (I.31) are positive semidefinite. Every coefficient $w_m\left(\mathsf{R}_m A \mathsf{R}_m^T\right)$ in its second term is positive. Its nullspace is therefore precisely $\ker\mathsf{R}$, which is also killed by S. The equations $C\theta = C\varphi = 0$ and $\theta = \varphi$ give the stated simultaneous-gradient kernel. ▫

The record block $B_{\varphi\varphi}$ is positive definite. Define the **diagnostic stationary reduction**

$$B_\theta^{\mathrm{red}} = B_{\theta\theta} - B_{\theta\varphi}B_{\varphi\varphi}^{-1}B_{\varphi\theta}, \quad B_{\mathrm{face}} = T_C^T B_\theta^{\mathrm{red}} T_C. \quad (I.32)$$

It is positive on all six hypercharge face directions. This is a local reduction of the scalar potential (I.30), not integration of record trajectories, not the full raw operator's effective action and not physical MASD auxiliary relaxation. It is consequently not labelled Z_q.

I.11. Exact mode formula and numerical execution

Let $s_C = 1.2$, $s_R = 0.9$, $s_B = 1.4$, and let a_u, a_v, a_{uv} be the three entries of the 2×2 diffusion block in (I.28). On a link mode with L-eigenvalue ℓ,

$$\mathsf{S}(\ell) = \begin{pmatrix} s_C\ell + s_B & -s_B \\ -s_B & s_R\ell + s_B \end{pmatrix}, \qquad d_A = a_u + a_v - 2a_{uv}.$$

Equation (I.31) reduces exactly to

$$B(\ell) = \frac{1}{2}\mathsf{S}(\ell)A_2\mathsf{S}(\ell) + \frac{389}{42}\begin{pmatrix} 3s_C a_u\ell + s_B d_A & -s_B d_A \\ -s_B d_A & 3s_R a_v \ell + s_B d_A \end{pmatrix}. \quad (I.33)$$

Here $389/42 = M_4/(2M_2)$. The factor three is each triangular incidence row's squared length. For $\ell > 0$, face compression gives

$$z_v(\ell) = \frac{B_{11}(\ell) - B_{12}(\ell)^2/B_{22}(\ell)}{\ell}. \quad (I.34)$$

At the frozen benchmark, the block entries are

$$B_{11} = \frac{63}{125}\ell^2 + \frac{1209}{50}\ell + \frac{7322}{375}, \quad B_{12} = \frac{27}{250}\ell^2 - \frac{987}{1000}\ell - \frac{7322}{375},$$
$$B_{22} = \frac{891}{2000}\ell^2 + \frac{200493}{7000}\ell + \frac{7322}{375}. \quad (I.35)$$

Face mode ℓ	Multiplicity	Exact z_v(ℓ)	Decimal
1	1	$36388754193/1020866500$	35.64496846
2	2	$5302275807/165041200$	32.12698288
4	2	$22420386507/741409000$	30.24024055
5	1	$21951994569/730262900$	30.06039958

These are exact rational results **of the declared benchmark**, not physical couplings or experimentally compared numbers. The record block minimum is approximately 19.52533333. Direct assembly gives the simultaneous-frame residual 1.08×10^{-16} relative to the parent norm. Exact rational mode assembly independently confirms the parent rank 18 and agrees with the numerical face matrix to maximum absolute discrepancy 7.11×10^{-15}.

Retaining only $SAS/2$ changes the face matrix by approximately 92.94% in the symmetric relative norm specified in §I.14. The omission is not a small normalization correction on this test. The fourth-derivative information demanded by (I.21) is material.

I.12. Sensitivity, full mixed derivatives and positive-rate convergence

I.12.1. Same stationary density and total spread, different response

Replace only the diffusion block by

$$\tilde{A} = \begin{pmatrix} 1.2 & -0.1 \\ -0.1 & 0.6 \end{pmatrix} \otimes I_{12}. \tag{I.36}$$

Both matrices are positive definite and have trace 21.6. Both processes have the identical stationary density e^{-S}/Z; their drifts are respectively $-A\nabla S$ and $-\tilde{A}\nabla S$. Their kinetic and raw-potential contributions are not identical.

Face mode	Primary z_v	Alternative z̃_v
1	35.64496846	51.21086394
2	32.12698288	49.85611939
4	30.24024055	49.43240227
5	30.06039958	49.69157684

The matrix difference is 36.51% in the symmetric relative norm. After dividing each face matrix by its own trace, the shape difference remains 4.982%. This is a test of the stated covariance/positivity/equilibrium constraints, not a proof that both laws satisfy all primitive VERSF axioms. It establishes why those particular constraints do not fix one universal multiplier.

I.12.2. All 300 independent second derivatives

The primary finite-difference check evaluates the exact nonlinear $v(x) - v(0)$, using stable trigonometric differences before forming the differences. It checks every diagonal and mixed entry of the 24-coordinate Hessian.

Symmetric field step	Relative Frobenius Hessian error	Maximum absolute entry error
0.004	1.07333×10^{-4}	4.86758×10^{-3}
0.002	2.68348×10^{-5}	1.21697×10^{-3}
0.001	6.70879×10^{-6}	3.04247×10^{-4}
0.0005	1.67720×10^{-6}	7.60622×10^{-5}

The approximately fourfold error decrease on halving the step is the expected second-order field-step behavior. Six additional dense directions are differentiated at 80-digit precision using a separate direct rim/spoke phase formula, not the primary residual-matrix evaluator. Their maximum scaled discrepancy from the exact rational quadratic form is 1.33×10^{-81}. This checks those directional identities at the working precision; it is not an 80-digit guarantee on all archived numerical calculations.

I.12A. A variable-diffusion configuration limit

A separate compact-circle model tests the kinetic reconstruction beyond constant coefficients. Let

$$a(x) = 1 + 0.2\cos x, \qquad S(x) = 0.7(1 - \cos x) + 0.1(1 - \cos 2x), \quad h = e^{-S/2}.$$

In flat reference volume the exact diffusion drift and reconstructed scalar potential are

$$b = a' - aS', \qquad v = -\frac{1}{2}(a'S' + aS'') + \frac{1}{4}a(S')^2. \tag{I.37}$$

On the periodic grid $x_i = i\delta$, use positive symmetric kinetic weights

$$c_{i,i+1} = a(x_i + \delta/2)/\delta^2, \qquad r_{ij} = c_{ij}h_j/h_i. \tag{I.38}$$

They give exact discrete detailed balance with $\pi_i \propto h_i^2$. Applying Theorem I.1 reconstructs the grid reference and

$$v_i^\delta = \sum_{j\sim i} c_{ij}\,(h_j/h_i - 1),$$

which converges to (I.37). Taylor expansion of the two midpoint terms shows that the odd terms cancel and that the remaining error is $O(\delta^2)$ for these smooth periodic coefficients. The same expansion yields the first two local moments:

$$b_i^\delta = \delta(r_{i,i+1} - r_{i,i-1}), \quad a_i^\delta = \frac{\delta^2}{2}(r_{i,i+1} + r_{i,i-1}). \tag{I.39}$$

Grid sites	Maximum drift error	Maximum diffusion error	Maximum v error
32	0.01394494	0.01352407	0.00837939
64	0.00354906	0.00341137	0.00211038
128	0.00088976	0.00085476	0.00052857
256	0.00022274	0.00021381	0.00013220

For each grid, an actual finite-time matrix exponential at time 0.003 has positive entries and row normalization residual at most 2.56×10^{-15}. The stationary residual is at most 2.57×10^{-14}. The smallest entries are very small on the finest grid; positivity is established structurally by the irreducible rate generator, not inferred from rounding.

A separate symbolic test uses the nonflat reference $w(x) = e^{\cos x/7}$. Substituting $d = (wa)'/w$, $b = d - aS'$ and (I.17) agrees exactly with $(wah')'/(wh)$. Thus the reference-density divergence term is tested, not silently omitted. These grids approximate a declared mathematical circle process. They are not physical space and emergent time refinements, and no physical regulator certificate follows from their convergence.

I.12B. Which update details disappear in the diffusion limit?

Fix the nonlinear 24-coordinate test at $x_i = 0.13\sin(i + 0.4)$ for zero-based indices. Let $b = -A\nabla S$ there, and take a unit vector proportional to $k_i = \cos(0.7i)$. Compare two small updates,

$$\delta x = b\tau + \sqrt{2\tau}\,A^{1/2}\xi, \tag{I.40}$$

where ξ is either standard Gaussian or has independent equiprobable ± 1 entries. Both have the same first two infinitesimal moments and obey (I.13). Their Fourier averages are evaluated exactly, without Monte Carlo:

$$P_G(\tau) = e^{i\tau k\cdot b - \tau k^T A k}, \quad P_R(\tau) = e^{i\tau k\cdot b}\prod_j \cos\left[\sqrt{2\tau}\left(A^{1/2}k\right)_j\right]. \tag{I.41}$$

Both discrete generator symbols $(P-1)/\tau$ approach $ik\cdot b - k^T A k$.

Step τ	Gaussian symbol error	Sign-update symbol error	Difference between symbols
0.04	0.01231515	0.01178932	0.00052583
0.02	0.00618991	0.00592299	0.00026693
0.01	0.00310309	0.00296861	0.00013448
0.005	0.00155358	0.00148609	0.00006750
0.0025	0.00077730	0.00074349	0.00003381

Expanding $\log\cos u = -u^2/2 - u^4/12 + O(u^6)$ explains the $O(\tau)$ difference after division by τ. The test verifies the local consistency statement, not convergence of a physically supplied VERSF transition family.

A finite-jump counterexample with matching first two moments

A symmetric unit jump occurring at rate one has mean increment zero and variance rate one, just like a diffusion with $a = 1/2$. Their generator symbols are nevertheless

$$\mathcal{L}_{\text{jump}}(e^{ikx})/(e^{ikx}) = \cos k - 1, \qquad \mathcal{L}_{\text{diff}}(e^{ikx})/(e^{ikx}) = -k^2/2. \tag{I.42}$$

At $k = 2$ they give approximately -1.41615 and -2. The third-moment remainder per unit time does not vanish for the jump process. First two moments are therefore not a general substitute for the full transition law. The source must justify the diffusion regime before that smaller input contract is used.

I.13. Handoff to the physical gauge calculation

The source audit supports two routes, neither of which is completed by the diagnostic tests. One is a complete admitted field-history law; another is an independently normalized physical force or forced susceptibility on the required coupled tangent. RCHS-24 already gives conditional deterministic reconstruction and quadratic connected-component sufficiency. A full stochastic law is not made a universal prerequisite here. [P5, §§3, 9I–9L, 14]

I.13.1. Requirements of the generator route

Within the finite continuous-time class, the required input is one source-derived rate generator on configurations containing the links, together with the reference measure and clock. Within the smooth local class it is the corresponding moment fields (b, A), a justified small-step limit, and the global integrability/domain conditions. The kinetic reference is then reconstructed rather than independently inserted. A single fixed-step K can be used only after the relevant logarithm is shown to be an admitted generator. Section I.4 demonstrates why this is a real condition.

The reconstructed raw operator still has to be connected to the physical defect/field response. HMGBC requires either a correctly typed tangent-to-history embedding with its adjoint and persistent projection, or a second variation directly defined on the physical tangent. Its kinetic field dependence, scalar potential, endpoint and record supports, currents, completion and matter contributions cannot be dropped because one scalar-potential test was positive. [P3, §§56A.3–56A.7]

I.13.2. Why the short-time increment metric is not the raw potential

For a smooth full defect map $\mathcal{D}(x)$ with differential J, a small increment $\Xi = \mathcal{D}(x + \delta x) - \mathcal{D}(x)$ satisfies

$$\lim_{\tau\downarrow 0} \tau^{-1} \operatorname{Cov}(\Xi \mid x) = 2JAJ^T. \tag{I.43}$$

Taylor expansion and (I.12)–(I.13) give this local conditional result. In the regular exponential tilt by Ξ, it is the corresponding local conditional score covariance per unit time. A stationary path rate also requires the correct observation, centering, averaging and memory conditions. It is not automatically $D^2 v$, W_{prim} or an action stiffness. At a fixed point the leading covariance sees A, whereas (I.21) additionally sees nonlinear drift derivatives. The difference is structural, not a missing numerical multiplier. [P3, §56A.5; P4, §10.1]

I.13.3. The downstream operation, not an executed physical output

Only after a common physical quadratic parent has been returned may its admitted auxiliary directions be relaxed:

$$H_g^{\text{eff}} = H_{gg} - H_{g\eta} H_{\eta\eta}^{\text{MP}} H_{\eta g}. \tag{I.44}$$

Here MP denotes the Moore–Penrose inverse. The range condition, positive quotient, retained curvature embedding and full Hessian-connected field set must be proved. Factorwise isotropy, cross-factor structure and continuum matching then determine whether physical Z_3, Z_2, Z_q exist in the claimed convention. Their eventual conversion is

$$g_s = Z_3^{-1/2}, \qquad g = Z_2^{-1/2}, \qquad g' = 6Z_q^{-1/2}. \tag{I.45}$$

The last factor is the inherited $q = 6Y$ convention. [P9] No number in §I.11 is substituted into (I.45). The physical curvature map, action conversion, scale, renormalization convention and regulator limit have not been supplied by this execution.

I.14. Verification, claim grades and failure tests

Grade N. The finite inverse, nonlinear derivatives, mode response and variable-diffusion checks support the results on their declared fixtures. The independent algorithms, numerical tolerances and complete verification inventory are in Technical Supplement S4.1. The failure conditions below delimit the mathematical and physical claims.

Failure tests tied to the actual claims

The finite inverse fails if its recovered conservative kinetic operator and potential do not reproduce the admitted rates. The diffusion inverse fails if (I.17) does not return the admitted operator, or if a claimed positive ground function is nonnormalisable or outside its domain. A nonzero circulation period or irreversible current rejects the reversible scalar class, not VERSF as a whole. The moment reduction fails when a retained jump or memory term invalidates (I.13)–(I.14). The nonlinear response fails if exact rational mode algebra disagrees with (I.31), or the full finite-field derivative fails its stated convergence. A physical release claim fails if it inserts the moment fields, changes the reference or clock after evaluating outputs, omits a coupled quadratic field, or promotes B_{face} to a continuum coupling without its action bridge.

Part II: Calibrated field response and quadratic completion

II.1. Direct response route and notation

This part integrates the RCHS-35C calculation [A2]. The known endpoint equation supplies only a partial source. A work-normalized external force provides a conditional way to eliminate a separate kinetic-map input when reconstructing an action, including some nonsymmetric kinetic maps. Both derivatives must belong to the same actual source; forcing defined after choosing a desired action only verifies that choice.

The full intended carrier includes amplitudes, independent currents, gauge links, complex record maps, support and completion data, and unresolved and matter contributions. A real tangent chart is used only where those objects have an admitted physical response representation. No positive probability density on Grassmann variables or absence of coupled record-stretch effects is assumed.

Here x is a complete local physical quotient coordinate, j its conjugate force, H the candidate action Hessian and Λ a kinetic map. In the endpoint calculation u is a real endpoint displacement and a a link displacement. D, C are the inherited incidence matrices, with $CD = 0$ and $F = CC^T$. Numerical values and verification claims in this part belong to archive [A2], not to a new integration run.

II.2. The explicit source generator rows

The constitutive–continuity subsystem is

$$j = K\Delta_U\psi, \qquad M_v\dot{\psi} + \Delta_U^\dagger j = 0, \qquad (\Delta_U\psi)_e = \psi_t - U_e\psi_s. \tag{II.1}$$

Consequently the endpoint drift is

$$\boxed{b_\psi = -M_v^{-1}\Delta_U^\dagger K\Delta_U\psi.} \tag{II.2}$$

This is inherited source content, re-evaluated here, not a newly chosen drift. Its scope is the stated constitutive shell; it does not define the evolution of all independent current fluctuations or supply equations for $\dot{U}$ and $\dot{\Phi}$. The canonical numerical convention is $K = I_{12}/31$ and $M_v = \mathrm{diag}(7,4,4,4,4,4,4)/31$. Its time parameter is not identified with a physical Fold duration. [P5, §9K.1]

At fixed links, and for the right-inserted generator variation $\delta U_e = iU_e\hat{T}_A\delta a_e^A$, complete differentiation gives

$$D_\psi b_\psi = -M_v^{-1}\Delta_U^\dagger K\Delta_U, \tag{II.3}$$

$$\left(\delta b_\psi\right)_s = -\frac{i\kappa_e}{m_s}\hat{T}_A U_e^\dagger\psi_t, \qquad \left(\delta b_\psi\right)_t = \frac{i\kappa_e}{m_t}U_e\hat{T}_A\psi_s. \tag{II.4}$$

Both the transport and its adjoint divergence are differentiated. Equation (II.4) is valid away from identity links. The representation remains the archived 50-dimensional one, including three neutral singlets and the Higgs doublet. The gauge insertion uses primitive $q = 6Y$; the separate native current instrument is not modified. [P5, §9K.2; A1, §9]

II.2.1. The conditional action recovered from these rows

Grant the source's fixed-conductance common-gradient interpretation, $b_\psi = -M_v^{-1}\,\partial_{\bar{\psi}}F_{\mathrm{end}}$. On a connected unrestricted endpoint patch,

$$F_{\mathrm{end}} = \sum_e \kappa_e \parallel \psi_t - U_e\psi_s \parallel^2 + \mathcal{G}(U, \Phi, J, \dots). \tag{II.5}$$

The difference between two such primitives has zero endpoint gradient, so it can be an arbitrary endpoint-independent functional subject to the remaining source requirements. This is not only an additive constant. The first term is the diffusion-generating energy, not automatically MASD's squared-defect action. It cannot be added to a separate action as a second physical contribution without an identification theorem. [P5, §9K.4]

Thus the actual source returns (II.2)–(II.4); the action statement (II.5) additionally uses its declared gradient interpretation. No manipulation of these rows alone supplies $\partial_U\mathcal{G}$ or $\partial_\Phi\mathcal{G}$.

II.3. Completing known source rows leaves the retained restoring block

Superscript MP denotes the Moore–Penrose inverse. The following standard Schur-complement result makes the residual source freedom exact. It is an application of positive block-matrix algebra, not a new general theorem. [M3]

Proposition II.1: completion of a partial positive parent. Suppose the upper blocks $A = A^T \succcurlyeq 0$ and B of a candidate quadratic action are known. A positive-semidefinite completion exists precisely when $\mathrm{Ran}B \subseteq \mathrm{Ran}A$. Every such completion is

$$H_\Sigma = \begin{pmatrix} A & B \\ B^T & B^T A^{\mathrm{MP}} B + \Sigma \end{pmatrix}, \qquad \Sigma = \Sigma^T \succcurlyeq 0. \tag{II.6}$$

Proof. Positivity implies that a vector in $\ker A$ has zero pairing with every column of B, establishing the range condition. Under that condition,

$$H_\Sigma = \begin{pmatrix} I & 0 \\ B^T A^{\mathrm{MP}} & I \end{pmatrix} \begin{pmatrix} A & 0 \\ 0 & \Sigma \end{pmatrix} \begin{pmatrix} I & A^{\mathrm{MP}} B \\ 0 & I \end{pmatrix}. \tag{II.7}$$

The triangular factors are invertible. Congruence therefore makes positivity equivalent to $\Sigma \succcurlyeq 0$. Equivalently, the quadratic form is

$$\frac{1}{2}(u + A^{\mathrm{MP}} B t)^T A (u + A^{\mathrm{MP}} B t) + \frac{1}{2} t^T \Sigma t. \tag{II.8}$$

Minimizing over u leaves exactly $t^T \Sigma t/2$. This proves the result, including singular A. ▫

This result grants more information than an uncalibrated partial drift: it supposes the corresponding action blocks have already been identified. Even then symmetry, positivity and reciprocal cross derivatives cannot select the remaining block. If a known gauge vector (g_u, g_t) obeys the upper-row identity $A g_u + B g_t = 0$, the remaining null condition is $\Sigma g_t = 0$. That constrains gauge directions, not the positive restoring values on the curvature quotient.

For (II.5), t may include links and any other unresolved action coordinates. Independent record, current and completion blocks still require their source data. The proposition does **not** assert that every Σ extends to a globally valid VERSF theory: a further primitive law may exclude or fix them. It establishes that the known rows plus these algebraic conditions do not do so.

II.3.1. What this prevents

Setting the lower block to its smallest positive completion selects $\Sigma = 0$; it does not derive zero physical gauge stiffness. Choosing Σ from the desired force strengths is equally impermissible. The source must return information transverse to the known endpoint rows, or establish that the physically retained response is independent of every still-admissible completion.

II.4. A calibrated field-response bridge without a separate mobility

The missing transverse information can be smaller than an entire transition kernel. Let x be a complete local real coordinate after only justified kinematic redundancies have been removed. Normalize a force j by the work term $-j^T x$. Suppose the same source has local evolution

$$b(x, j) = -\Lambda(x)\,[\nabla\Gamma(x) - j] + O(\| j \|^2), \quad \nabla\Gamma(x_\star) = 0. \tag{II.9}$$

The invertible map $\Lambda_\star$ may be nonsymmetric. No Gaussian process or particular fluctuation law is required by this deterministic statement. Both the unforced drift and its response to the specified work source must be supplied independently of the unknown Hessian.

Define

$$B = D_x b(x_\star, 0), \qquad R = D_j b(x_\star, 0). \tag{II.10}$$

Theorem II.2: calibrated local action recovery. Under (II.9),

$$B = -\Lambda_\star H, \qquad R = \Lambda_\star, \qquad \boxed{H = -R^{-1} B}, \quad H = D^2\Gamma(x_\star). \tag{II.11}$$

Proof. The derivative of Λ multiplies $\nabla\Gamma(x_\star) = 0$ and vanishes. The two displayed derivative identities then give the inverse. No commutation or symmetry of Λ is used. ▫

Symmetry of $-R^{-1}B$ is a necessary quadratic integrability test. Positivity and the physical-null conditions must also be checked; the calculation may not symmetrize a failed candidate. If $H \succ 0$ and $(\Lambda + \Lambda^T)/2 \succ 0$, the linear evolution $\dot{x} = -\Lambda H x$ is stable: the positive quadratic energy obeys $\dot{\Gamma} = -(Hx)^T \mathrm{sym}(\Lambda)(Hx) < 0$ away from equilibrium.

II.4.1. Nonlinear integrability is a separate condition

On a patch where $R(x)$ is invertible, define the one-form

$$\alpha(x) = -R(x)^{-1} b(x, 0). \tag{II.12}$$

If this is the source's conjugate-response map, a scalar action exists locally when $d\alpha = 0$, and on a simply connected patch it is recovered by $\Gamma(x) - \Gamma(x_\star) = \int_{x_\star}^{x} \alpha$. Noncontractible periods, regularity and domains must be treated separately. Symmetry at one point certifies only the local quadratic candidate, not global nonlinear integrability. An arbitrary extension of b to a forcing variable cannot establish physical action selection merely by making this test pass.

II.5. Retained curvature response and the complete quadratic reduction

Full forcing in every coordinate is unnecessary when the desired retained coordinate is already physically specified. Let $f = E^T x$, with E full column rank, and introduce its normalized conjugate source through

$$\Gamma_h(x) = \Gamma(x) - h^T E^T x, \qquad P = D_h b(x_\star, 0) = \Lambda_\star E. \tag{II.13}$$

On a positive physical quotient $H \succ 0$, the stationary linear response satisfies $B\delta x + Ph = 0$. Therefore

$$\boxed{\chi = -E^T B^{-1} P = E^T H^{-1} E.} \tag{II.14}$$

The unknown kinetic map cancels before any eigenvalue is interpreted as stiffness. This identity permits circulating kinetics when the same map acts on both the action covector and its conjugate source. Using only the dissipative part for the source while retaining circulation in the unforced drift is a different experiment.

Proposition II.3: action of the retained coordinate. The minimum quadratic action at fixed $f = E^T x$ is

$$\Gamma_{\mathrm{ret}}^{(2)}(f) = \frac{1}{2} f^T K_f f, \qquad \boxed{K_f = \chi^{-1}.} \tag{II.15}$$

Proof. A Lagrange multiplier h for $E^T x = f$ gives $Hx = Eh$, so $x = H^{-1}Eh$ and $f = \chi h$. Substitution into $x^T H x/2$ yields (II.15). For a direct split $x = (f, \eta)$, this is

$$K_f = H_{ff} - H_{f\eta} H_{\eta\eta}^{-1} H_{\eta f}. \tag{II.16}$$

Thus the forced response and Schur reduction describe the same specified stationary quadratic action. ▫

The theorem assumes all relevant coupled variables are in x. A resolved process with memory cannot be treated as a memoryless local drift simply to obtain B. One must retain sufficient state, justify a zero-frequency response treatment, or measure the correctly defined stationary response directly. Observation-null directions are not reclassified as gauge. Singular auxiliary directions require the range condition and a justified quotient or constrained minimum, not an indiscriminate inverse.

This is stationary quadratic reduction. It is not automatically integration of fluctuating fields, a terminal-record likelihood or the Hessian of RCHS-35's raw scalar potential. When the desired action already includes fluctuation corrections, the response must belong to that same effective action. Its physical action units and curvature map remain part of the source identification. [A1, §13; P5, §§9I–9J]

II.6. What calibration removes, and what it does not

A common change of the local time parameter multiplies B and R by the same positive factor at equilibrium. It therefore cancels from (II.11); a state-dependent factor also cancels there because its derivative multiplies the zero reference drift. This does not derive a physical time from a stochastic normalization.

Nor does it eliminate the work convention. Replacing a force by an arbitrarily rescaled input changes $D_j b$ and hence the inferred action normalization. The physical content is that j is the force in the specific term $-j^T x$, not just any laboratory or algorithmic control parameter.

For an invertible linear coordinate change $y = Tx$, the conjugate source transforms as $j_y = T^{-T} j_x$. Then

$$B_y = TB_xT^{-1}, \quad R_y = TR_xT^T, \quad H_y = T^{-T}H_xT^{-1}. \tag{II.17}$$

Thus the calibrated construction has the correct Hessian transformation law. The tangent geometry and source pairing are not erased by the inverse.

II.6.1. The raw-potential derivative order does not transfer to this action

RCHS-35's reversible scalar reconstruction, at constant diffusion A, gives

$$v = \frac{1}{2}\mathrm{div}b + \frac{1}{4}b^TA^{-1}b. \tag{II.18}$$

Consequently D^2v may depend on third spatial derivatives of b. That does not imply the Hessian of an independently identified gradient action always needs those derivatives. For the exact one-dimensional example

$$S(x) = \frac{kx^2}{2} + \frac{\lambda x^4}{4}, \quad b = -aS', \quad R = a,$$

$$-R^{-1}b'(0) = k, \qquad v''(0) = \frac{ak^2}{2} - 3a\lambda. \tag{II.19}$$

Both statements are correct, but they answer different questions. RCHS-35 explicitly retained that distinction. This continuation executes the conjugate-action route rather than relabelling D^2v or its stationary minimum as that response. [A1, §7.2]

II.6.2. A necessary caution about successful tests

A symmetric positive susceptibility is not sufficient to prove correct source calibration. Section II.10 constructs an incorrectly forced version of the unchanged benchmark whose susceptibility remains symmetric, yet whose retained coefficient differs by about four percent. The independent work pairing and the source's coupling to it cannot be inferred just from output symmetry or positive rank.

II.7. A pure retained-curvature term survives all auxiliary handling

Let f be the retained curvature and let η stand for any auxiliary variables, with all their couplings included. Suppose a still-undetermined local contribution has the form

$$\Gamma_\lambda(f,\eta) = \Gamma_0(f,\eta) + \frac{\lambda}{2}f^T\Sigma_C f. \tag{II.20}$$

Proposition II.4: pure retained-term persistence. For the same admissible auxiliary domain,

$$\inf_\eta \Gamma_\lambda(f,\eta) = \inf_\eta \Gamma_0(f,\eta) + \frac{\lambda}{2}f^T\Sigma_C f. \tag{II.21}$$

For a common λ-independent measure and finite nonzero integrals,

$$-\log\int e^{-\Gamma_\lambda(f,\eta)}d\mu(\eta \mid f) = -\log\int e^{-\Gamma_0(f,\eta)}d\mu(\eta \mid f) + \frac{\lambda}{2}f^T\Sigma_C f. \tag{II.22}$$

Proof. The added term is constant in the optimization variables, giving (II.21). Its exponential factors out of the integral, giving (II.22). Neither proof assumes a Gaussian auxiliary action, factorization of its internal variables or absent cross-couplings. ▫

These are two separate identities; they do not equate integration with minimization. Domains or measures that themselves change with the source parameter require their additional contributions. The result says that completing an auxiliary calculation cannot determine an independent retained term merely because the auxiliary calculation is complete.

II.7.1. Application to the inherited closure convention

On the identity-branch finite gauge chart, $f = (C \otimes I_{12})a$. The represented generator trace is

$$G_{\mathrm{rep}} = \mathrm{diag}(6I_8, 13/2\, I_3, 378), \qquad \Sigma_C = I_6 \otimes G_{\mathrm{rep}}. \tag{II.23}$$

A common closure-weight variation therefore produces

$$\frac{\partial K_f}{\partial \lambda} = \Sigma_C, \quad \mathrm{rank}\Sigma_C = 72, \quad \mathrm{tr}\Sigma_C = 2673. \tag{II.24}$$

It leaves the endpoint rows in (II.2) unchanged and annihilates every link-gradient frame direction because $CD = 0$. The calculation evaluates this sensitivity, not a selected value of λ. One common free coefficient is already enough to show non-identification from the stated partial data; no separately chosen colour, weak or Abelian prices are needed. A fuller VERSF source may fix or forbid such a variation. This is not a no-go theorem against that fuller source. [P5, §§9K–9L; P4, §§9–10]

II.8. Connection to the complete physical quadratic action

At an admitted common defect-zero stationary background, MASD's intended bosonic response has the form

$$H_{\mathrm{bos}} = H_V + J_D^T W_{\mathrm{prim}} J_D, \quad H_{\mathrm{phys}} = H_{\mathrm{bos}} + H_{\mathrm{other}}^{(2)}, \quad J_D = D\mathcal{D}(x_\star). \tag{II.25}$$

Here $H_{\mathrm{other}}^{(2)}$ denotes only source-derived quadratic contributions not already counted in the bosonic expression; it is not an adjustable completion assigned a numerical value. All typed defect embeddings and their physical magnitudes are included in J_D. All cross-defect metric blocks are included in W_{prim}. Any additional matter, support, measure or completion contribution present at this order must be included in the same physical parent, not silently discarded. Away from a common defect zero, derivatives of the metric, embeddings and nonzero residuals contribute further terms. [P3, §56A.3; P4, §§9, 17]

The calibrated identity (II.11) would return this complete parent only if b and its conjugate-source response are the dynamics of that same action on that same full tangent. Equations (II.2)–(II.5) alone do not establish that identity for the missing fields. Conversely, a source-derived retained susceptibility (II.14) can return the required quadratic reduction without reconstructing every irrelevant microscopic transition.

II.8.1. Which unresolved source information can actually change the answer?

Write an admitted parent as $H = \begin{pmatrix} H_{ff} & H_{f\eta} \\ H_{\eta f} & N \end{pmatrix}$ with $N \succ 0$, and define its stationary lift

$$L_\star = \begin{pmatrix} I \\ -N^{-1} H_{\eta f} \end{pmatrix}.$$

For a variation on this fixed local quotient,

$$\boxed{dK_f = L_\star^T (dH) L_\star.} \tag{II.26}$$

Proof. $K_f = L_\star^T H L_\star$ and $HL_\star = \left(K_f, 0\right)^T$. The top block of $dL_\star$ is zero. Both terms involving $dL_\star$ in the differential therefore vanish. This is the quadratic envelope identity; it retains variations of the auxiliary and cross blocks. ▫

If only the common residual metric varies while the background, J_D and H_V are fixed,

$$dK_f = (J_D L_\star)^T \left(dW_{\mathrm{prim}}\right)(J_D L_\star). \tag{II.27}$$

For a positive-semidefinite candidate variation, this derivative vanishes precisely when

$$\left(dW_{\mathrm{prim}}\right)^{1/2} J_D L_\star = 0. \tag{II.28}$$

Equation (II.28) supplies a concrete response-independence test. It does not require deriving an all-order sector that cannot affect this response, but it does require accounting for every variation that can. The closure variation (II.23) acts directly on retained curvature and fails that invariance test. If the background or embeddings move, their derivatives must also be retained; (II.27) is not an excuse to hold physical quantities fixed artificially.

II.9. Verification using the unchanged RCHS-35 configuration cost

The next calculation tests the bridge, not a newly selected physical law. It consumes RCHS-35's archived stationary Hessian and its declared phase cost unchanged. On the same $\mathbb{T}^{24}$ link–record carrier,

$$S(\theta,\varphi) = \lambda_C \sum_p f_q\left((C\theta)_p\right) + \lambda_R \sum_p f_q\left((C\varphi)_p\right) + \lambda_B \sum_e f_q\left(\varphi_e - \theta_e\right), \tag{II.29}$$

where $f_q(y) = \sum_r d_r\,[1 - \cos(q_r y)]$, $q = (1,4,-2,-3,-6,0,3)$ and $d = (18,9,9,6,3,2,2)$. The source blockwise signed-generator check is performed directly, not inferred from even moments. The prices remain $(\lambda_C, \lambda_R, \lambda_B) = (1.2,0.9,1.4)/378$. This periodic closure is the predecessor's explicit diagnostic completion, not the full logarithmic closure functional. [A1, §§9–10]

With $L = C^T C$, the stationary Hessian is

$$S_2 = D^2 S(0) = \begin{pmatrix} (6/5)L + (7/5)I & -(7/5)I \\ -(7/5)I & (9/10)L + (7/5)I \end{pmatrix}. \tag{II.30}$$

It has the same six simultaneous frame gradients and a positive 18-dimensional quotient. For each kinetic map Λ below, the explicitly declared verification forcing is

$$b_h(x) = -\Lambda[\nabla S(x) - E_{\text{full}} h], \qquad E_{\text{full}} = \begin{pmatrix} C^T \\ 0 \end{pmatrix}. \tag{II.31}$$

The two diffusion choices and the antisymmetric perturbation are inherited from RCHS-35:

$$A_1 = \begin{pmatrix} .7 & .2 \\ .2 & 1.1 \end{pmatrix} \otimes I_{12}, \qquad A_2 = \begin{pmatrix} 1.2 & -.1 \\ -.1 & .6 \end{pmatrix} \otimes I_{12},$$

$$\Omega = .13 \begin{pmatrix} 0 & I_{12} \\ -I_{12} & 0 \end{pmatrix}. \tag{II.32}$$

The four tested kinetic maps are $A_1, A_2, A_1 - \Omega$ and $(7/3)A_1$. The last is an explicit clock-rescaling check. All source derivatives and response matrices are computed on the kinematic quotient; the full analytic cost (II.29) remains the basis for the finite-field checks. None of these inputs is promoted to VERSF's physical generator. In particular, specifying (II.31) verifies cancellation but does not derive the physical conjugate-force law.

II.10. The retained action is unchanged although the raw potentials differ

For every kinetic choice in (II.32), the calibrated inverse and stationary response return

$$H_{\text{cal}} = Q^T S_2 Q, \qquad Z_S = \frac{6}{5} I_6 + \frac{63}{50}\left(\frac{9}{10}F + \frac{7}{5} I_6\right)^{-1}. \tag{II.33}$$

Here Q is an orthonormal basis matrix for the 18-dimensional test quotient; $S_{2,Q} = Q^T S_2 Q$, $\Lambda_Q = Q^T \Lambda Q$ and $E = Q^T E_{\text{full}}$. This is a finite stationary action coefficient, not a continuum Z_q. The response follows directly from the Schur complement of (II.30), or independently from $-E^T B^{-1} P$.

Face eigenvalue	Multiplicity	Exact coefficient	Decimal
1	1	$201/115$	1.74782608696
2	2	$51/32$	1.59375000000
4	2	$363/250$	1.45200000000
5	1	$417/295$	1.41355932203

The separately reconstructed primary and alternative static action matrices differ by 3.82×10^{-16} relatively. In contrast, their archived RCHS-35 raw-potential reductions retain the reported relative difference 0.36511572. This is not a contradiction: $D^2 v$ and the calibrated Hessian of S are different responses. A change in the former alone does not establish a change in the latter. RCHS-35 did not identify either with the complete physical gauge action. [A1, §§7.2, 10, 12.1]

II.10.1. Incorrect forcing can pass a symmetry check

Keep circulating unforced dynamics $b_0 = -(A_1 - \Omega)\nabla S$, but incorrectly force only its dissipative part, using $P_{\text{wrong}} = A_1 E_{\text{full}}$. Then

$$\chi_{\text{wrong}} = E^T S_{2,Q}^{-1} \Lambda_Q^{-1} A_{1,Q} E. \tag{II.34}$$

On a face mode ℓ, its inverse is exactly

$$z_{\mathrm{wrong}}(\ell) = \frac{3201(18\ell + 49)}{100(486\ell + 665)}. \tag{II.35}$$

It differs from (II.33). The full face discrepancy is 4.04997%, while its antisymmetry residual is only 2.39×10^{-16}. Thus apparent reciprocity is insufficient evidence that the response uses the source's conjugate work convention. Equation (II.35) is a verification countercheck, not another candidate physical interaction law.

II.11 Executed source and response checks

Grade N. The 844-coordinate transport parent reproduces the stated endpoint reduction to 3.90×10^{-16} relative discrepancy. All 144 source-link derivative columns show second-order convergence. Independently calibrated finite-response solves and the separate verifier complete 22 checks.

Technical Supplement S4.2 retains the source endpoint construction, equations (II.36)–(II.37), the three convergence tables and the separate verification route. The background is the specified neutral-orthogonal chirp; the physical source and carrier requirements remain those of II.1–II.10.

Part III: Six-defect transverse calculus and compatibility

III.1. Source-audited derivative extension

This part integrates RCHS-35D [A3]. The earlier fixed-support closure, composition and polar-bond covectors are inherited from [P11]; they are not newly discovered here. The additions retain all six defect families, independent current and continuity contributions, general matrix records, local completion and moving occupied supports. The printed MASD support derivative is explicitly corrected in §III.5.

All pairings are real: $\langle A, B\rangle = \mathrm{ReTr}\left(A^\dagger B\right)$ and the corresponding real complex-vector pairing. A star on a differential is its adjoint in these pairings. The gauge insertion is $\delta U_e = iU_e\alpha_e$, with $\alpha_e = \sum_A \delta\, a_e^A \hat{T}_A$ and primitive Abelian generator $q = 6Y$.

Spatial records Φ_e^{tr} and local completion maps $\Phi_{H,i}$ remain different fields. The general differential accepts their source-specified embeddings and metric. The 97,044-argument wheel fixture is an enlarged derivative test, not an admitted physical carrier. Its numerical results and the separate moving-support checks retain the scope of archive [A3].

III.2. Which functional can be identified with the transverse remainder?

The known source equations and their conditional integration are

$$b_\rho = -M_v^{-1}\Delta_U^\dagger K \Delta_U \rho, \qquad F_{\mathrm{end}} = F_{\mathrm{diff}} + \mathcal{G}(t), \tag{III.1}$$

$$F_{\mathrm{diff}} = \sum_e \kappa_e \parallel \rho_t - U_e\rho_s \parallel^2, \qquad t = (U, J, \Phi^{\mathrm{tr}}, \Phi_H, \dots). \tag{III.2}$$

The integration assumes a connected unrestricted endpoint patch, fixed conductances and the stated gradient convention. It is not an off-shell derivation of independent current dynamics. If a candidate full functional Γ is proposed as this same energy, it must satisfy

$$D_\rho(\Gamma - F_{\mathrm{diff}}) = 0. \tag{III.3}$$

At a stationary point, equality of the endpoint–endpoint and endpoint–transverse Hessian blocks is a necessary local test. Merely writing $\Gamma = \Gamma_V + 1/2\,\langle d, Wd\rangle$ does not prove (III.3). The residual functional measures defects of equations that can already vanish on a solution; the diffusion energy generates the endpoint equation. [A2, §2; P5, §9K.4]

III.2.1. An exact current–continuity compatibility test

Consider one real nonzero incidence mode of eigenvalue $\ell > 0$, at zero frequency, and retain an independent current j and endpoint amplitude u. The orthogonal constant-weight J, T subaction is

$$\Gamma_{JT} = \frac{w_J}{2}\left(j - \kappa\sqrt{\ell}\, u\right)^2 + \frac{w_T}{2}\ell j^2, \qquad w_J, w_T, \kappa > 0. \tag{III.4}$$

Stationary elimination of j gives

$$j_* = \frac{w_J \kappa \sqrt{\ell}}{w_J + w_T \ell} u, \qquad H_{u,\mathrm{eff}}^{JT} = \frac{\kappa^2 w_J w_T \ell^2}{w_J + w_T \ell}. \tag{III.5}$$

The transported endpoint energy is $F_{\mathrm{diff}} = \kappa\ell u^2$, with Hessian $2\kappa\ell$. Equality requires

$$\left(\kappa w_J - 2\right) w_T \ell = 2 w_J. \tag{III.6}$$

Proposition III.1. With strictly positive constant w_J, w_T, κ, this equality cannot hold at two distinct positive incidence eigenvalues.

Proof. Subtract the two equations. Since the eigenvalues differ and $w_T > 0$, one obtains $\kappa w_J = 2$. Substituting into either equation gives $w_J = 0$, a contradiction. The elimination and the two-mode contradiction are checked in exact symbolic arithmetic. ▫

This rejects a specific naive identification of a squared J, T subaction with the diffusion-generating energy. It does not reject the full MASD action, a general cross-metric, additional physical fields or another justified action bridge. The following calculation therefore differentiates the residual action, not an established physical remainder.

III.3. Complete first differential: closure, current and conservation

Let $d = \left(D_C, D_J, D_T, D_R, D_B, D_H\right)$ include the actual typed embeddings. The formulas below first display the unembedded residuals; derivatives of any field-dependent embedding must then be applied by the product rule. Geometric weights are frozen only in the numerical fixture, not asserted physically constant. [P4, §§9, 12–17]

III.3.1. Closure with the ordered holonomy retained

For a face p, write $Q_p = H_{p,*}^{-1} H_p(U)$, with the reference and logarithm branch fixed. Then

$$D_C(p) = -\frac{i}{|p|}\mathrm{Log}_0 Q_p, \qquad \delta D_C(p) = -\frac{i}{|p|} D\mathrm{Log}_{Q_p}\left[H_{p,*}^{-1}\delta H_p\right]. \tag{III.7}$$

Each occurrence of a link in the ordered product is differentiated. For $H_p = U_{02}^{\dagger} U_{12} U_{01}$,

$$\delta H_p = \delta U_{02}^{\dagger} U_{12} U_{01} + U_{02}^{\dagger} \delta U_{12} U_{01} + U_{02}^{\dagger} U_{12} \delta U_{01}. \tag{III.8}$$

No commutation of a holonomy with its variation is assumed. If physical face area varies, the additional derivative of $|p|^{-1}$ belongs in (III.7).

III.3.2. Independent current

With $\Delta_U \rho = \rho_t - U_e \rho_s$,

$$\delta D_J(e) = \delta J_e - \kappa_e(\delta\rho_t - U_e\delta\rho_s - \delta U_e \rho_s) - \delta\kappa_e\, \Delta_U \rho. \tag{III.9}$$

The current is an independent field. Replacing δJ by a constitutive-shell value would constrain the action before evaluating its coupled response. The numerical fixture fixes $\kappa_e = 1/31$ only as the inherited derivative-check convention.

III.3.3. Covariant continuity

The oriented divergence is $(\partial_U J)_i = \sum_{t(e)=i} J_e - \sum_{s(e)=i} U_e^{\dagger} J_e$. Therefore

$$\delta D_T(i) = \delta\dot{\rho}_i + (\partial_U \delta J)_i + \sum_{s(e)=i} i\,\alpha_e U_e^{\dagger} J_e. \tag{III.10}$$

The last term is present at a nonzero current background. It is a direct link response, not a derivative of the current coordinates. It cannot be omitted from a transverse calculation simply because the continuity defect is named a current sector.

At zero frequency, $\delta\dot{\rho} = 0$ in a static variation. At nonzero frequency or on a discrete physical history, its derivative is fixed by that history's actual time operator. Treating it as an independently and freely relaxed velocity would be a new assumption. The engine accepts an extra supplied $\delta\dot{\rho}$ term but does not derive the physical time law.

III.4. Spatial records, Gram support and the full bond chain

The full spatial-record differential on a triangle is

$$\delta D_R = \delta\Phi_{12}^{\mathrm{tr}}\Phi_{01}^{\mathrm{tr}} + \Phi_{12}^{\mathrm{tr}}\delta\Phi_{01}^{\mathrm{tr}} - \delta\Phi_{02}^{\mathrm{tr}}. \tag{III.11}$$

This includes positive stretches and arbitrary matrix variations, not only gauge-unitary phases. It does not differentiate the local completion morphism, which has its own residual in §III.6.

For identity realization maps, the source Gram and its differential are

$$G_i = \rho_i \rho_i^\dagger + \sum_{t(e)=i} \Phi_e \Phi_e^\dagger + \sum_{s(e)=i} \Phi_e^\dagger \Phi_e + G_i^{\mathrm{term}}, \tag{III.12}$$

$$\begin{aligned} \delta G_i &= \delta\rho_i \rho_i^\dagger + \rho_i \delta\rho_i^\dagger + \delta G_i^{\mathrm{term}} \\ &+ \sum_{t(e)=i} \left(\delta\Phi_e \Phi_e^\dagger + \Phi_e \delta\Phi_e^\dagger \right) \\ &+ \sum_{s(e)=i} \left(\delta\Phi_e^\dagger \Phi_e + \Phi_e^\dagger \delta\Phi_e \right). \end{aligned} \tag{III.13}$$

The source's tilde realization maps, if not identity, must also be differentiated or explicitly frozen. The terminal Gram cannot be dropped merely because its background value is positive. Its derivative depends on the actual terminal construction. [P4, §§8A, 16.1]

Let Π_i select a separated occupied spectral band. With $M_e = \Pi_t \Phi_e \Pi_s$ and $V_e = \mathrm{Pol} M_e$, the complete chain is

$$\delta M_e = \delta\Pi_t \Phi_e \Pi_s + \Pi_t \delta\Phi_e \Pi_s + \Pi_t \Phi_e \delta\Pi_s, \tag{III.14}$$

$$\begin{aligned} \delta D_B(e) &= \delta\Pi_t U_e \Pi_s + \Pi_t \delta U_e \Pi_s + \Pi_t U_e \delta\Pi_s \\ &- D\mathrm{Pol}_{M_e}[\delta M_e]. \end{aligned} \tag{III.15}$$

A fixed rank does not mean fixed subspaces. Discarding $\delta\Pi$ or the support-motion terms in the polar derivative changes (III.15). Conversely, on an open full-support patch $\Pi_i = I$, its derivative is identically zero; the earlier full-support calculations need no projector correction.

The required support and polar formulas are supplied next. They are valid only on separated spectral bands and a constant-rank polar stratum. A gap closing, an actual rank change, or a moving physical cutoff across an eigenvalue requires different analysis.

III.5. Correction to the printed support-projector derivative

The MASD Appendix B formula on PDF page 78 reads

$$\delta\Pi = \Pi^\perp \delta G\, S_G + S_G \delta G\, \Pi^\perp, \qquad S_G = (G - g_{\mathrm{occ}})^+ \text{ on the occupied support.} \tag{III.16}$$

The wording and displayed expression were checked against the rendered backing PDF, not inferred from a damaged extraction. With the reduced resolvent defined as printed, (III.16) is not the general derivative of $1_{[g_{\mathrm{occ}},\infty)}(G)$. The correction below is explicit; it is not silently imported into the source claim. [P4, Appendix B]

III.5.1. The correct spectral derivative

Let $G = Z\mathrm{diag}(\lambda_a)Z^\dagger$ and let p_a be one or zero according to the selected band. On a gap-preserving perturbation,

$$D\Pi_G[E] = Z\left[\mathsf{K} \circ \left(Z^\dagger E Z\right)\right]Z^\dagger, \quad \mathsf{K}_{ab} = \begin{cases} \dfrac{p_a - p_b}{\lambda_a - \lambda_b}, & p_a \neq p_b, \\ 0, & p_a = p_b. \end{cases} \tag{III.17}$$

Proof. Differentiate $\Pi^2 = \Pi$: the within-band blocks of $\delta\Pi$ vanish. Differentiate $G\Pi = \Pi G$: in the eigenbasis, $(\lambda_a - \lambda_b)(\delta\Pi)_{ab} = (p_a - p_b)E_{ab}$. The separated bands permit exactly the divisions in (III.17), including repeated eigenvalues within a band. ▫

The arbitrary cutoff disappears as long as it stays in the same gap. Equation (III.17) is also the contour-resolvent derivative of the spectral projector. It is self-adjoint as a real linear map on Hermitian matrices.

III.5.2. Exact counterexample to the printed formula

For a planar rotation $R(t)$, take $G(t) = R(t)\mathrm{diag}(3,0)R(t)^T$. For every $0 < g_{\mathrm{occ}} < 3$, the selected projector is $\Pi(t) = R(t)\mathrm{diag}(1,0)R(t)^T$, so

$$G'(0) = \begin{pmatrix} 0 & 3 \\ 3 & 0 \end{pmatrix}, \qquad \Pi'(0) = \begin{pmatrix} 0 & 1 \\ 1 & 0 \end{pmatrix}. \tag{III.18}$$

The printed formula instead gives off-diagonal value $3/(3 - g_{\mathrm{occ}})$: $6/5$ at cutoff $1/2$, $3/2$ at cutoff 1, and 3 at cutoff 2. The correct answer is always one. The family is positive semidefinite and rank one throughout, with a persistent gap. This correction affects moving-support use of that formula; it is not evidence against previous fixed-full-support results or the entire VERSF action programme.

III.6. Moving polar support and local completion

III.6.1. Constant-rank polar differential

Let $M = U_r \Sigma V_r^\dagger$ be its thin singular-value decomposition with all active singular values positive. Put $Q = U_r U_r^\dagger$, $P = V_r V_r^\dagger$, $E_r = U_r^\dagger E V_r$. For a constant-rank tangent, $(I - Q)E(I - P) = 0$. Then

$$\begin{aligned} &D\mathrm{Pol}_M[E] = U_r \mathsf{A} V_r^\dagger + (I - Q)EV_r\Sigma^{-1}V_r^\dagger \\ &+U_r\Sigma^{-1}U_r^\dagger E(I - P), \\ &\mathsf{A}_{ab} = \frac{\left(E_r - E_r^\dagger\right)_{ab}}{\sigma_a + \sigma_b}. \end{aligned} \tag{III.19}$$

To derive it, resolve E into active–active, complement–active and active–complement blocks. Differentiating the polar factorization gives the active Sylvester equation; differentiating the two subspaces gives the last two terms. Their sum is the differential of the canonical partial isometry. The expression is also its real adjoint map on the tangent pairing. Standard polar differential calculus underlies this construction. [P11, §7; M4]

On full support this reduces to the familiar right-polar equation for $M = VS$,

$$S\Omega + \Omega S = V^\dagger E - E^\dagger V, \qquad \delta V = V\Omega. \tag{III.20}$$

The numerical rank-two test in Technical Supplement S4.3 moves both subspaces. The active-only contribution vanishes there while the full derivative is nonzero, so (III.20) cannot be used with silently frozen supports on that test.

III.6.2. Local completion strain is a different field

Use the source's left polar factor $B_H = \left(\Phi_H \Phi_H^\dagger\right)^{1/2}$, a frozen positive symmetric reference, and its scalar target:

$$A_0 = B_{H,\mathrm{sym}}^{-1/2}, \quad Y_H = A_0 B_H A_0, \quad D_H = \log Y_H - \frac{\phi_H}{\Lambda_*} P_H^R. \tag{III.21}$$

On positive supported coordinates, its derivative is

$$\begin{aligned} &B_H \delta B_H + \delta B_H B_H = \delta\Phi_H \Phi_H^\dagger + \Phi_H \delta\Phi_H^\dagger, \\ &\delta D_H = D\log_{Y_H}[A_0 \delta B_H A_0] - \delta(\phi_H/\Lambda_*)P_H^R - (\phi_H/\Lambda_*)\delta P_H^R. \end{aligned} \tag{III.22}$$

A changing A_0 adds its two product-rule terms. The minimal MA9 branch freezes P_H^R; it does not derive the physical scalar target or local chiral realization. Those maps remain explicit inputs. The numerical engine tests seven independent target arguments, not seven newly asserted physical scalar fields. [P4, §§31, 47F]

III.7. The transverse force covectors with all six families retained

For a supplied common residual metric set $\tau_X = \sum_Y W_{XY} D_Y$. Every cross-family contribution is already in τ_X; it is not an optional later correction. The complete first variation is

$$D\Gamma_D[\xi] = \langle \tau, J\xi \rangle + \frac{1}{2}\langle d, W_\xi d \rangle, \qquad J = Dd. \tag{III.23}$$

III.7.1. Explicit link derivative

At fixed geometric conventions and with the support data independent of U in this variation, the positive action covector on a right-inserted gauge direction is

$$
\begin{aligned}
&\left(\mathfrak{f}_a\right)_e^A = \sum_{p \ni e} \left\langle \tau_{C,p}, -\frac{i}{|p|} D\log_{Q_p}\left[H_{p,*}^{-1} \delta_e H_p\right] \right\rangle \\
&+\left\langle \tau_{J,e}, i\kappa_e U_e \hat{T}_A \rho_s \right\rangle + \left\langle \tau_{T,s}, i\hat{T}_A U_e^\dagger J_e \right\rangle \\
&+\left\langle \tau_{B,e}, \Pi_t i U_e \hat{T}_A \Pi_s \right\rangle + \left(\mathfrak{f}_{\text{extra}}\right)_e^A.
\end{aligned}
\tag{III.24}
$$

Here $\mathfrak{f}_{\text{extra}}$ means the explicitly required derivatives of metric, realization, geometric data and any other physical action terms; it is not a coefficient assigned a test value. Equation (III.24) shows why closure and bond covectors alone are not the complete transverse derivative of the six-defect functional. Current and continuity both contribute. Although R, H have no direct link variation on this fixed independent-field chart, they can enter every τ_X through the common metric.

The restoring force is minus this covector. Turning it into a velocity still requires the source's kinetic map; a covector is not an independently calibrated drift.

III.7.2. Current and direct record pullbacks

The current covector is

$$
\mathfrak{f}_J = \tau_J + \partial_U^\dagger \tau_T.
\tag{III.25}
$$

For one composition triangle, the record covectors are

$$
\left(\mathfrak{f}_{\Phi_{01}}\right)_R = \Phi_{12}^\dagger \tau_R, \quad \left(\mathfrak{f}_{\Phi_{12}}\right)_R = \tau_R \Phi_{01}^\dagger, \quad \left(\mathfrak{f}_{\Phi_{02}}\right)_R = -\tau_R.
\tag{III.26}
$$

Each shared edge receives all incident terms. These composition formulas are inherited from [P11], not a new result. The remaining direct and support-induced bond terms follow in §III.7A.

III.7A. Support-induced record forces and completion pullback

Let $Z_e = \left(D\mathrm{Pol}_{M_e}\right)^* \left[\tau_{B,e}\right]$. For an edge from s to t, the partial bond pullbacks are

$$
\begin{aligned}
\left(\mathfrak{f}_U\right)_{B,\text{direct}} &= \Pi_t \tau_B \Pi_s, \\
\left(\mathfrak{f}_\Phi\right)_{B,\text{direct}} &= -\Pi_t Z_e \Pi_s, \\
Q_t &= \mathrm{Herm}\left(\tau_B \Pi_s U^\dagger - Z_e \Pi_s \Phi^\dagger\right), \\
Q_s &= \mathrm{Herm}\left(U^\dagger \Pi_t \tau_B - \Phi^\dagger \Pi_t Z_e\right).
\end{aligned}
\tag{III.27}
$$

The Q_i are covectors for support variations. Sum them over incident edges, then apply the corrected self-adjoint projector derivative:

$$
R_i = D\Pi_{G_i}\left[\sum_{e \ni i} Q_i^{(e)}\right].
\tag{III.28}
$$

For the explicit Gram (III.12), the induced additional covectors are

$$
\left(\mathfrak{f}_{\rho_i}\right)_{\text{supp}} = 2R_i \rho_i, \qquad \left(\mathfrak{f}_{\Phi_e}\right)_{\text{supp}} = 2R_t \Phi_e + 2\Phi_e R_s.
\tag{III.29}
$$

They also pair with δG_i^{term} and with any varying realization maps. Equation (III.29) follows by differentiating the products in (III.13) and cycling the real trace. It is not a freedom to hold an actual physical terminal realization fixed. Combining (III.26)–(III.29) with metric and other source terms gives the spatial-record covector on the stated branch.

These expressions supply the part absent from a fixed-support calculation. A separate four-dimensional, rank-two test differentiates supports built from amplitude and record Grams, carries them through the supported polar factor, and verifies the complete bond chain and its adjoint. It is not a second full-carrier simulation.

III.7A.1. Completion covector

For the frozen references in (III.21), let $\mathcal{L}_{B_H}(X) = B_H X + X B_H$ and set

$$\Theta_H = A_0 \left(D\log_{Y_H}\right)^* [\mathrm{Herm}\tau_H] A_0.$$

Then the local completion and target covectors are

$$\mathfrak{f}_{\Phi_H} = 2\mathcal{L}_{B_H}^{-1}(\Theta_H)\Phi_H, \qquad \mathfrak{f}_{\phi_H} = -\Lambda_*^{-1}\langle \tau_H, P_H^R \rangle. \tag{III.30}$$

The intermediate matrix Θ_H is the strain pullback. The target covector must be pulled back through the source's actual ϕ_H map. A varying projector, reference or scale adds the terms already shown in (III.22). No Higgs representation or completion law is inferred from this derivative identity.

III.8. The quadratic action: off-zero terms and exact common-zero reduction

In a fixed residual chart, permit a self-adjoint field-dependent $W(x)$. Let $J\xi = Dd[\xi]$, $d_{\xi\zeta} = D^2 d[\xi, \zeta]$ and $W_\xi = DW[\xi]$. Direct differentiation of (III.23) gives

$$\begin{aligned} D^2\Gamma_D[\xi, \zeta] &= \langle J\xi, WJ\zeta \rangle + \langle d, W d_{\xi\zeta} \rangle \\ &+ \langle J\xi, W_\zeta d \rangle + \langle J\zeta, W_\xi d \rangle + \frac{1}{2}\langle d, W_{\xi\zeta} d \rangle. \end{aligned} \tag{III.31}$$

The second term is residual stress. Both first metric-derivative terms are needed away from a common zero. A symbolic three-coordinate test with nonlinear residuals and nonconstant positive W verifies this entire identity independently.

At a common defect zero $d(x_*) = 0$, every term except the first vanishes. Thus

$$H_D = J_*^* W_* J_*, \qquad D\mathfrak{f}_D[\xi] = J_*^* W_* J_* \xi. \tag{III.32}$$

This is MASD's inherited Gauss–Newton result, with the enlarged differential and adjoint explicitly implemented. It does not mean that W_* has been derived, that a physical common zero has been selected, or that the underlying scalar completion premise has been proved. [P4, §§20–21]

III.8.1. Every physical contribution must belong to the same action

The intended full physical parent, when supplied, is schematically

$$H_{\mathrm{phys}} = H_V + J_*^* W_{\mathrm{prim}} J_* + H_{\mathrm{remaining}}^{(2)}. \tag{III.33}$$

The last term denotes source-derived contributions not already counted: for example matter, measure and unresolved effects, where present. It is not assigned zero by the current execution. The original bosonic fields, scalar-target map, physical support realization, time operator and every same-order mixed block must be retained. Fermionic bilinears and their effective fluctuations require their correctly typed source construction; this manuscript does not invent a positive measure on Grassmann coordinates or append a determinant model.

A gauge-orbit tangent is a Hessian null at a stationary common zero when all fields move together under the actual gauge action. An observation-null direction is not automatically gauge. Away from stationarity, a coordinate Hessian on a curved field manifold also carries the relevant chart/connection terms; one cannot infer a gauge-null Hessian merely from a nonzero-residual test. The numerical frame test below is performed at the compatible common-zero fixture.

The physical quadratic parent is therefore not emitted by the code when its physical metric or complete-carrier certificate is absent. That refusal is tested rather than replaced with an identity metric.

III.9. Transverse reduction and calibrated curvature forcing

Let f be the source-normalized retained curvature coordinate, r the explicitly retained record variables, and s every other coupled auxiliary. On an admitted stable quotient the complete Hessian has all blocks

$$H = \begin{pmatrix} H_{ff} & H_{fr} & H_{fs} \\ H_{rf} & H_{rr} & H_{rs} \\ H_{sf} & H_{sr} & H_{ss} \end{pmatrix}. \tag{III.34}$$

When the stated inverses exist, first eliminating s gives

$$\bar{H}_{ab} = H_{ab} - H_{as} H_{ss}^{-1} H_{sb}, \quad a, b \in \{f, r\}, \qquad K_f = \bar{H}_{ff} - \bar{H}_{fr} \bar{H}_{rr}^{-1} \bar{H}_{rf}. \tag{III.35}$$

This equals the one-step Schur complement over (r, s). The exact symbolic test retains all cross blocks. Singular cases require the appropriate range conditions, admitted constraints and pseudoinverse on the correct subspace. These standard identities do not determine any of the missing blocks. In particular, a closure–record–bond-only inverse is not the full physical reduction until the effects of J, T, H, support and all other coupled sectors have been included or proved irrelevant. [A2, §§5, 8; P4, §§23–24]

III.9.1. What an equivalent calibrated response would supply

For a conjugate source with work $-h^T E^T x$, suppose the actual dynamics and source satisfy $B = D_x b = -\Lambda H$ and $P = D_h b = \Lambda E$. Then

$$\chi = -E^T B^{-1} P = E^T H^{-1} E, \qquad K_f = \chi^{-1}. \tag{III.36}$$

This is the calibrated identity already derived and tested in RCHS-35C. It is not a new result of this execution. It cancels the kinetic map only when the two derivatives come from the same physical work-normalized source. The inspected prior papers do not supply those full transverse derivatives. Defining $B = -\Lambda H$ after choosing W_* and then recovering H would only check the definition.

For a finite flat wheel, C and its lift $T_C = C^T (C C^T)^{-1}$ can define a test curvature chart. On a nonflat physical branch, the actual linearized holonomy map and its physical embedding must replace that special chart. A numerical coordinate lift is not the missing calibration.

If a memory-bearing reduced response is used, the correct zero-frequency response must retain the eliminated dynamics. Treating it as a short memoryless process would change the experiment. Stationary minimization, integration of fluctuating fields and a normalized-record Fisher matrix remain distinct operations.

III.10 Executed six-defect derivative fixture

Grade N. The fixture contains all twelve wheel edges, six faces and the archived 50-dimensional representation. Matrix-free differential and adjoint operations cover 97,044 real matrix/vector arguments. The direct tests use six dense directions and all 144 gauge-link columns; they do not constitute an exhaustive Hessian census.

III.11 Numerical verification and exact source checks

Twenty primary and nine separate-verifier checks exercise the full derivative, adjoint pairing and common-zero reduction. Moving-support tests use a separate gapped fixture; freezing those supports changes its derivative by about 2.13%. The complete inputs, tolerances and per-sector results are in Technical Supplement S4.3.

III.11A Provenance of the derivative result

The general Gauss–Newton, Schur and calibrated-response identities are inherited mathematical tools. The source-specific contribution is the complete six-family derivative and adjoint, current/continuity link terms, completion pullback, moving-support correction and the compatibility test of III.2. Technical Supplement S4.3 distinguishes exact symbolic checks from floating-point comparisons and preserves their verification conventions.

Part IV: History–action matching and the selection test

IV.1. Time-dependent identification and its assumptions

This part integrates RCHS-35E [A4]. Part III's static two-mode test does not identify the current–continuity residual penalty with the endpoint diffusion energy. Retaining time permits a different relationship: a normalized history law can contract to the endpoint Gibbs energy without its instantaneous squared residual being that energy. The construction below calculates that relationship and the resulting covariance constraint.

The fluctuation–dissipation input is inherited from the conditional gradient–Gibbs continuation [P12], not newly derived from the complete VERSF primitives. The calculation assumes real finite-dimensional linear fluctuations, a fixed reference volume, centered time-local Gaussian residual noise, fixed transport coefficients during each test and a stable endpoint subspace. It imposes the Gibbs density of the same transport energy as its identification condition. The inverse temperature remains a parameter.

The general relation between Gaussian histories, dissipation and equilibrium belongs to the established Onsager–Machlup setting [M6]. The source-specific calculation normalizes the finite transitions, classifies compatible current–continuity metrics, performs the whole-history contraction and separately tests the explicit capacity, activity and entropy constraints. All numerical returns below are those of archive [A4].

The endpoint fixture retains its additional assumptions. The operational Gaussian proposal and exact bath reduction are specified separately in §IV.13. The fixture's unselected Gaussian input therefore does not imply absence of a Gaussian construction in the corpus. [P28–P30]

IV.2. Restoring time in the current–continuity mode

Let $\ell > 0$ be a spatial incidence eigenvalue and $\kappa > 0$ the declared conductance in the scalar mode convention. Keep the endpoint amplitude u and current j independent. Put $a = \kappa\ell$ and

$$r_J = j - \kappa\sqrt{\ell}\,u, \qquad r_T = \dot{u} + \sqrt{\ell}\,j. \tag{IV.1}$$

The proposed quadratic history exponent is

$$\mathcal{A}_\ell[u,j] = \frac{1}{2}\int_0^T \left[w_J r_J^2 + w_T r_T^2\right] dt, \qquad w_J, w_T > 0. \tag{IV.2}$$

Time t is the stated evolution parameter, not an independently derived physical Fold. Equation (IV.2) is not yet an absolute path measure. Section IV.3 supplies a finite-step normalized construction; the integrals subsequently denote its quadratic control/history expression for smooth test paths, not a density against an infinite-dimensional flat measure.

Proposition IV.1: time-dependent residual elimination. Pointwise minimization over the current gives

$$j_\star = \frac{\sqrt{\ell}\left(\kappa w_J u - w_T\dot{u}\right)}{w_J + w_T\ell}, \qquad c_\ell = \frac{w_J w_T}{w_J + w_T\ell}, \tag{IV.3}$$

and

$$\boxed{\mathcal{A}_\ell^{\mathrm{red}}[u] = \frac{c_\ell}{2}\int_0^T (\dot{u} + au)^2\, dt.} \tag{IV.4}$$

Proof. Differentiate the quadratic expression in j, solve its positive scalar normal equation, and substitute. Equivalently, complete the square:

$$w_J r_J^2 + w_T r_T^2 = \left(w_J + w_T\ell\right)(j - j_\star)^2 + c_\ell(\dot{u} + au)^2. \tag{IV.5}$$

All terms are retained and the identity is verified symbolically. ▫

A history obeying the inherited diffusion equation $\dot{u} = -au$ therefore has zero quadratic residual cost. This is compatible with a nonzero transport energy $F_\ell(u) = au^2$. The two quantities need not be equal to describe the same mean relaxation.

At zero frequency, (IV.4) gives the coefficient $c_\ell a^2$, whereas $F_\ell'' = 2a$. The previous static mismatch therefore remains correct, but it does not by itself reject a whole-history interpretation. The remaining questions are normalization, equilibrium identification and selection of c_ℓ.

IV.3. A normalized transition law, not only a squared expression

Use a forward time step $h > 0$ and set $\dot{u} = (u' - u)/h$. For any positive 2×2 residual precision W, including a cross term, define

$$p_h(u', j \mid u) = \frac{\sqrt{\det W}}{2\pi} \exp\left[-\frac{h}{2} r^T W r\right], \qquad r = \left(r_J, r_T\right)^T. \tag{IV.6}$$

This is exactly normalized on $du'\,dj$. A centered residual Gaussian with covariance W^{-1}/h has density $h\sqrt{\det W}/(2\pi)$; the map $(u', j) \mapsto r$ has absolute Jacobian $1/h$. Their product gives (IV.6).

For $W = \mathrm{diag}(w_J, w_T)$, Gaussian integration of j gives

$$\boxed{p_h(u' \mid u) = \sqrt{\frac{c_\ell}{2\pi h}} \exp\left[-\frac{c_\ell}{2h}\{u' - (1 - ah)u\}^2\right].} \tag{IV.7}$$

Minimization and Gaussian integration have the same quadratic exponent here because the eliminated current has a constant positive quadratic block. Their normalization factors are not discarded, and this statement is not extended to nonlinear, field-dependent or constrained auxiliary integrals.

Equation (IV.7) is the Euler transition of the explicitly added diffusion

$$du = -au\,dt + c_\ell^{-1/2} dB_t. \tag{IV.8}$$

It is a valid normalized transition at every positive h, but it does not have the exact continuous semigroup composition law. Its stationary variance exists only for $0 < ah < 2$ and equals $[c_\ell(2a - a^2 h)]^{-1}$.

The continuous diffusion has exact transition

$$u' \mid u \sim \mathcal{N}(e^{-ah}u, C_h), \qquad C_h = \frac{1 - e^{-2ah}}{2ac_\ell}. \tag{IV.9}$$

The code tests the finite joint integral, the marginalized normalization, the Euler-to-continuous limit and the exact semigroup separately. It never calls an Euler step an exact physical update. At fixed a, c_ℓ, the determinant factors in (IV.6)–(IV.9) are path-independent constants; if those coefficients vary with a link background, their contributions must be retained when comparing that background.

No assertion is made that the full VERSF process is Gaussian, that its time is infinitesimal, or that the absolute HMGBC source should be normalized row by row. Equation (IV.6) defines the particular normalized experiment being tested.

IV.4. What the history–energy match actually selects

The known modal drift is the ordinary-real-coordinate gradient of $F_\ell = au^2$ with mobility $1/2$. Require the stationary density of (IV.8) to be the source's stated Gibbs form for that same energy:

$$p_{\mathrm{Gibbs}}(u) \propto e^{-\beta a u^2}, \qquad \mathrm{Var}_{\mathrm{Gibbs}}(u) = \frac{1}{2\beta a}. \tag{IV.10}$$

The positive number β is still a source parameter. Setting it to one in the numerical test is not its physical determination. [P12, §§1–3]

Theorem IV.2: selected endpoint history precision. Within the scalar additive Gaussian class with fixed drift $-au$, matching (IV.10) is equivalent to

$$\boxed{c_\ell = \beta.} \tag{IV.11}$$

Proof. Stationarity of the second moment in (IV.8) requires $2a\mathrm{Var}(u) = c_\ell^{-1}$. Substituting (IV.10) gives (IV.11), and conversely (IV.11) gives exactly that stationary Gaussian. ▫

Thus the observable history precision is no longer independently selectable on different spatial modes once the same drift, Gibbs energy and β have been fixed. This is a conditional selection, not a new determination of β, the physical action unit or the gauge coefficients.

Independent positive constant residual weights require

$$\frac{1}{w_T} + \frac{\ell}{w_J} = \frac{1}{\beta}. \tag{IV.12}$$

They cannot satisfy this on two distinct positive ℓ values. Subtracting the equations would require $1/w_J = 0$, outside the finite positive-weight class. Their finite mismatch is not repaired by a single common multiplier.

A local positive cross-metric does solve the matching:

$$\boxed{W_\ell = \begin{pmatrix} \alpha + \beta\ell & -\beta\sqrt{\ell} \\ -\beta\sqrt{\ell} & \beta \end{pmatrix}, \qquad \alpha > 0.} \tag{IV.13}$$

Indeed $\det W_\ell = \alpha\beta > 0$, and

$$r^T W_\ell r = \alpha r_J^2 + \beta\left(r_T - \sqrt{\ell}\, r_J\right)^2 = \alpha r_J^2 + \beta(\dot{u} + au)^2. \tag{IV.14}$$

The current integrates out and leaves (IV.11) for every mode. The negative cross entry is a correlation in a positive full metric, not a negative action. The free α changes conditional current fluctuations while leaving the endpoint history unchanged. Nothing in this calculation identifies (IV.13) as the primitive full W_{prim}.

IV.5. The complete compatible Gaussian metric family

Work in mass-normalized real endpoint coordinates on a specified stable subspace. Let $\mathsf{D}: \mathbb{R}^n \to \mathbb{R}^m$ have full column rank, $L = \mathsf{D}^T\mathsf{D} > 0$, and absorb the fixed conductances into D. The residuals are

$$r = j - \mathsf{D}u, \qquad s = \dot{u} + \mathsf{D}^T j, \qquad \zeta = s - \mathsf{D}^T r = \dot{u} + Lu. \tag{IV.15}$$

Let $\Sigma_e = W^{-1}$ be the covariance-rate matrix of (r, s). The exact Gaussian marginal has endpoint covariance rate

$$\mathsf{S} = R\Sigma_e R^T, \qquad R = (-\mathsf{D}^T \quad I_n). \tag{IV.16}$$

For drift $-Lu$ and energy $F = u^T L u$, the matching Gibbs covariance is $(2\beta L)^{-1}$. The Lyapunov equation therefore fixes

$$\boxed{RW^{-1}R^T = \beta^{-1} I_n.} \tag{IV.17}$$

This is the operator-valued matching condition on the residual metric. It keeps all current–continuity cross blocks. It is neither $W = I$ nor a statement that the full metric is uniquely selected.

Theorem IV.3: complete Gaussian classification. Put $\mathsf{S} = \beta^{-1} I_n$ and

$$T = \begin{pmatrix} I_m & 0 \\ -\mathsf{D}^T & I_n \end{pmatrix}.$$

Every positive residual covariance satisfying (IV.17), and only those covariances, is

$$\boxed{\Sigma_e = T^{-1} \begin{pmatrix} N + Z\mathsf{S}Z^T & Z\mathsf{S} \\ \mathsf{S}Z^T & \mathsf{S} \end{pmatrix} T^{-T}, \qquad N > 0, \quad Z \in \mathbb{R}^{m\times n}.} \tag{IV.18}$$

Proof. In (r, ζ) coordinates the lower covariance block is fixed to S. Every positive block covariance has conditional mean $\mathbb{E}[r \mid \zeta] = Z\zeta$ and positive conditional covariance N. Its Schur decomposition is exactly the middle matrix in (IV.18). Conversely that decomposition is positive and has the required lower block. The invertible triangular change of coordinates completes the proof. ▫

For $Z = 0$, its precision is the matrix counterpart of (IV.13):

$$W = \begin{pmatrix} N^{-1} + \beta\mathsf{D}\mathsf{D}^T & -\beta\mathsf{D} \\ -\beta\mathsf{D}^T & \beta I_n \end{pmatrix}. \tag{IV.19}$$

Before the stable-subspace restriction, incidence-local D and scalar N give a local graph expression. Gauge covariance of a transported version requires transforming every typed residual and noise frame consistently; the present calculation does not establish the full physical embedding.

IV.6. Conserved mean, hard continuity and the current-cycle freedom

The numerical endpoint test uses the source's weighted wheel:

$$K = I_{12}/31, \qquad M = \text{diag}(7{,}4{,}4{,}4{,}4{,}4{,}4)/31, \qquad \mathsf{D}_{\text{full}} = K^{1/2} D M^{-1/2}. \tag{IV.20}$$

This follows from $u = M^{1/2}\rho$ and $j = K^{-1/2}J$ in the stated mass-weighted source convention. The transformed residuals are $K^{-1/2}D_J$ and $M^{-1/2}D_T^{(M)}$, where $D_T^{(M)} = M\dot{\rho} + D^T J$ is the mass-weighted continuity residual. This is not the unweighted MASD display with its time convention left unchanged. The real transport energy is $u^T Lu$, and the real mobility is $I/2$. [P5, §9K]

The uniform mass-weighted endpoint coordinate is a zero mode of this isolated transport subsystem. For the stationary Gaussian test, its value is fixed and the six orthogonal modes are used. It is not relabelled as gauge or silently discarded from a claimed full physical theory. Without this restriction or an independently confining source, that free endpoint mode has no normalizable Gaussian equilibrium.

On this subspace, $m = 12, n = 6$. Equation (IV.17) fixes 21 independent entries of the endpoint covariance. The unrestricted symmetric residual covariance has 171 entries and retains

$$171 - 21 = 150 = \frac{12 \cdot 13}{2} + 12 \cdot 6 \tag{IV.21}$$

parameters in the N, Z description. These are mathematical family dimensions, not a count of new physical constants. The map onto symmetric endpoint matrices is surjective because $R(0, I_n)^T = I_n$.

IV.6.1. Exact continuity is a different residual model

Imposing $s = 0$ exactly removes continuity noise rather than choosing a finite w_T. If current noise has covariance rate Q_J, then endpoint noise is $\mathsf{D}^T Q_J \mathsf{D}$. Matching the same Gibbs energy requires

$$\boxed{\mathsf{D}^T Q_J \mathsf{D} = \beta^{-1} I_n.} \tag{IV.22}$$

A positive family satisfying it is

$$Q_J = \beta^{-1}\mathsf{D}L^{-2}\mathsf{D}^T + \nu P_{\text{cyc}}, \quad P_{\text{cyc}} = I_m - \mathsf{D}L^{-1}\mathsf{D}^T, \quad \nu > 0. \tag{IV.23}$$

Its longitudinal and cycle subspaces are orthogonal, so it is positive, and multiplication by D^T and D gives (IV.22). The six current-cycle variances remain adjustable. In one mode, hard continuity requires current precision $w_J(\ell) = \beta\ell$, not a constant w_J.

The projection enforces the stated mean conservation in this mathematical process. It is not a derivation that the endpoint amplitude is VERSF's conserved bit capacity. Moreover, a representation-valued current cycle is not automatically a gauge-link curvature coordinate. No gauge weight is read from the arbitrary ν.

IV.7. Recovering the endpoint action from whole histories

With the matched coefficient, the scalar history expression is $\beta \int (\dot{u} + au)^2 dt/2$. The exact transition variance after duration T is

$$C_T = \frac{1 - e^{-2aT}}{2\beta a}.$$

Starting from $u(0) = 0$, the endpoint-dependent negative log density is

$$\boxed{I_T(U) = \frac{U^2}{2C_T} = \frac{\beta a U^2}{1 - e^{-2aT}}.} \tag{IV.24}$$

Its long-duration limit is exactly $\beta F_\ell(U)$. The normalization constant in the endpoint density is independent of U for this fixed harmonic operator. It is not independent of arbitrary changes of the operator.

The minimum quadratic history with these fixed endpoints is

$$u_\star(t) = U\frac{\sinh(at)}{\sinh(aT)}, \qquad 0 \le t \le T. \tag{IV.25}$$

Substituting into the integral yields exactly (IV.24). The same answer follows by eliminating every intermediate coordinate of the Gaussian chain. Thus the boundary contraction is explicit, not an identification of the static energy with the zero-frequency path kernel.

For any smooth test path, reversing its time order gives the boundary relation

$$\mathcal{A}[u] - \mathcal{A}[u^{\mathrm{rev}}] = \beta a\{u(T)^2 - u(0)^2\} = \beta \Delta F_\ell. \tag{IV.26}$$

This follows by expanding the two squares. The exact continuous transition kernel also obeys the corresponding detailed-balance ratio at finite time. The Euler discretization approximates this relation; it is not asserted exact at finite step.

IV.7.1. What this resolves

The static penalty evaluated at $\dot{u} = 0$ is $\beta a^2 u^2/2$. The long-history endpoint action is $\beta a u^2$. They differ because one holds an entire path constant while the other sums over, or contracts, the allowed histories ending at a prescribed point. This explains the restricted mismatch in RCHS-35D without changing its algebra.

It does not prove that MASD's physical gauge action is the boundary action of this Gaussian process. That further identification must say which history boundary, measure and observable define the physical action, and must retain the other coupled fields. A raw transfer pressure, normalized path likelihood, boundary rate and instantaneous free energy remain distinct until such a bridge is established. [A3, §2; P3]

IV.8. The same bridge on a complete coupled harmonic action

Let x now contain all variables of a *specified* positive harmonic system, with $F(x) = x^T Hx/2$, $H > 0$, symmetric mobility $\Lambda > 0$, and matching noise covariance $2\Lambda/\beta$. No assumption that H and Λ commute is needed. The quadratic history expression is

$$\mathcal{A}[x] = \frac{\beta}{4}\int (\dot{x} + \Lambda Hx)^T \Lambda^{-1} (\dot{x} + \Lambda Hx)\, dt. \tag{IV.27}$$

Completing the square with the reversed drift gives

$$\mathcal{A}[x] = \beta\{F(x_T) - F(x_0)\} + \frac{\beta}{4}\int (\dot{x} - \Lambda Hx)^T \Lambda^{-1} (\dot{x} - \Lambda Hx)\, dt. \tag{IV.28}$$

For the infinite-past trajectory approaching the stable origin, reversed relaxation realizes the lower bound. The boundary action is βF. Equivalently, the stationary covariance is $(\beta H)^{-1}$ by the inherited Lyapunov relation. These are exact harmonic identities; no claim is made that all full VERSF histories are of this form.

For a retained physical coordinate $f = E^T x$, the stationary marginal is Gaussian with covariance $\beta^{-1} E^T H^{-1} E$. Its quadratic action is

$$I_{\mathrm{ret}}(f) = \frac{\beta}{2} f^T K_f f, \qquad \boxed{K_f = (E^T H^{-1} E)^{-1}.} \tag{IV.29}$$

On a direct split $x = (f, \eta)$, this is the usual Schur complement $H_{ff} - H_{f\eta} H_{\eta\eta}^{-1} H_{\eta f}$. All auxiliary cross blocks are included in H. Gaussian integration and constrained minimization have the same quadratic part here; they are not equated for a nonlinear fluctuating action with field-dependent determinants.

The Fourier history kernel, by contrast, has

$$\mathcal{K}(0) = \frac{\beta}{2} H\Lambda H, \qquad \int_{-\infty}^{\infty} \frac{d\omega}{2\pi}\, \mathcal{K}(\omega)^{-1} = (\beta H)^{-1}. \tag{IV.30}$$

Reading $\mathcal{K}(0)$ itself as the static action Hessian would make a kinetic coefficient look like a force strength. The numerical endpoint test verifies the integral separately. Equation (IV.29) agrees with the calibrated static response in RCHS-35C under its stated common-action and work conventions. It does not supply an unknown H by naming that response. [A2, §§4–5]

For a physical VERSF application, all same-order coupled current, link, record, completion, support, unresolved and matter effects must enter the same admitted action or its justified response. Their selection is not implied by the small harmonic example.

IV.9. Does the matched endpoint history select a changing-link law?

No such selection follows merely from the normalization just established. Suppose a prescribed link history is $U_0, \ldots, U_{N-1}$, and each conditional endpoint/current step is a normalized kernel $p_k(x_{k+1}, j_k \mid x_k, U_k)$. For a fixed initial endpoint, free integration of every later endpoint and current gives

$$\boxed{\int \prod_{k=0}^{N-1} p_k\,(x_{k+1}, j_k \mid x_k, U_k) \prod_{k=0}^{N-1} d\,x_{k+1}\,dj_k = 1.} \tag{IV.31}$$

Proof. Integrate the last normalized step first, and repeat backwards. The identity holds for arbitrary prescribed schedules, not only constant links. A normalized initial distribution can also be integrated without changing the result. ▫

Thus a normalized conditional endpoint process does not by itself assign relative prior weights to the link schedules. Equation (IV.31) does not say that endpoint observations cannot distinguish them: their transition means, covariances and measured-path likelihoods can differ. It also does not apply unchanged to fixed final endpoints, loop traces, unnormalized transfers or constraints on intermediate histories.

For those different experiments, an induced link-dependent functional can remain. One must derive why that boundary condition or raw weight belongs to the physical source, rather than select whichever functional produces the desired gauge response. Missing determinant or Jacobian factors cannot be omitted to manufacture a loop cost. The primary code verifies free-terminal normalization on two different changing-coefficient schedules while retaining different final means and variances.

IV.9.1. How a pure-link source would enter

Given a separately supplied link process and a configuration cost $V(U)$, a raw history weighting could contain

$$\exp\left[-\lambda \int_0^T V\,(U_t)dt\right]. \tag{IV.32}$$

Such a weighting modifies the joint history ensemble; after conditioning or normalization it generally changes the driven dynamics. The Feynman–Kac/Doob distinction is standard. [M1] It is not an invisible change to a *known complete* configuration law.

Here the complete link law and λ are not known. Normalizing only the endpoint conditional factors cannot determine them. This extends the fixed-link conditional warning to prescribed changing-link histories without proving that the full VERSF source admits every possible V or λ.

The history match has therefore selected the endpoint projection (IV.17), not the independent curvature-restoring dynamics. That is the exact point where its constructive result stops.

IV.10. Testing capacity balance and the one-bit condition explicitly

BTAC-1 represents BCB by a fixed total capacity and zero-sum changes, and uses a one-bit branch condition $\dot{\Sigma} = \ln 2$ at its declared clock. Its reported bath-adjacency alternatives were not selected uniquely. [P13, §§2, 4] We do not discard those principles. We test what their explicit budget and entropy constraints determine in a small rate family, adding the stronger requirement of equal mean jump activity.

This family is a mathematical countercheck, not the physical gauge carrier. Its seven states represent one conserved capacity token occupying a hub or one of six rim sites. Every jump preserves the sum of those seven capacity entries. The amplitude coordinates of the earlier Gaussian calculation are not identified with this token budget.

Let $\lambda > 0$ be a declared rim-versus-hub configuration price and $A > 0$ an oriented rim affinity. Use the canonical wheel's off-diagonal rate bases, with one common scale γ:

$$\begin{aligned} r_{hb_i} &= \frac{\gamma}{7} e^{-\lambda/2}, & r_{b_i h} &= \frac{\gamma}{4} e^{\lambda/2}, \\ r_{b_i b_{i+1}} &= \frac{\gamma}{4} e^{A/2}, & r_{b_i b_{i-1}} &= \frac{\gamma}{4} e^{-A/2}. \end{aligned} \tag{IV.33}$$

The diagonal generator entries are minus the outgoing rates. This is continuous time, not a claim that the canonical discrete refinement step has been derived or preserved.

With $Z = 7 + 24e^{-\lambda}$, stationarity is exact:

$$\pi_h = \frac{7}{Z}, \qquad \pi_{b_i} = \frac{4e^{-\lambda}}{Z}. \tag{IV.34}$$

Hub–rim flows balance; the rim circulation is uniform. The mean jump activity and stationary entropy-production rate are

$$J = \gamma \frac{12\left(e^{-\lambda/2} + e^{-\lambda}\cosh(A/2)\right)}{Z}, \qquad \dot{\Sigma} = \gamma \frac{12e^{-\lambda}A\sinh(A/2)}{Z}. \tag{IV.35}$$

Requiring $J = 1$ and $\dot{\Sigma} = \ln 2$ fixes A and γ *given* λ:

$$\boxed{\frac{A\sinh(A/2)}{e^{\lambda/2} + \cosh(A/2)} = \ln 2, \qquad \gamma = \frac{Z}{12\left(e^{-\lambda/2} + e^{-\lambda}\cosh(A/2)\right)}.} \tag{IV.36}$$

For every $\lambda > 0$, the left side of the first equation is strictly increasing from zero to infinity. Its derivative numerator is positive: with $d = e^{\lambda/2}$, it is $d\sinh(A/2) + (Ad/2)\cosh(A/2) + \sinh(A/2)\cosh(A/2) + A/2$. Hence each price admits a unique drive and rate scale satisfying both constraints.

The relative configuration price remains free in this family. This is not a proof that all those laws satisfy every BCB/TPB or VERSF axiom. Additional source relations, operational capacities, spatial embeddings and irreversible-record semantics may reject or select them. It shows that the stated conservation, entropy and activity conditions alone do not do so.

Source-scope qualification. PFRA-1 already computes a conditional one-bit affinity, and the interface papers impose an additional bit-commitment normalization on their declared Wilson action. These are retained in §VII.5. The price family in this section tests only its specified conservation, activity and entropy constraints; its admissibility under those additional source principles has not been established. [P19–P20]

IV.11 Numerical identification and selection tests

Grade N. Independent current integration and a separate residual least-squares calculation reproduce the matched history quadratic form. Normalization, stationary kernels, half-step composition and reversal are checked on the declared harmonic model. Euler covariance errors decrease at first order in the time step.

Technical Supplement S4.4 retains the transport spectrum (IV.37), the modal comparison table, conditional-current fixtures and every reported tolerance. Its β = 1 and residual widths are verification choices. The analytic matching conditions remain in IV.1–IV.10.

IV.12. Whole-history contraction and the remaining price family

For $a = 31/28$, $\beta = 1$, horizon $T = 2$ and endpoint $U = 0.7$, the exact boundary action (IV.24) is

$$I_T(U) = 0.5490510145534239. \tag{IV.38}$$

The complete Euler history is minimized over all intermediate endpoints. These are time discretizations of the declared mathematical test, not physical space and emergent time regulators.

Time intervals	Minimized Euler history cost	Relative endpoint-variance error
16	0.509294713596	0.0780615
32	0.529106449160	0.0376948
64	0.539061922668	0.0185305
128	0.544052242264	0.0091880

The finite-history Schur result agrees with the closed discrete controllability variance at every level. A separate least-squares elimination of the 32-step path agrees to 4.11×10^{-15} absolute discrepancy. Sampling the exact continuous kernel instead gives the same exact endpoint variance for every listed partition. Direct integration along (IV.25) agrees with the boundary result to ordinary floating-point accuracy.

The six-dimensional history spectrum is integrated independently over frequency. Its equal-time covariance agrees with $(2\beta L)^{-1}$ to relative discrepancy 8.83×10^{-17}. The quadrature routine's internal error estimate is recorded separately; this agreement is not an interval-certified error bound.

IV.12.1. Conserved-capacity and equal-activity entropy test

Inserted price λ	Solved affinity A	Solved rate scale γ	Hub stationary mass
0.2	1.754060529259	1.078499475834	0.262668717957
0.7	1.864165164953	1.100095481572	0.370017047337
1.4	2.048795410223	1.217393379961	0.541865825742

Every row conserves its one-token capacity, has mean jump activity one and entropy production $\ln 2$ to the reported numerical accuracy. The stationary ratios still reconstruct their distinct inserted prices as $-\log[7\pi_b/(4\pi_h)]$. Exact symbolic stationarity and the entropy-rate expression are verified separately.

These are not three predicted VERSF force strengths. They show why imposing one entropy number and an average update number does not, in this stated family, select the relative state cost. They also do not rerun BTAC-1's representation-resolved bath calculation or identify its alternative adjacencies.

IV.13 The inherited Gaussian proposal and its exact response

The continuous-amplitude Gaussian construction is already present in the prior corpus. RSMPC §64.4.1B–H specifies its geometry, minimum-norm defect lift, likelihood normalization and core information metric; the standalone proposal theorem records the same formulas. PSAC §§10H–K consumes this construction and proves its Gaussian bath result. These sources supplement the conditional endpoint model in §§IV.1–IV.12; their probability family is not selected anew here. [P28–P30]

At a frozen defect-zero vacuum, let J_D be the complete defect differential and Q_{kin} span the physical tangent quotient. With G_{op} the inherited operational metric, define

$$J_p = J_D Q_{\text{kin}}, \qquad G_p = Q_{\text{kin}}^{\dagger} G_{\text{op}} Q_{\text{kin}}. \qquad \text{(IV.39)}$$

The minimum-operational-norm lift and continuous-amplitude proposal are

$$E_D = Q_{\text{kin}} G_p^{-1} J_p^{\dagger} \big(J_p G_p^{-1} J_p^{\dagger}\big)^{+}, \qquad \text{(IV.40)}$$

$$\xi \mid (X, D) \sim \mathcal{N}\big(a_t E_D D,\, a_t G_{\text{op}}^{-1}\big), \qquad X' = \operatorname{Exp}_X^{\text{op}} \xi. \qquad \text{(IV.41)}$$

The inverse metric in (IV.41) acts on the admitted tangent quotient. For this declared Gaussian amplitude law, with its metric and lift frozen, the exact likelihood ratio is

$$\log \frac{dQ_D}{dQ_0} = \langle E_D D, \xi \rangle_{G_{\text{op}}} - \frac{a_t}{2} \parallel E_D D \parallel_{G_{\text{op}}}^2. \qquad \text{(IV.42)}$$

Consequently, its KL divergence per time step and its core Fisher metric are

$$\frac{D_{\text{KL}}(Q_D \| Q_0)}{a_t} = \frac{1}{2} D^{\dagger} W_{\text{core}} D, \qquad W_{\text{core}} = E_D^{\dagger} G_{\text{op}} E_D. \qquad \text{(IV.43)}$$

The linear score and quadratic normalization are fixed together. An independently chosen amplitude width or defect-dependent normalizer would change this source law. On the evaluated finite cell, the source reports a 243-dimensional defect metric of rank 183 and a minimum-norm right-inverse residual of 6.86×10^{-15}. The 187-dimensional physical tangent also contains defect-silent directions; a defect-image calculation does not erase them. These are prior finite-carrier returns. [P28, §64.4.1; P29]

RSMPC's full statement calls (IV.41) the declared quadratic-order form, in a rank-stable normal chart, of the global operational heat-kernel proposal. Its likelihood calculation is at the frozen linearized vacuum. Thus the Gaussian formulas are exact for the specified amplitude construction; the source does not thereby identify every complete nonlinear configuration history with a Gaussian distribution on one affine space. Nonlinear defects and the exponential link map do not refute conditional Gaussian amplitudes. In particular, the later roughness-operator calculation in §VII.12 does not establish a change of G_{op}. This corrects an overbroad implication in the intermediate applicability discussion. [A27, §§11–12; P28, §64.4.1C–H]

On the positive unresolved-bath quotient, the prior exact Ornstein–Uhlenbeck transition is

$$q' \mid q \sim \mathcal{N}\big(e^{-a_t A_Q} q, A_Q^{+}[I - e^{-2a_t A_Q}]\big). \qquad \text{(IV.44)}$$

For a centered Gaussian bath bilinearly coupled to defects, completion of the square gives

$$W_{\mathrm{prim}} = W_{\mathrm{core}} - C^{\dagger} A_Q^{+} C, \quad \mathrm{ran} C \subseteq \mathrm{ran} A_Q, \quad W_{\mathrm{prim}} \succcurlyeq 0. \qquad \text{(IV.45)}$$

PSAC Theorem 1C additionally proves that a resolved orientation-odd linear source survives this elimination unchanged. Its three premises remain explicit: a centered Gaussian bath, bilinear coupling and the stated source placement. Its scalar closure normalization does not automatically fix all faithful weak-sector norms. Later RSMPC §67 derives the canonical K7 bath spectrum and $C = 0$ on the separable branch; §67.3's correction and §71.2 withhold physical promotion of the whitened identity response. This supplies the bath calculation on that branch without selecting a physical electroweak boundary. [P28; P30, §§10H–O]

IV.14 Complete Gaussian history contraction with coupled auxiliaries

The continuation in [A27, §10] establishes a sufficient long-history Fisher–Schur identity without requiring a factorizing Perron function. Work at a fixed spatial regulator and fixed nonzero physical mode. Let $z = (x, q)$ denote retained and hidden real coordinates and use the symmetric Gaussian transfer

$$T(z, z') = \exp\left[-1/2\, z^{\mathsf{T}} D z - 1/2\, z'^{\mathsf{T}} D z' + z^{\mathsf{T}} E z'\right], \quad E \succ 0, \quad D - E \succ 0. \qquad \text{(IV.46)}$$

Here D and E are trajectory-kernel matrices, distinct from the defect vector in §IV.13. They may fail to commute and may couple x to q. The positive Perron function is Gaussian, with matrix $R = D - E(D + R)^{-1}E$. Its stationary Doob process has transition matrix $A = (D + R)^{-1}E$ and innovation covariance $\Sigma = (D + R)^{-1}$. The bulk trajectory precision is $\mathcal{H}(\omega) = 2D - 2E\cos\omega$. Eliminating every hidden sample, including its temporal memory, gives

$$Z = \mathcal{H}_{xx}(0) - \mathcal{H}_{xq}(0)\mathcal{H}_{qq}(0)^{-1}\mathcal{H}_{qx}(0) = S_x(0)^{-1}, \qquad \text{(IV.47)}$$

where $S_x(0)$ is the retained covariance summed over all integer time lags. The last identity follows independently from $S_z(0) = (I - A)^{-1}\Sigma(I - A^{\mathsf{T}})^{-1}$ and the Perron equation. It is an identity of trajectory precision and covariance, not an identification of $-\log T$ with a configuration-potential Hessian.

For a constant retained mean displacement m with covariance unchanged, the Fisher matrix of N observations is

$$I_{m,N} = (\mathbf{1}_N \otimes I)^{\mathsf{T}} Q_{x,N} (\mathbf{1}_N \otimes I), \qquad \lim_{N\to\infty} \left(\frac{I_{m,N}}{N}\right) = Z. \qquad \text{(IV.48)}$$

Here $Q_{x,N}$ is the exact marginal path precision. A periodic constant mode gives NZ directly. Opening the history and introducing stationary Perron weights changes only its endpoint blocks. The uniform positive gap confines the change of the hidden minimizer to bounded boundary layers, so the total quadratic correction is $O(1)$ and the rate correction is $O(1/N)$. Nonzero retained–hidden Perron blocks are allowed. This proves the stated rate identity without asserting equality of one-step marginalized kernels.

The physical source coordinate matters. If the parameter is instead a conjugate force h, entering by $h^{\mathsf{T}} \sum_t x_t$, its information rate is

$$\lim_{N\to\infty} \left(\frac{I_{h,N}}{N}\right) = S_x(0) = Z^{-1}, \qquad \frac{\partial m}{\partial h} = Z^{-1}. \qquad \text{(IV.49)}$$

The existing physical field-to-law map must determine which contraction applies. An arbitrary normalized tilt or terminal-record Fisher matrix cannot be substituted for that map. The four-coordinate nonfactorizing verification fixture in [A27] gives agreement between the full-path and covariance routes to 3.7×10^{-15} and exhibits the predicted finite-history boundary correction. Its matrices carry no physical weak/Y normalization. The long-history limit does not license an uncontrolled spatial infrared or regulator limit. This supplies a sufficient case of the HMGBC bridge, not universal closure of its physical source conditions. [P3, §16 and §56A]

IV.15 The prior quadratic innovation theorem

Complete-history Gaussianity and statistical independence of total event counts are stronger than the local quadratic score calculation requires. SMC-1U, SGPL-1 Gate 2, Theorem 12, already proves the relevant innovation statement. For primitive mark counts N_e with predictable intensities λ_e, set $M_e = N_e - \int \lambda_e \, dt$. One mark per primitive Fold gives orthogonal compensated innovations. With the complete shared state retained, the score rate is

$$W_{ab} = \lim_{T\to\infty}\left[\frac{1}{T}\mathbb{E}\int_0^T \sum_e s_{ae}\, s_{be}\lambda_e\, dt\right]. \qquad \text{(IV.50)}$$

Correlated histories and unequal accepted rates remain admissible. The theorem expressly distinguishes this quadratic result from an all-orders product law. Gate 4 constructs the measure-valued Doob/Kraus kernel and retains the physical evaluation of its complete carrier. Thus this manuscript consumes an existing quadratic source theorem; it does not require a new proof of global Gaussianity before using the stationary response theorem in Parts II–III. The actual physical mark derivatives, accepted intensities and action identification still belong to the source calculation. [P31, SGPL-1 Gates 2–4]

IV.16 Testing the Gaussian proposal as autonomous evolution

The inherited proposal in §IV.13 prescribes a displacement for a supplied defect increment. A later test asks whether replacing that increment by the instantaneous defect itself generates autonomous evolution. On the frozen linear chart, let J be the defect differential, G the positive operational metric and E_D the minimum-norm right lift on the supported defect range. Then

$$P = E_D J, \qquad P^2 = P, \qquad \dot{m} = \pm\alpha P m. \qquad \text{(IV.51)}$$

The positive substitution amplifies every realizable defect. Reversing its sign yields only the rates zero and α; it leaves unconstrained kernel coordinates without a restoring drift. If a fixed surjective readout R recovered an endpoint flow $\dot{u} = -Lu$, it would require $LR = \alpha RP$ and hence $L^2 = \alpha L$. The six positive endpoint rates already retained in (IV.37) do not satisfy that identity for one common α. The original Gaussian proposal remains valid on its stated terms. This test excludes the two particular feedback identifications as complete evolution on that branch. Additional physical drift or memory was not excluded. [A29, §21; calculation C36]

The check uses the inherited reduced 226-coordinate and 243-residual archive, whose supported response rank is 183. Idempotence holds to 3.63×10^{-14}, and a separate singular-value construction reproduces the lift to 3.86×10^{-15} relative error. The rates are source-parameter rates, not physical seconds or gauge strengths. No new covariance, force normalization or fitted clock is selected.

IV.17 Coupled histories with the continuity derivative restored

A separate construction retains the entire 187-coordinate kinematic quotient of that archive and inserts the time derivative only where the original continuity defect requires it. Let J denote its static defect map, T_ρ the insertion of density velocities, W the inherited candidate residual metric and V its additional quadratic potential. The declared harmonic history action is

$$\mathcal{A}[x] = \frac{1}{2}\int \left[(Jx + T_\rho\dot{x})^T W(Jx + T_\rho\dot{x}) + x^T V x\right] d\sigma. \qquad \text{(IV.52)}$$

Define $H = J^T W J + V$, $M = T_\rho^T W T_\rho$ and $F = J^T W T_\rho$. Although T_ρ has rank 39, the priced velocity form M has rank 36. The three additional unpriced directions remain algebraic variables; they are not removed as gauge. With U spanning the support of M and N its kernel, write $x = Uy + Nz$. The identity $FN = 0$ allows the algebraic square to be completed. Setting $H_{zz} = N^T H N$, $H_{zy} = N^T H U$ and $F_z = N^T F U$ gives

$$\widehat{M} = U^T M U - F_z^T H_{zz}^{-1} F_z, \qquad \text{(IV.53)}$$

$$\widehat{F} = U^T F U - H_{zy}^T H_{zz}^{-1} F_z, \qquad \widehat{H} = U^T H U - H_{zy}^T H_{zz}^{-1} H_{zy}. \qquad \text{(IV.54)}$$

The archived $\widehat{M}$ and $\widehat{H}$ are positive, and $\widehat{F}$ is symmetric to 2.31×10^{-15}. The resulting causal representation has 36 evolving coordinates and 151 algebraic coordinates:

$$dy = -L_y y\, d\sigma + \widehat{M}^{-1/2} dB_\sigma, \qquad L_y = \widehat{M}^{-1/2}\Omega\widehat{M}^{1/2}, \qquad \text{(IV.55)}$$

$$\Omega = \left(\widehat{M}^{-1/2}\widehat{H}\widehat{M}^{-1/2}\right)^{1/2}, \qquad z = -H_{zz}^{-1}H_{zy}y - H_{zz}^{-1}F_z\dot{y} + \eta. \qquad \text{(IV.56)}$$

Here η is algebraic white noise with covariance $H_{zz}^{-1}\delta(\sigma - \sigma')$. It is a generalized process rather than a pointwise smooth auxiliary field. Boundary terms and finite-step normalization are retained in the source derivation. An independent stabilizing Riccati solve reproduces L_y to 1.62×10^{-13}; reconstructed full frequency covariance agrees with direct inversion to 2.76×10^{-15} relative error. These checks validate the stated Gaussian model, whose metric remains a candidate. [A29, §22; C37]

For the three previously retained transverse gauge directions, let E be their fixed embedding and define

$$Z = (E^T H^{-1} E)^{-1}, \qquad R = H^{-1} E Z. \qquad \text{(IV.57)}$$

The archive satisfies $MR = FR = F^T R = 0$ to numerical precision, with $T_\rho R = 0$ as well. Since $HR = EZ$ and $E^T R = I$, the complete frequency precision $\mathcal{D}(\omega) = H + \omega^2 M + i\omega(F - F^T)$ obeys

$$[E^T \mathcal{D}(\omega)^{-1} E]^{-1} = Z. \qquad \text{(IV.58)}$$

Thus restoring this continuity derivative does not change the candidate's retained transverse response at any invertible frequency. Its previously archived diagonal remains ($0.773030349411, 0.769270248459, 0.789448515937$). This is a finite-model result, not zero physical gauge dynamics. HMGBC already supplies direct operational evolution through its full kinetic operator; that sector was omitted from (IV.52) by construction. A physical temporal completion must attach that existing operator and any Wilson temporal structure consistently, without counting the same contribution twice. [P3, §§56A.1–56A.3; A29, §§22.6–22.7]

Part V: Refinement geometry and the F19 source gate

V.1. Role of the refinement gate

The physical GNC-EX3/4 calculation requires a source-derived nonfactorising reduced Hessian, not a benchmark metric. MASD and HMGBC relocate the missing source weighting to an operational history construction in which refinement must preserve the relevant generator. Earlier formulations bundled this into a requirement that the actual coarse maps be sufficiently regular. RCHS-36F [A5] separates the gauge-link and completion maps rather than assuming that one scalar refinement rule applies to both. The calculation uses no Standard Model coupling, weak angle or electromagnetic target.

V.2. Binary ordered holonomy

Let G be the compact link group with an inherited bi-invariant, equivalently Ad-invariant, inner product on its Lie algebra. For binary refinement the coarse link is the ordered product

$$m(g_1,g_2) = g_1 g_2. \quad \text{(V.1)}$$

Using left-trivialised tangent coordinates $\delta g_1 = g_1 X_1$ and $\delta g_2 = g_2 X_2$, with $h = g_1 g_2$, the coarse tangent is

$$h^{-1}\delta h = \mathrm{Ad}_{(g_2^{-1})} X_1 + X_2. \quad \text{(V.2)}$$

Write $Q = \mathrm{Ad}_{(g_2^{-1})}$. Ad-invariance makes Q orthogonal, so the differential is $A = [Q, I]$ and

$$A A^\dagger = 2 I. \quad \text{(V.3)}$$

The minimum-norm fine lift of a coarse tangent Y is $A^\dagger(AA^\dagger)^{-1}Y = (\tfrac{1}{2}Q^\dagger Y, \tfrac{1}{2}Y)$, with squared fine norm $\tfrac{1}{2}\|Y\|^2$. Therefore the target metric is not a freely selectable blocking coefficient:

$$g_{\mathrm{link},n} = \tfrac{1}{2}\, g_{\mathrm{link},n+1}. \quad \text{(V.4)}$$

For an ordered product of k fine links the same calculation gives $g_{\mathrm{link,coarse}} = (1/k) g_{\mathrm{link,fine}}$. This fixes relative refinement scaling only; it does not determine the absolute metric normalisation at one reference level.

V.3. Minimal fibres and basic Haar measure

For fixed coarse holonomy h the fibre is $F_h = \{(g, g^{-1}h) : g \in G\}$, the graph of inversion followed by right translation. Both are isometries for a bi-invariant metric. The fibre is therefore an isometric image of the diagonal in G×G, hence totally geodesic and minimal. The mean-curvature drift that would spoil the older submersion argument is absent on this link block.

Haar invariance also gives $dg_1\, dg_2 = dg_1\, dh$ after the change of variables $h = g_1 g_2$. The fibre measure is independent of h and the pushforward of product Haar is Haar on the coarse link. Thus the ordered-holonomy block satisfies the minimal-fibre and basic-measure conditions exactly at the stated metric grade.

V.4. Exact link Laplacian intertwining

A constant metric rescaling $g \to cg$ gives $\Delta_{(cg)}=c^{-1}\Delta_g$. For a basic function $f\circ m$ on the fine product, the two fine link Laplacians add:

$$\Delta_{(G\times G)}(f\circ m) = 2\,(\Delta_g f)\circ m. \quad \text{(V.5)}$$

Since the forced coarse metric is $g/2$, $\Delta_{(g/2)}=2\Delta_g$. Hence

$$\Delta_{(G\times G)}(f\circ m) = (\Delta_{(g/2)} f)\circ m. \quad \text{(V.6)}$$

This is the scalar operational generator intertwining required on the ordered-holonomy link block. HMGBC independently obtains a raw multiplicity-two relation on its persistent H^1 refinement carrier before multiplicity normalisation. The matching factor is a structural consistency check only; the two carriers are not identified. [P3, §§23–25]

V.5. Karcher midpoint at the diagonal

The completion coarse map is qualitatively different. Let $q(x,y)$ be the binary Karcher midpoint on a smooth geodesically convex completion chart. At a coincident pair $x=y=p$,

$$dq_{(p,p)}(X,Y) = \tfrac{1}{2}(X+Y). \quad \text{(V.7)}$$

The minimum-norm fine lift of a coarse tangent Z is (Z,Z), whose squared norm is $2\|Z\|^2$. The diagonal target metric forced by the midpoint is therefore

$$g_{comp,n} = 2\, g_{comp,n+1}. \quad \text{(V.8)}$$

Link multiplication and completion averaging consequently renormalise in opposite directions:

$$g_{link,n} = \tfrac{1}{2}\, g_{link,n+1}, \quad g_{comp,n} = 2\, g_{comp,n+1}. \quad \text{(V.9)}$$

A single universal scalar blocking factor therefore cannot make both maps Riemannian submersions if their fine sector metrics share one common normalisation.

V.6. Curved-midpoint obstruction away from the diagonal

The diagonal result is not the whole completion problem. In a constant negative-curvature chart of sectional curvature $-\kappa^2$, place the fine completion states at $\gamma(-r)$ and $\gamma(r)$. A symmetric transverse Jacobi field with equal endpoint value a obeys $J''-\kappa^2 J=0$, so

$$J(t) = a \cosh(\kappa t) / \cosh(\kappa r). \quad \text{(V.10)}$$

To obtain a fixed midpoint variation Z one needs $a=Z\cosh(\kappa r)$. The minimum symmetric fine norm is therefore

$$\|X\|^2 + \|Y\|^2 = 2 \cosh^2(\kappa r)\, \|Z\|^2. \quad \text{(V.11)}$$

The induced quotient metric depends on the fine representative r inside the same midpoint fibre. In positive constant curvature, before the first conjugate point, the local factor is $2\cos^2(\kappa r)$, again representative dependent. Therefore, if the actual VERSF completion chart contains a retained direction of nonzero sectional curvature, the binary Karcher midpoint cannot generically be a fixed-metric Riemannian submersion away from the diagonal. This is a geometric counterexample, not a claim that the physical completion chart is curved. A flat commuting chart would evade the obstruction.

V.7. Numerical verifier and claim grade

RCHS-36F checks the ordered-holonomy differential on 100 random orthogonal adjoint-frame witnesses. The maximum relative residual in $AA^\dagger=2I$ is 3.59×10^{-16}, the maximum horizontal-lift image residual is 2.16×10^{-16}, and the maximum lift-norm scaling residual is 4.13×10^{-16}. The Karcher diagonal lift returns a norm ratio 2.0000000000000004. These are implementation checks of the exact formulas, not physical-regulator evidence.

The honest grade is therefore: ordered-holonomy refinement regularity: DERIVED conditional on the inherited bi-invariant link metric; relative binary link scaling: DERIVED; Karcher diagonal scaling: DERIVED; curved fixed-metric obstruction: DERIVED as a general geometric counterexample, with physical application conditional on the actual completion curvature; absolute operational metric, physical bath operator/coupling, W_prim, G_red and gauge couplings: OPEN.

V.8. Consequence for F19 and GNC-EX3/4

F19 should no longer be treated as one undifferentiated refinement-regularity premise. The gauge/link portion can be inserted into the physical history calculation as an analytic theorem at its stated metric grade. The completion portion should instead be tested through HMGBC's blockwise HP3 commuting-square identities unless the selected completion chart is independently proved flat on the retained branch. The genuine two-regulator requirement remains: two interacting regulator complexes must independently return the physical operational metric, bath operator A_Q, defect-bath coupling C, W_prim and reduced Hessian. Profile enlargement or tensor-factorised duplication is not physical refinement evidence. [P3; P4]

W_prim = W_core − C† A_Q⁺ C. (V.12)

The next load-bearing execution is therefore not another gauge benchmark. It is the completion/bath HP3 and common-history-operator return needed to evaluate A_Q and C on the physical branch. Only after that return can GNC-EX3/4 construct the nonfactorising G_red and pass it to the already-closed gauge evaluator.

Part VI. Native record laws and identifiable curvature response

VI.1. The post-freeze gauge comparison and its limits

RCHS-36G–I [A6–A8] test whether two previously calculated regulator responses can already support the proposed gauge identification. On the frozen six-premise HCMR six-level branch, the reported values give $Z_3/Z_2 = 6.780509044617$ and $g_s/g = 0.384033269920$. Within the specified full-content Standard Model one-loop comparison, the positive-domain ultraviolet floor is $\sqrt{19/42} = 0.672592709135$. A common normalization cannot repair this ratio. This excludes that frozen branch within that comparison class; it does not exclude every threshold theory or every VERSF continuation. The numbers are a post-freeze comparison of rounded source returns, not newly derived physical couplings.

The separate factor-blind irreversible lift has colour and weak multipliers 0.773030 and 0.769270. Their ratio, 1.004887750725, moves the comparison in the wrong direction. Repetition with positive powers cannot reverse that direction. However, the lift and the HCMR return were generated from different objects. Their multiplication is a declared comparison model, not an established common-action composition. In that model only, holding the weak multiplier at 0.769270 requires the colour multiplier to be at most 0.250791137916 to enter the stated compatibility band. The corresponding 74.92% screen and 52.22-percentage-point increment are conditional bounds, not universal physical requirements on D41.

RCHS-36I [A8] distinguishes covariance from a fixed-background commutant condition. Covariance means

$$D(g \cdot z) = U_g D(z) U_g^{\dagger}. \qquad \text{(VI.1)}$$

It does not imply that $D(z)$ commutes with every U_g at a non-invariant background. A commutant restriction applies to an invariant operator or background, or to the appropriate stabilizer. The native current-dependent instrument is a covariant, generally noncentral family. This correction is essential to the positive response calculations below.

VI.2. Native current response, strength and observation capacity

RCHS-36J [A9] differentiates the published current residual, including its induced change in the instrument. For an oriented link, the background endpoint vectors define

$$j_{xy} = \psi_y - U_{xy}\psi_x, \qquad \rho_{xy} = \frac{j_{xy} j_{xy}^{\dagger}}{j_{xy}^{\dagger} j_{xy}}. \qquad \text{(VI.2)}$$

The twelve Hermitian generators define $K_a = i[T_a, \rho]$ and $S = \sum_a K_a^2$. The admissible strength family is

$$\eta = \frac{t}{\lambda_{\max}(S)}, \quad C_0 = \sqrt{I - \eta S}, \quad C_a = \sqrt{\eta}\, K_a, \quad \sum_{a=0}^{12} C_a^{\dagger} C_a = I. \qquad \text{(VI.3)}$$

No desired score matrix or coupling is inserted. On the two declared random endpoint witnesses, both the seven-role terminal readout and the current-resolved readout have curvature rank 72 at every tested strength

$t = 0.05, 0.20, 0.50, 0.80, 0.95$. These are finite numerical witnesses, not an all-background or all-strength theorem. The selected physical strength remains open.

For twelve separately resolved edges and n terminal labels, normalization gives the exact capacity bound $\mathrm{rank} J_{\mathrm{terminal}} \leq 12(n-1)$. Removing the neutral role changes the full source carrier from dimension 50 to 47 and reduces the observed terminal rank from 72 to 60. Retaining the current label restores rank 72 on that six-role carrier. Thus terminal-only capacity does not establish that a neutral particle is compulsory; it constrains a specific observation architecture.

Strength controls information size as well as rank. Under the stated regular-support assumptions, the weak-strength expansions are $F_{\mathrm{mark}}(t) = tF_1 + O(t^2)$ and $F_{\mathrm{terminal}}(t) = t^2 F_2 + O(t^3)$. At fixed observation protocol, discarding the current label loses the conditional score covariance and cannot increase Fisher information. These statements concern the J experiment. They do not order the two distinct sequential measurement protocols in VI.4.

VI.3. What the free-endpoint tests ruled out

RCHS-36K [A10] profiles the 693 real tangent coordinates of seven normalized complex 50-dimensional endpoint vectors. Across its four witness settings the single-step terminal curvature score is entirely confounded by those endpoint variations. The marked response retains rank 72, but only about 0.015–0.040% of its direct information trace. Profiling nuisance parameters is not integration over a specified physical prior and is not elimination of a physical bath from a common action.

RCHS-36L [A11] sharpens this obstruction. Endpoint rotations $\delta\psi_v = i\phi_v^a T_a \psi_v$ preserve the local sector populations, including the finer neutral-vector plus twelve-sector decomposition. Yet their nuisance score spans the entire 72-dimensional terminal curvature score on the tested backgrounds. The residual is zero at the original score scale. Finite nonflat link changes can consequently be hidden by endpoint orientation changes while preserving both terminal probabilities and those local populations. Fixed-link endpoint rotations are not being mistaken for gauge transformations of the complete configuration.

The obstruction is local to that experiment and nuisance family. Population records alone do not fix relative orientation, but this does not prove that every ordered history is uninformative. Nor does it require a deterministic pre-event ray: a uniquely specified stochastic conditional law would suffice. The revised HCMR-P1 source explicitly permits that route. The next calculation therefore retains state updates and record order.

VI.4. Exact prepared-input averaging and ordered predictions

RCHS-36M [A12] returns to the archived PFDMI-EX2F endpoint chirps, generators, history probabilities and projectors. Its background is not either random J–L witness. The seven-vertex wheel has twelve undirected edges and 31 directed history transitions: seven self steps and 24 nonself traversals. Resolving thirteen current outcomes on a nonself traversal gives 319 full marks on a 350-dimensional history–internal carrier.

Two different variables must be kept distinct. The background vectors $X = (\psi_v)_v$ define the instrument through (VI.2). The separately prepared input state is averaged exactly. The primary preparation is the Fubini–Study mean on the 49-dimensional innovation space orthogonal to the neutral vector Ω:

$$R_{0,49} = \frac{I - |\Omega\rangle\langle\Omega|}{49}, \qquad \varrho_0 = \sum_x \pi_x \, |x\rangle\langle x| \otimes R_{0,49}. \tag{VI.4}$$

The full-carrier check uses $R_{0,50} = I/50$. Initial preparation in the innovation subspace does not impose a projection back to that subspace after each event: evolution takes place on the full 50-dimensional internal carrier. Combining the archived history distribution with this preparation at each address is a declared conditional assembly, not a derivation of the unique primitive joint law.

Use (VI.3) at the archived saturated strength $t = 1$, with the archived hypercharge generator Y. For traversal $h: x \to y$,

$$M_{h,a} = \sqrt{p_h} |y\rangle\langle x| \otimes C_{xy,a} U_{xy}. \tag{VI.5}$$

Self steps have identity internal transport; reverse traversals use $U_{yx} = U_{xy}^\dagger$ and $j_{yx} = -U_{xy}^\dagger j_{xy}$. The finite-field continuation is assembled from the native edge formula. At identity links it reproduces the archived frozen effects to maximum error 1.94×10^{-14}. This continuation is an explicit construction, not an assertion that the archived frozen matrix file already contained a finite-field family.

For an ordered record $\rho = (e_1, \ldots, e_n)$, write $M_\rho = M_{e_n} \cdots M_{e_1}$. Then

$$Z_\rho = \mathrm{tr}\big(M_\rho \varrho_0 M_\rho^\dagger\big), \qquad \sigma_\rho = \frac{M_\rho \varrho_0 M_\rho^\dagger}{Z_\rho}. \tag{VI.6}$$

$$P(e \mid \rho, \theta, X) = \frac{Z_{\rho e}}{Z_\rho} = \mathrm{tr}\big(M_e \sigma_\rho M_e^\dagger\big). \tag{VI.7}$$

The prepared-state integral is exact by linearity in its density matrix; it is not Monte Carlo sampling. The current state after the record, including the ordered updates, determines the next prediction. Multiplying probabilities evaluated on an unchanged initial vector would give a different law.

The terminal experiment sums over the current outcome and projects onto one of seven terminal blocks of dimensions (3,3,6,2,9,9,18) after each step:

$$\mathcal{T}_{h,r}(R) = p_h P_r \sum_a C_{h,a}\, U_h R U_h^\dagger C_{h,a}^\dagger P_r. \tag{VI.8}$$

Composition of these completely positive maps gives the ordered terminal probabilities. These seven projectors are distinct from the twelve innovation-sector projectors used in L. Because intermediate terminal projection changes the state, this protocol is not merely classical deletion of labels from the fully marked protocol. No Fisher ordering between those two experiments is inferred.

Current marks, traversals, terminal observations and completed Facts are also distinct. The archived first closed-cover completion clock has minimum seven updates and mean 21.277682950918 in its specified model. The two-step calculation below is not a two-Fact experiment. Whether completed physical records retain these ordered microscopic observations remains a source question.

VI.5. Predictions and curvature information actually returned

All 15,841 compatible full two-mark histories were evaluated. The terminal calculation has 7,105 ordered rows, of which 1,302 are structural zeros from sector changes on a final self step. Structural zeros are excluded from the regular score calculation; no artificial probability floor supplies their information. With $\mathcal{A} = \mathrm{diag}(p)^{-1/2} J_{\mathrm{raw}} Q$ and the archived orthonormal 144×72 curvature injection Q, the direct Fisher matrix is $F = \mathcal{A}^\top \mathcal{A}$.

Prepared-input mean and protocol	Numerical rank	Smallest Fisher eigenvalue	Fisher trace
Innovation mean, one full mark	72	1.88122×10^{-8}	4.34818×10^{-4}
Innovation mean, two full marks	72	7.64899×10^{-7}	1.57921×10^{-3}
Innovation mean, two terminal observations	72	1.22374×10^{-10}	2.44376×10^{-3}

The one-terminal innovation-mean matrix is numerically full rank but has condition number approximately 6.06×10^{12}; it is not used as the robust positive result. For the full-carrier mean, the single-terminal response vanishes exactly by unitality, while the two-record response survives. Record order and state update therefore supply information absent from that single-event mean.

The prediction is concrete. In the archived example of two hypercharge-current marks, first $6 \to 1$ and then $1 \to 2$, the joint probability is $9.19152706914 \times 10^{-6}$. Conditioning on this record changes the probability of the next no-current mark $2 \to 3$ from 0.50135572325 to 0.43298596657. The total-variation distance between the complete unconditioned and conditioned next-mark distributions is 0.13758171129. These are conditional model predictions in the archived convention, not observed frequencies or fitted force strengths.

To test the L obstruction, let D be the vertex incidence map and use the weighted endpoint-orientation nuisance score $N_g = -\mathrm{diag}(p)^{-1/2} J_{\mathrm{raw}} (D \otimes I_{12})$. Gauge covariance supplies this Ward relation; the prepared means and terminal projectors are invariant under the corresponding representation. With the Moore–Penrose inverse, define

$$\mathcal{R} = \left(I - N_g N_g^{+}\right)\mathcal{A}, \qquad F_{\text{eff}} = \mathcal{R}^{\top}\mathcal{R}. \tag{VI.9}$$

The nuisance rank is 72, with twelve global rotation null directions. Profiling is performed after the exact prepared-input average. Rank is assessed at relative threshold 10^{-8} against the original direct-score scale, not against an arbitrarily rescaled residual.

Two-terminal experiment	Residual curvature rank	Retained direct trace	Smallest residual singular value
Innovation mean $R_{0,49}$	72	10.36298%	3.98778×10^{-6}
Full-carrier mean $R_{0,50}$	72	10.34951%	1.87946×10^{-6}
Innovation mean, both traversals nonself	72	10.45047%	3.73042×10^{-6}

The nonself restriction has 4,410 positive outcomes and selection probability 0.657540632861685, independent of curvature in the declared history law. The positive result does not depend on reading a terminal sector during an idle step. It establishes local statistical identifiability of all 72 tested curvature directions against the stated orientation nuisance at this background. It is not a certified rank theorem for all backgrounds, a profile over all 693 endpoint degrees of freedom, or a physical gauge-action Hessian.

Numerical checks support the returned law: probability sums differ from unity by at most 2.3×10^{-16}; terminal marginal consistency has maximum error 3.47×10^{-17}; two-step finite-difference derivative errors are below 2.01×10^{-8}; and the independent orientation Ward check is below 9.45×10^{-10}. Exact averaging was separately checked against an orthonormal 49-state preparation basis. These are archived execution checks, not new executions performed by this manuscript integration.

VI.6. What has been restored, and what the full law still requires

The combined result changes the frontier. The single-step population-preserving orientation obstruction does not survive the specified ordered two-terminal experiment: the residual has all 72 curvature directions. A deterministic selected input ray is unnecessary for this calculation. The exact prepared-input mean, native state update and retained order already produce an identifiable conditional response.

This does not contradict fixed-independent-current hypercharge invisibility results. Here the current changes with the link through (VI.2), and only the stated nuisance family is profiled. Nor does M supersede every earlier endpoint calculation: RCHS-25 supplies a conditional completion clock, RCHS-26 supplies a conditional stationary-traffic generator, and RCHS-27 supplies quadratic moments. Those returns do not by themselves specify the full nonlinear joint marked-background law.

If a longer observed record retains this same prefix, marginalizing its added outcomes recovers the prefix law. The Fisher chain rule then preserves the prefix information, including efficient information when the same nuisance family is used throughout. This argument does not apply automatically to a completed Fact that discards the prefix, to a different measurement protocol, or to an enlarged nuisance model.

The fully background-averaged physical prediction would instead require

$$P(\rho \mid \theta) = \int \operatorname{tr}\left[M_\rho(\theta, X)\varrho_0(\theta, X)M_\rho(\theta, X)^{\dagger}\right]\mu_\theta(dX). \tag{VI.10}$$

The source must specify the background law μ_θ, its correlations with preparation and history, and the physical retained-record map. Averaging a separately prepared state to I/d does not integrate background variables that also define the operators. Likewise, statistical nuisance profiling cannot substitute for this integral. HCMR-P1 supplies the ordered conditional-posterior rule for a specified frozen instrument and prior; component-count reductions alone are not the full ordered law.

Finally, M uses archived Y and an edge order of six rim edges followed by six spokes. J–L use $q = 6Y$ and the opposite edge grouping. Their rank statements can be compared at their declared grades, but their raw traces and coefficients cannot be combined as a common physical response. To obtain physical gauge coefficients still requires source selection of the complete interacting law, calibrated same-action response or action identification, the coupled bath/completion reduction, operational units and regulator matching. For predictions averaged over those backgrounds, the joint background-and-record law is still required. Sections VI.7–VI.10 and Part VII add the later endpoint, completion and direct-action results and give the updated physical handoff.

Continuation note. The endpoint extension proposed above is now executed in N–O, and the completion-record question is tested in P–S. The direct current-action route remains authoritative for physical force-strength calculation. The sections that follow replace the earlier generic handoff to another occurrence or endpoint-rank test.

VI.7 Ordered continuation with the full normalized endpoint family

RCHS-36N and O extend the experiment of M without changing its archived carrier, preparation, generator convention or curvature injection. They allow 99 real normalized endpoint coordinates at each of seven vertices, shared across incident edges, giving 693 nuisance coordinates. This includes the orientation family used in §VI.5. The endpoint score has numerical rank 537 in both experiments. "Full endpoints" means this specified normalized family, not every possible physical-background uncertainty. [A14–A15]

For record length L, let A_L and N_L be the probability-weighted curvature and endpoint derivative matrices. The efficient information is obtained by profiling the same endpoint displacement across the entire record:

$$F_L = A_L^{\top}(I - N_L N_L^{+})A_L. \qquad \text{(VI.11)}$$

Quantity	Two retained observations N	Three retained observations O
Endpoint nuisance coordinates	693	693
Surviving curvature rank	72	72
Efficient Fisher trace	$5.48800968 \times 10^{-10}$	$2.51617925 \times 10^{-5}$
Smallest efficient Fisher eigenvalue	$2.92276189 \times 10^{-15}$	$6.48895998 \times 10^{-10}$
Own fixed-endpoint trace retained	0.0000224572%	0.455900%

The third observation increases the efficient trace by about 45,848.7 and the smallest eigenvalue by about 222,014.7. The stronger coordinate-invariant comparison solves $F_3 v = \gamma F_2 v$ and gives $5816.8393 \leq \gamma \leq 551012.0769$. Every tested curvature direction therefore gains information. These comparisons are per prepared record of the stated length, not equal-duration measurements or independent overlapping windows.

The prefix marginal reproduces N's probability vector to 2.08×10^{-17} maximum error and its joint derivatives to 3.38×10^{-15} relative error. O's independently rebuilt dense maps and finite differences also resolve its strongest and weakest efficient directions. The reported ranks are stable over the archived nuisance thresholds, referenced to the original curvature score. They are numerical local witness results, not interval-certified global identifiability theorems.

The same-prefix argument in §VI.6 becomes quantitative here. Conditional scores have zero conditional mean, so the joint information increases when the third observation is retained. Minimizing over the same endpoint nuisance displacement preserves $F_3 \succcurlyeq F_2$. That inequality predicts monotonicity; the executed calculation supplies the size of the gain. This supersedes the suggestion that the next unresolved observational test is merely to enlarge M's nuisance family to these normalized endpoints.

VI.8 What survives at a genuine completion

RCHS-36P and Q test the earliest closed-cover completion stratum of the existing wheel process. Completion requires return to the start after visiting all seven addresses. The 84 rooted directed seven-step covers have total probability $p_7 = 0.0066940605981213$, or about 0.669406% of starts. Instrument updates inside such a cover are not individually relabelled as completed Facts. [A16–A17]

Filed content conditional on seven-step completion	Residual curvature rank
Whole address path and final terminal outcome	0
Whole address path and terminal outcomes at updates six and seven	72
Last directed edge and those two ordered terminal outcomes	72

Filed content conditional on seven-step completion	Residual curvature rank
Starting address and those two terminal outcomes	0
Those two terminal outcomes alone	0

P's final-outcome result requires resolving weak nuisance directions. A loose nuisance cutoff misleadingly returns rank 72; the resolved rank-504 nuisance space fills the within-path probability tangent, and a normalization-reduced fit reproduces the curvature derivative to relative error 4.88×10^{-12}. Q then retains one additional internal terminal outcome and recovers rank 72, even after discarding the path except for its last directed edge. The last-edge/pair readout has efficient trace 4.901524×10^{-10} and retains only 0.0000168582% of its fixed-endpoint trace. The positive rank is accompanied by a weak information strength.

The completion calculation is a sufficient-record witness, not a derivation of the physical filing rule or a proof of the globally smallest record. If the complete stopped record retains the flag distinguishing seven-step completion, retains Q's sufficient record on that stratum, and uses the same parameter and nuisance family, its efficient information obeys

$$F_{\text{stopped,eff}} \succcurlyeq p_7 F_{7,\text{eff}}. \qquad \text{(VI.12)}$$

This follows by splitting the squared score norm into flagged strata before minimizing over the common nuisance displacement. Q's witness gives a trace lower bound $3.28111007 \times 10^{-12}$ and a smallest-eigenvalue lower bound $1.03434462 \times 10^{-17}$. Later completion lengths were not evaluated by that calculation, and the inequality does not establish that the physical record retains the flag and terminal pair.

VI.9 Binary Facts and carried continuation state

RCHS-36R shows that weaker filing arguments do not establish Q's record. A last-edge label with a same/different terminal flag has zero efficient curvature response in the tested maps. Keeping both sector identities but forgetting their order greatly reduces the response. Two complete histories with the same address path and final sector can leave different carried states and next-record distributions; the archived example has total-variation separation 0.1921501. Record capacity, retained labels and the carried conditional state must therefore be distinguished. [A18]

RCHS-36S consumes the prior one-bit completion and renewal maps. Its rank-three theorem adds the assumptions that only two fixed reopened states influence the next completion, the same history-independent cycle acts each time, and no parameter-dependent timing or additional contexts are observed. Then every word likelihood depends on the initial-bit probability and two transition probabilities. At regular interior points its Fisher rank is at most three, or at most two conditional on the first bit. This restriction follows from that two-state fixed-cycle closure, not from one bit per Fact. [A19]

The reconciled source reading retains the already developed coarse-record conditional state, commitment-memory field and conditional occurrence/type response. A history-dependent binary sequence can carry many independent parameter responses without adding a primitive bit. The factorized native occurrence zero and passive endpoint-projection tests retain their stated scopes; they do not exclude those wider source constructions. [A19–A20]

VI.10 Relation to the force-strength programme

The current-rigidity successor already supplies a positive relaxed current action on its declared source family and explicitly prefers direct continuum action attachment in §14 Branch D and §40. Reconstructing 72 curvature coordinates from a bare binary sequence is not a universal prerequisite for that action route. The published factorized occurrence law can be current-independent while the conditional record identity, phase and source-action response remain nonzero. [P18; A20]

Parts VI.7–VI.9 settle additional observational questions and identify source-sensitive filing requirements. The physical strength question proceeds from the existing current action, its faithful metric and normalized continuum embedding. Part VII integrates that calculation and the prior coupling constraints. This preserves the positive ordered-record results without converting Fisher information into an energy Hessian by definition.

VI.11 Evolving internal state and the joint current response

A later calculation uses the native PFDMI current instrument with the archived endpoint fields, Fold history kernel and common unit-face field mode. It evaluates the complete opportunity channel, including the no-jump current operator and all terminal outcomes:

$$\mathcal{E}_{e,A}(X) = \sum_{r,\alpha} P_r\, C_{e,\alpha}(A) U_e(A) X U_e(A)^\dagger C_{e,\alpha}(A)^\dagger P_r. \qquad \text{(VI.13)}$$

The thirteen current alternatives include the source's positivity-saturating complement. The current itself varies with the link through $j_e = \psi_t - U_e\psi_s$. The derivative therefore includes the current ray, the maximal allowed instrument amplitude and the constant-rank square root of the complement. Holding these quantities fixed while varying the field would differentiate a different source. [A29, §17; C32]

Each edge channel has 49 fixed operators at the archived zero-link witness, but their stationary-flow-weighted average has only the identity as a fixed operator. Its smallest positive fixed-space gap is $2.23834611545 \times 10^{-6}$. Together with the connected Fold carrier and the channel contraction bound, this identifies the joint stationary instrument density as $\sigma_x = \pi_x I_{50}/50$. The gap is a dimensionless certificate for this operator; it is not a physical decay rate. The density describes the evolving internal state conditional on the supplied instrument, and does not select the endpoint-field ensemble or its phases.

One stationary terminal marginal is $d_r/50$ and has zero field derivative. Two consecutive terminal observations, retaining the second edge, have

$$p_e(r,s) = \frac{1}{50}\sum_{\alpha} \| P_s C_{e,\alpha} P_r \|_{\mathrm{HS}}^2. \qquad \text{(VI.14)}$$

For the fixed endpoint witness and the common (W_3, Y) mode, the resulting Fisher matrix is

$$F_{W_3,Y} = 10^{-6}\begin{pmatrix} 0.543365578664 & 3.048673921064 \\ 3.048673921064 & 35.936005460391 \end{pmatrix}. \qquad \text{(VI.15)}$$

Its eigenvalues are $2.82677079189 \times 10^{-7}$ and $3.61966939599 \times 10^{-5}$. Sequential Kraus evaluation agrees with the block formula to 6.9×10^{-16}, and an independent directional relative-entropy Hessian agrees to 7.1×10^{-13} relative error. This is a two-observation response with endpoint phases and the other two weak directions held fixed. It is not an asymptotic information rate, two committed Facts, an energetic metric or evidence for physical neutral kinetic mixing. Its readout and source family also differ from those in §§VI.7–VI.8.

VI.12 Endpoint phases and their dynamical compatibility

The next calculation allows the 350 component phases of the seven endpoint fields to vary while preserving every component magnitude. The current remains $j_e = \psi_t - U_e\psi_s$. For the specified pair statistic, write its phase and four-field score matrices as B_s and S_f. The shared-endpoint phase matrix has rank 252 and spans all independent symmetric fixed-marginal pair probabilities in this readout. Profiling gives

$$S_{\mathrm{eff}} = (I - B_s B_s^+) S_f \simeq 0. \qquad \text{(VI.16)}$$

The remaining relative score norms are below 3.5×10^{-14} at the retained rank threshold. Explicit phase compensators and an independent finite-field check confirm first-order cancellation; the compensated finite relative entropy scales quartically with the field step. These are statistical source ambiguities, not pure-gauge field changes or proof of zero action cost. The endpoint phases have not been shown freely variable in the full physical action. [A29, §18; C33]

Continuity supplies a stronger test. On the stated current and continuity zero-defect shell, $\partial_\sigma \psi = -\mathrm{div}_U j$. A phase history $\delta\psi = i\psi b$ has velocity variation $i\dot{\psi} b + i\psi\dot{b}$. Both terms and the direct link derivative of the divergence must be retained. Eliminating the arbitrary real phase rates leaves a radial compatibility equation $H_b b + G_f a = 0$, in addition to $B_s b + S_f a = 0$. The combined system has rank 328, and an archived left-null certificate excludes simultaneous cancellation for every nonzero tested four-field direction. A finite check confirms that a pair-score-preserving phase change requires a first-order change in component-magnitude velocity. This is a conditional obstruction on that shell, not the complete action's evolution or an energetic lower bound. [A29, §19; C34]

The inherited scalar potential prices seven endpoint norms,

$$\Gamma_V = \sum_v \frac{\mathrm{vol}_v \lambda_{\mathrm{sub}}}{4} (\| \psi_v \|^2 - \rho_c^2)^2. \qquad \text{(VI.17)}$$

It does not price all 350 component magnitudes independently. A further calculation finds phase compensators that hide all four field scores while preserving first-order velocities of all seven endpoint norms, and even all 49 central-sector norms. Their instantaneous norm preservation is exact. Consequently the component-history obstruction cannot be multiplied by this potential coefficient to manufacture a physical stiffness. The complete source can still price transport, record, current, completion or finite-history changes. This narrower conclusion preserves the earlier obstruction at its actual scope. [A29, §20; C35]

Together these results identify the physical task more precisely: the complete source must select or price the joint endpoint, current and field directions. A positive fixed-background Fisher matrix, a statistical compensator and an unweighted radial residual are three different response objects. None alone is the full energetic gauge metric.

Part VII Current response and electroweak normalization

VII.1 Exact response of the inherited current and link mode

RCHS-36T applies the current-link reciprocity theorem to one real member of the existing nonuniform cycle doublet. Let p be its retained current coordinate, h the conjugate-helicity current partner, θ the matched link coordinate and y the relaxable record phase. We use h here to avoid confusing the partner with the primitive charge generator $q = 6Y$. The variable y is not the stored bit of a committed Fact. [A21; P18, §§39A–39G]

On the declared positive diagonal source-metric family,

$$\Gamma^{(2)} = \frac{w_J}{2}\left(p - \frac{\kappa\theta}{\sqrt{2}}\right)^2 + \frac{w_J}{2}\left(h + \frac{\kappa\theta}{\sqrt{2}}\right)^2 + 2w_C\theta^2 + \frac{w_B}{2}(\theta - y)^2 + 2w_R y^2. \qquad \text{(VII.1)}$$

All four weights are positive. Introduce conjugate sources by subtracting $f_p p + f_\theta \theta$ and relax h, y. The resulting link coefficient and two-coordinate response are

$$K_\theta = 4w_C + \frac{4w_B w_R}{4w_R + w_B}, \qquad \chi_{p\theta} = \begin{pmatrix} w_J^{-1} + \kappa^2/(2K_\theta) & \kappa/\left(\sqrt{2}K_\theta\right) \\ \kappa/\left(\sqrt{2}K_\theta\right) & K_\theta^{-1} \end{pmatrix}. \qquad \text{(VII.2)}$$

Thus the relaxed current stiffness is $K_J = w_J K_\theta / \left(K_\theta + \kappa^2 w_J/2\right)$. At the inherited unit-weight benchmark with $\kappa = 1$, $K_\theta = 24/5$, $K_J = 48/53$ and $\chi_{pp} = 53/48$. These are exact evaluations of the prior family, not newly source-selected physical numbers. Direct stationary equations and a separately assembled Hessian verify the response to floating-point precision. The full physical source need not preserve this scalar diagonal family.

If $P = a_p p$, $\Theta = a_\theta \theta$ and the physical functional is $S = S_* \Gamma$, conjugate sources must refer to that same functional. The physical response then scales as

$$\chi_{PP}^{\mathrm{phys}} = \frac{a_p^2}{S_*}\left(w_J^{-1} + \frac{\kappa^2}{2K_\theta}\right), \qquad \chi_{\Theta P}^{\mathrm{phys}} = \frac{a_p a_\theta}{S_*}\frac{\kappa}{\sqrt{2}K_\theta}. \qquad \text{(VII.3)}$$

Here S_* converts units; it is not permission to add a new free physical normalization after the source and continuum conventions have been fixed. An action-conjugate source is not automatically a mechanical force or an electric current in amperes.

VII.2 Electromagnetic charge and face flux

The later electromagnetic calculation constructs the photon charge direction directly in the archived carrier. With the neutral lower Higgs component and the archive's conventional hypercharge generator,

$$Q_{\mathrm{em}} = T_3 + Y = T_3 + q/6, \qquad \mathrm{Tr}Q_{\mathrm{em}}^2 = 17, \qquad \mathrm{Tr}(T_3 Y) = 0. \qquad \text{(VII.4)}$$

The lower Higgs component is annihilated by this generator. This checks the charge direction in the inherited representation; it does not newly derive electroweak symmetry breaking. Specifying the charge-normalized photon direction does not require selecting a weak mixing angle. Separating canonically normalized weak and hypercharge fields does require their kinetic coefficients. [A26]

Let C be the oriented six-face boundary map with six rim edges followed by six spokes. For the selected normalized cosine face mode $s_k = \cos(2\pi k/3)/\sqrt{3}$, $CC^\top s = 4s$. The gradient-orthogonal edge lift is $a = C^\top s\,\phi/4$. Writing $t = C^\top s/2$ gives

$$a = t\theta, \qquad \phi = 2\theta, \qquad \phi = \frac{e\Phi}{\hbar}. \qquad \text{(VII.5)}$$

The face-to-link factor is therefore fixed for this mode. The flux amplitude Φ is not a magnetic field in tesla unless physical face areas are additionally supplied. Geometric residuals in the native calculation are at most 1.3×10^{-15}.

VII.3 Calibrated link strength and its limits

In the declared effective Wilson convention, the quadratic Euclidean action is $S_E^{(2)}/\hbar = (\beta_{\mathrm{EM}}/2)\sum_k f_k^2$. Using measured low-energy electromagnetic alpha as a calibration gives

$$\beta_{\mathrm{EM}} = \frac{1}{4\pi\alpha} \simeq 10.9049783253, \qquad K_\phi = \beta_{\mathrm{EM}}, \qquad K_\theta = 4\beta_{\mathrm{EM}} \simeq 43.6199133013. \qquad \text{(VII.6)}$$

These are dimensionless action coefficients at the stated effective scale, not an independent derivation of alpha or a primitive high-energy boundary value. The numerical input is the CODATA value documented in the electromagnetic archive; no new experimental fit is performed here. [A26; M7] Sections VII.19–VII.23 show why this calibration cannot be replaced merely by the scalar K7 admission probability: the latter is a structural admission weight and, on the saturated closure-projection branch, its support trace is field-rigid rather than the physical gauge stiffness.

If this electromagnetic mode is represented by the same reduced scalar parent as §VII.1, its link contribution to current compliance is now calibrated:

$$\chi_{pp} = w_J^{-1} + \frac{\pi\alpha}{2}\kappa^2, \qquad \chi_{\theta\theta} = \pi\alpha, \qquad \chi_{\theta p} = \frac{\pi\alpha}{\sqrt{2}}\kappa. \qquad \text{(VII.7)}$$

The numerical coefficients are $0.0114626546033\kappa^2$ for the additional current compliance, 0.0229253092067 for link self-compliance and 0.0162106416008κ for the mixed compliance. Total physical current response still uses the source's w_J, κ and conjugate-unit conversion. Fixed light speed constrains propagation and dimensional conversion; it does not by itself supply the internal weak–hypercharge contrast. The rigidity and electromagnetic route in *Void Tensile Strength* is retained at its stated grade; its Appendix H.4 does not provide that microscopic coupling calculation. [P25]

Calibrating a relaxed coefficient must not count its record relaxation twice. Within the same four-variable family, the difference between holding the record phase fixed and relaxing it is

$$K_\theta^{\text{phase fixed}} - K_\theta^{\text{relaxed}} = \frac{w_B^2}{4w_R + w_B}. \qquad \text{(VII.8)}$$

Equation (VII.6) fixes one relaxed combination of weights, not this separate difference. Holding y fixed is also not automatically the physical operation effected by retaining a Fact.

VII.4 A numerical next-record prediction for physical flux

The electromagnetic projection uses M's archived endpoints, initial density $(I - |\Omega\rangle\langle\Omega|)/49$, stationary history mixture, saturated instrument and finite-field continuation. The selected cosine mode has the following Fisher coefficients with respect to the face phase ϕ. [A26]

Retained observation	Information per phase squared
One terminal observation	$5.649535594 \times 10^{-9}$
Two ordered terminal observations	$4.279619328 \times 10^{-5}$
Two observations after the tested endpoint gauge rotations are profiled	$9.642709812 \times 10^{-6}$

This electromagnetic subspace has rank six before and after that orientation profiling. The selected mode retains 22.5317% of its unprofiled information. These results use M's orientation nuisance, not the larger N–O endpoint family; those retention fractions must not be interchanged. In physical flux units the profiled coefficient is $2.225704801 \times 10^{25}$ Wb^{-2} per stated two-update record. It is information, not energy stiffness or an event rate.

For the predetermined prefix consisting of history $1 \to 2$ and the right charged-lepton terminal sector, the probability that the next history is $2 \to 0$ with that same sector is

$$P_{\text{next}}(\phi) = 0.1884852035475 - 0.0003264551352\,\phi + O(\phi^2). \qquad \text{(VII.9)}$$

At $\phi = 0.01$, equivalent to flux amplitude $6.582119570 \times 10^{-18}$ Wb, direct finite-field evaluation gives $P_{\text{next}} = 0.1884819428842$, a change of $-3.260663355 \times 10^{-6}$. The linear remainder is 3.89×10^{-9}. Independent finite-field differences verify the conditional derivative to relative error below 6.6×10^{-9}. This is a concrete prediction of the specified native conditional instrument under its electromagnetic identification; no laboratory observation or fully background-marginalized physical law is claimed.

VII.5 Prior normalization and coupling results carried forward

The broader source comparison requires several earlier results to be retained explicitly. They constrain different objects and cannot be replaced by a blanket statement that normalization has never been calculated. [A28]

First, PFRA-1 already uses the conditional one-bit entropy result to solve the irreversible-affinity equation

$$\frac{24a\sinh a}{7 + 6(2 + 2\cosh a)} = \ln 2, \qquad a = 0.959001109719975. \qquad \text{(VII.10)}$$

The affinity a is not the fine-structure constant. Its clock convention, entropy premises and physical unit conversion are retained. PFRA-1 also computes the no-fit precursor $(g_s, g, g') \simeq (0.804242, 0.632439, 0.347331)$; it explicitly leaves the score magnitude whitened and factor-blind and does not certify the physical Standard Model boundary. These are prior quantitative results. [P19, §§2–5]

Second, the interface bit-commitment normalization BCN is

$$\beta\left[1 - \cos\left(2\pi/N_\phi\right)\right] = \ln 2. \qquad \text{(VII.11)}$$

At fixed phase resolution and the stated interface action, this condition determines beta. It remains a conditional calibration: the reviewed minimal-commitment argument imposes its reliability conversion and does not independently derive the minimum it selects; XII.12 records the correction. Its attachment to a complete physical source must also be established. The interface-structure paper prints the purported unique phase-resolution value as a placeholder and retains an enumeration/scale qualification; it supplies no unstated integer here. [P20, §§3–5; P24, §§2–3; A46, §8]

Third, GNC-EX2A fixes the source generator convention and the Wilson continuum map, giving $\beta = 1/g^2$ and $c_{\text{norm}} = 1$. A factorwise generator rescaling or additional continuum multiplier is therefore unavailable on that route. The physical source response between those fixed conventions remains the object to calculate. [P21, §§6–8]

Two prior weak-angle constructions must be compared with their own premises:

Construction	Conditional result	Assumptions controlling the result
Hexagonal Geometry Appendix H	$\sin^2\theta_W = 3/13$	Active-mode isotropy H9; weak/complement assignment of dimensions 3 and 10; susceptibility-to-coupling rule
RRHF neutral-extended relaxation ledger	$\sin^2\theta_W = 45/194$	Direct traces $(6, 13/2, 378)$; score relaxations $(5, 4, 80)$; primitive charge $q = 6Y$

Appendix H and the numerical gauge-closure papers state both conditional routes. Their numerical proximity cannot establish a common physical carrier, response metric or matching scale. The later current-rigidity analysis further states that different faithful wheel modes generally have different current stiffnesses in the common separable family; equality of primitive mark gains does not alone prove equality of physical gauge stiffnesses. [P18, F7–F10; P22–P23]

VII.6 Source response shape and the electroweak contrast

The current-factor geometry supplies a conditional response test independent of the overall scalar scale. Use the inherited positive matrix

$$H = \frac{1}{49}\begin{pmatrix} 36 & 18 & 36 \\ 18 & 26 & 26 \\ 36 & 26 & 47 \end{pmatrix}, \qquad M = \ell H - rr^{\top}. \qquad \text{(VII.12)}$$

Here the single-portal form is a branch assumption inherited from the hazard/clock/current chain. In the reference-normalized coordinates, $B = H^{-1/2} M H^{-1/2} = \ell I - uu^{\top}$, so its ordered generalized eigenvalues obey $b_2 = b_3 = \ell$. Conversely, this equality for a positive semidefinite response with $\ell > 0$ reconstructs the single-portal form. If finer marks yield a compatible positive effective refinement term, $B = \ell I + R - uu^{\top}$ with $R \succcurlyeq 0$, the upper two eigenvalues satisfy $b_2, b_3 \geq \ell$. For $b_2 > 0$ the minimum trace of such an effective refinement term is

$$\operatorname{mintr} R = b_3 - b_2. \qquad \text{(VII.13)}$$

The minimum is over the displayed algebraic decompositions with $\ell > 0$. It is achieved at $\ell = b_2$, $u = \sqrt{b_2 - b_1}\, e_1$ and $R = (b_3 - b_2) e_3 e_3^{\top}$. This is a diagnostic for a source-returned matrix in the same chart; it does not identify the current-factor matrix with the photon kinetic matrix or assert a primitive realization of every decomposition. [A25; P26–P27]

The electroweak calculation isolates a different contrast. On the restricted RRHF parent family, $D_A = (6, 13/2, 378)$ and $Z_A = D_A - r_A$. The positive deformation

$$r_3 = 5, \quad r_2 = 4 - \delta, \quad r_q = 80 + 36\delta, \qquad -20/9 < \delta < 4 \qquad \text{(VII.14)}$$

preserves the photon sum while changing the split:

$$Z_2 + Z_Y = \frac{97}{9}, \qquad Z_Y = Z_q/36, \qquad \sin^2\theta_W = \frac{45 + 18\delta}{194}. \qquad \text{(VII.15)}$$

The native representation calculation verifies positivity, gauge covariance and the photon-null variation. It does not verify compatibility of every member with BCN, Appendix H, the unique full source, or all later admissibility principles. Therefore this family is not a corpus-wide theorem of free physical couplings. Nor does electromagnetic calibration authorize an otherwise forbidden continuum rescaling. [A27–A28]

For the full source parent and normalized retained embeddings, the quantity to derive is

$$G_{\text{red}} = D - C^{\dagger} B^{+} C, \qquad Z_2 = 1/3\, \operatorname{Tr}\big(E_2^{\dagger} G_{\text{red}} E_2\big), \qquad Z_Y = E_Y^{\dagger} G_{\text{red}} E_Y. \qquad \text{(VII.16)}$$

The retained-to-auxiliary coupling must lie in the supported range of the auxiliary block. Here B denotes that auxiliary Hessian, not the normalized comparison matrix used earlier in this section. Defining $\Sigma = Z_2 + Z_Y$ and $\Delta = Z_2 - Z_Y$ gives

$$\sin^2\theta_W = \frac{1}{2}\left(1 + \frac{\Delta}{\Sigma}\right). \qquad \text{(VII.17)}$$

The source must establish whether the Appendix H assumptions, the RRHF ledger, or a different response is returned. A fixed photon coefficient and fixed characteristic speed do not by themselves calculate this internal contrast. Physical matching uses a common declared scale, followed by the applicable radiative and threshold treatment.

VII.7 Amplitude moments and the feedback compatibility result

RCHS-36U identifies the field-moment calculation inside the inherited marked-update law. For a normalized one-opportunity kernel K on the complete current state, define $G = K - I$. For $X = (P, \Theta)$,

$$b_i = G X_i, \qquad A_{ij} = G\big(X_i X_j\big) - X_i G X_j - X_j G X_i. \qquad \text{(VII.18)}$$

The fixed-one-proposal covariance is $A - bb^{\top}$; the quadratic-variation rate at proposal intensity ν is νA. Applying G to $P, \Theta, P^2, P\Theta, \Theta^2$ therefore supplies the first two moments for this pair, provided those are the correctly typed field observables. Fact-conditioned moments instead use the restricted mark kernel and its occurrence probability. The source's one-bit normalization and time convention remain intact; these identities do not select an unprovided amplitude measure. [A22]

The trial score-feedback update introduced in RCHS-36V was subsequently rejected for physical promotion by RCHS-36W. At fixed apparatus and carried memory, a fixed joint quantum instrument must be affine in the incoming density matrix. For native effects E_m, derivatives $D_m = \partial_\theta E_m$, probabilities $p_m = \mathrm{Tr}(E_m\rho)$ and scores $s_m = \mathrm{Tr}(D_m\rho)/p_m$, the added deterministic displacement $\xi_m = \gamma s_m$ generally violates that requirement. [A23–A24]

Let $\rho_{\mathrm{mix}} = t\rho_1 + (1-t)\rho_2$, $p_{m,\mathrm{mix}} = tp_{1m} + (1-t)p_{2m}$ and $V(\rho) = \mathbb{E}[\xi^2]$. The exact mixture defect is

$$tV(\rho_1) + (1-t)V(\rho_2) - V(\rho_{\mathrm{mix}}) = \gamma^2 \sum_m \frac{t(1-t)p_{1m}p_{2m}}{p_{m,\mathrm{mix}}}(s_{1m} - s_{2m})^2. \qquad \text{(VII.19)}$$

For nonzero gamma and an open full-rank state patch, fixed-instrument realization requires $D_m = c_m E_m$ for every supported mark. The selected native effect fails that proportionality with best relative residual 0.999886. Native probabilities and the unconditioned native state update themselves pass the mixture test. The obstruction belongs to the added score-dependent field displacement, not to the inherited Born instrument or all physical record feedback.

Accordingly, RCHS-36V's ratios $27/310$ and $3/155$ are retained only as outputs of its imposed model and are not admitted physical predictions in this manuscript. A source-derived joint field/record operation with its actual carried memory can supply another law; its unnormalized moments must satisfy the required affinity. A replacement feedback rule requires independent source selection.

VII.8 Integrated physical interpretation

The accumulated work now supplies conditional curvature identifiability with broader endpoint uncertainty, a large executed gain from ordered continuation, a completion-record information boundary, a charge-consistent electromagnetic flux prediction, a calibrated link reference and an explicit same-source electroweak contrast. The current-response inversion and one-bit normalization use results already present in prior papers. The feedback exclusion and restricted-family corrections remove claims that those constructions do not support.

The next physical derivation starts from the positive current action with the fixed source generator and Wilson conventions. Its task is to evaluate the full physical branch, retained embeddings and coupled response in (VII.16), and determine the assumptions actually enforced by that source. The complete marked-background law remains necessary for predictions that explicitly average that law. It is not imposed as a universal prerequisite for every direct action calculation. Completion/refinement and physical scale matching retain their separately stated requirements.

Sections VII.9–VII.12 retain the earlier joint source calculations and Gaussian foundations. Sections VII.13–VII.18 integrate the later source mapping, calibration and attachment tests. Part VIII supplies the conditional temporal configuration operation and its remaining physical dependencies.

VII.9 Joint evaluation of the archived retained parent

The existing FCHI construction supplies a 102-coordinate retained quadratic parent. The 11 September execution in [A27, §7] retains the weak and hypercharge coordinates jointly and relaxes the other 100 coordinates. The auxiliary block has rank 94 with six terminal nulls and satisfies the range condition. At regulator levels 3 and 4, the same calculation returns

$$K_{\mathrm{EW}}^{\mathrm{FCHI}} = \begin{pmatrix} 5/2 & 0 \\ 0 & 149/18 \end{pmatrix}, \qquad (Z_2, Z_Y) = (5/2, 149/18), \qquad \text{(VII.20)}$$

$$g = 0.6324555320, \quad g' = 0.3475706678, \quad \sin^2\theta_W = 45/194. \qquad \text{(VII.21)}$$

This verifies the prior neutral-extended RRHF pair on the archived larger parent. It is not a new physical coupling prediction: the representation-score prescription remains an input to this parent, and its other sectors are direct-summed with the gauge block. The evaluation preserves the earlier result and its conditions while preventing its repeated recovery from being presented as a fresh derivation. [A27, §7; P23; P31, FCHI-1]

VII.10 Return reduction retaining the physical duration

The subsequent calculation in [A27, §8] combines the common raw-transfer convention with prior renewal results. Let $T(\theta)$ be a smooth finite irreducible nonnegative raw transfer with Perron root λ. Partition its states into a nonempty return section P and hidden set Q. For spectral discount s, define

$$\mathcal{R}(s,\theta) = e^{-s}T_{PP} + e^{-2s}T_{PQ}\left(I - e^{-s}T_{QQ}\right)^{-1}T_{QP}. \qquad \text{(VII.22)}$$

The inverse exists when $\rho\left(e^{-s}T_{QQ}\right) < 1$. Its expansion sums every first-return excursion with its original duration. Eliminating the hidden components of the Perron eigenvector proves $\rho\left(\mathcal{R}(\log\lambda,\theta)\right) = 1$. If $r > 0$ is that eigenvector and $D_r = \operatorname{diag} r$, the return kernel of $K = \lambda^{-1}D_r^{-1}TD_r$ is

$$K^{\text{return}} = D_{r_P}^{-1}\mathcal{R}(\log\lambda,\theta)D_{r_P}. \qquad \text{(VII.23)}$$

Thus return elimination and Doob normalization commute in this construction, with no removal of retained–hidden coupling. This is a state-return reduction, not an arbitrary tensor-factor marginalization, and it does not by itself establish the Gaussian Fisher–Schur bridge of §IV.14.

Write $\varphi = \rho(\mathcal{R}) - 1$, $s_\star = \log\lambda$ and $\tau_{\mathrm{r}} = -\varphi_s > 0$ at the root. Implicit differentiation gives the complete joint response

$$s_a = \frac{\varphi_a}{\tau_{\mathrm{r}}}, \qquad s_{ab} = \frac{\varphi_{ab} + \varphi_{sa}s_b + \varphi_{sb}s_a + \varphi_{ss}s_as_b}{\tau_{\mathrm{r}}}. \qquad \text{(VII.24)}$$

The mixed duration terms are retained. For raw cost $-\log\lambda$, the response is $-s_{ab}$ per original step, with the existing physical time and curvature normalization applied subsequently. A positive source cumulant Hessian is not automatically a positive energetic stiffness.

The inherited K7 current/persistence test gives mean return duration $31/7$ and

$$\nabla^2_{u,v}\log\lambda = \frac{1}{29791}\begin{pmatrix} 10536 & -3216 \\ -3216 & 5316 \end{pmatrix}. \qquad \text{(VII.25)}$$

Direct Perron differentiation and the return-resolvent calculation agree exactly in rational arithmetic. The labels u, v are current and persistence, not weak and hypercharge, and hub return is not newly identified with physical Fact formation. This establishes the source-preserving operation with nonzero mixed response; the physical transfer and its gauge deformation must supply its physical inputs. [A27, §8; P3; P27; P34]

VII.11 Physical weak and hypercharge vertices on the common source

The derivative continuation [A27, §9] attaches the fixed gauge generators to Part III's six-defect calculus and to the later shared-link matter reconstruction [P33]. In the inherited right-link chart, for specified geometric profiles a_e, b_e,

$$U_e(w,y) = U_{e,*}\exp[i(wA_e + yB_e)], \quad A_e = a_eT^3, \quad B_e = b_eY, \qquad \text{(VII.26)}$$

$$U_{e,w} = iU_eA_e, \quad U_{e,y} = iU_eB_e, \quad U_{e,wy} = -1/2\, U_e\{A_e, B_e\}. \qquad \text{(VII.27)}$$

The conventional Y is used. Although $[T^3, Y] = 0$, the mixed derivative need not vanish. On the inherited 50-dimensional representation, $\operatorname{Tr}(T_3Y) = 0$ while $\operatorname{Tr}\left(T_3^2Y^2\right) = 5/8$. The latter is a representation identity, not a mixed kinetic coefficient. The unbroken gauge symmetry and complete action determine which mixed response survives.

Let $d_a = \partial_a\mathbf{D}|_\star$ collect all six defect vertices. At a defect zero, their direct quadratic contribution is $d_a^\dagger W_{\text{prim}}d_b$, with the real part understood for real field coordinates. Off zero, the residual, metric and second-vertex product-rule terms in §III.8 remain necessary. The occupied-support correction in §III.5 is retained; vanishing residuals never justify discarding their first derivatives or the common auxiliary columns. On the frozen Gaussian proposal of §IV.13, the already established score contraction is

$$s_a = \langle E_Dd_a, \xi\rangle_{G_{\text{op}}}, \qquad \frac{\mathbb{E}_0[s_as_b]}{a_t} = d_a^\dagger W_{\text{core}}d_b. \qquad \text{(VII.28)}$$

For the shared-link matter source, use the inherited incidence pullbacks S, T and carrier pairing Γ_E:

$$\mathcal{B} = \mathsf{T} - \mathcal{U}_f\mathsf{S}, \quad K_f = \mathsf{T}^\dagger\Gamma_E\mathcal{B} + \text{h.c.}, \quad L_f = \mathcal{B}^\dagger\mathcal{B}. \qquad \text{(VII.29)}$$

At fixed incidence and pairing, $\mathcal{B}_a = -\mathcal{U}_{f,a}\mathsf{S}$ and $\mathcal{B}_{ab} = -\mathcal{U}_{f,ab}\mathsf{S}$. In particular,

$$(L_f)_{ab} = \mathcal{B}_{ab}^\dagger \mathcal{B} + \mathcal{B}^\dagger \mathcal{B}_{ab} + \mathcal{B}_a^\dagger \mathcal{B}_b + \mathcal{B}_b^\dagger \mathcal{B}_a. \qquad \text{(VII.30)}$$

The corresponding kinetic and source-Wilson derivatives follow by the same product rule. Any physically moving incidence, pairing, support or normalization map must also be differentiated. The later MFKR infrared spatial-normalization result is consumed; its kinetic seed is not substituted for the complete physical chiral operator, and matter traces exclude the two Higgs entries of the common carrier. [P33]

The archived independent checks give maximum relative errors 1.10×10^{-9} for the six first variations, 6.65×10^{-9} for the shared-link mixed matter vertices and 7.91×10^{-10} for the variable-metric product rule. Pure-gauge variation of all six defects at a compatible zero cancels to 6.48×10^{-16} absolute error. These checks validate derivatives and covariance, not a selected physical vacuum or numerical W_{prim}. The full weak/Y response then uses one common auxiliary relaxation, as in (VII.16); separate factorwise relaxations would discard cross terms. [A27, §9]

VII.12 Stationary response and full marginal response

The restored Gaussian source theorem changes the physical continuation. Exact Gaussianity of every complete history is not a prerequisite for the stationary quadratic Schur theorem already established by MASD and Quadratic Gauge-Release Sufficiency. Its local target is the actual same-source Hessian. The stronger full-history information identity in §IV.14 additionally requires its stated physical displacement map and covariance conditions. [P4–P5; P28–P31]

The native operator check in [A27, §11] finds, on the inherited K7 curvature representative and 48 matter rows,

$$\partial^2_{(w,y)} \mathrm{Tr}_{48} L_U^3 \big|_0 = \begin{pmatrix} 36 & 0 \\ 0 & 60 \end{pmatrix}. \qquad \text{(VII.31)}$$

Independent spectral and closed-walk evaluations agree to 3.8×10^{-16} relative discrepancy. These coefficients describe a field-dependent native roughness spectrum. They are not gauge stiffnesses, do not identify L_U with the operational metric, and do not refute the conditional Gaussian proposal (IV.41). The inference from nonlinear field dependence to failure of that proposal is withdrawn. [A27, §12]

For a full fluctuation marginal, a Gaussian bath whose precision itself depends on the retained field contributes a determinant term. On a fixed positive support and reference volume, its Hessian contribution is

$$\Delta H_{ab} = 1/2\, \mathrm{Tr}(A^{-1}A_{ab} - A^{-1}A_b A^{-1} A_a). \qquad \text{(VII.32)}$$

This term vanishes when that precision is field independent. It is not generated merely by calling the bath Gaussian. The physical source must determine its presence, along with fermionic, record, measure and normalization contributions. An already integrated action must not count the same fluctuation correction twice. The positive-transfer construction in Full-Carrier Provenance uses a Gaussian reference path integral with a local retained-potential weight; it does not assert joint Gaussianity of all interacting fields. [P32, Appendix F]

The physical target is therefore concrete: evaluate the inherited source operators on their physical branch, contract the existing weak/Y vertices, and perform the appropriate common relaxation or full-history contraction. The fixed Wilson convention then reads the transverse kinetic coefficients as $g = Z_2^{-1/2}$ and $g' = Z_Y^{-1/2}$. A broken-phase field Hessian must have its mass terms separated from its kinetic response. Neither the conditional pair (VII.21), the verification matrices in §IV.14 nor the spectral coefficients (VII.31) are promoted to this physical output. The Gaussian proposal, bath theorem and quadratic innovation theorem remain established inputs to that evaluation.

VII.13 Magnitude bearing source response and the field map

The later source-weight analysis first distinguishes the endpoint-field ensemble from the evolving quantum state propagated by the marked instrument. For a local current residual with supplied positive metric M_e, its direct zero-defect link Hessian is

$$K_{ab}^{(J)} = \mathrm{Re}[(T_a\psi_s)^\dagger M_e (T_b \psi_s)]. \qquad \text{(VII.33)}$$

This expression retains amplitude and coherence. Under the additional scalar specialization $M_e = m_e I$, representation trace averages reduce to unnormalized endpoint-field second moments. They cannot generally be calculated from normalized terminal populations alone. The native equal-population witness reproduces the known trace averages while retaining a nonzero weak–hypercharge cross vector. The full action and background symmetry determine whether any physical mixed response survives. [A29, §§6–7]

A common rescaling of endpoint fields and currents leaves the normalized current instrument unchanged while scaling this direct unit-metric Hessian quadratically. That algebraic invariance concerns the specified instrument; it does not establish admissibility of the rescaling in the full action or reopen the fixed generator and Wilson conventions. Once a complete physical source is supplied, its endpoint moments, coherences and bath are related outputs of that source. They are not independent fit parameters.

For a nonzero random current j, normalized representation weights require a ratio expectation. With representation projector P_r and $X = j^\dagger j > 0$ almost surely,

$$\mathbb{E}\frac{j^\dagger P_r j}{X} = \int_0^\infty \mathbb{E}\left[(j^\dagger P_r j)e^{-tX}\right] dt. \qquad \text{(VII.34)}$$

The source note evaluates the integrand for a genuinely Gaussian current law, including nonzero mean and noncircular covariance. This analytic reduction does not establish that law from a Gaussian proposal for a different variable. Its normalized current-ray weights also remain distinct from the unnormalized moments in (VII.33).

The physical map can be stated exactly at score level. On one history law, let u be the declared source scores and s the actual field scores. Define $W_s = \mathbb{E}[uu^T]/T$, $B_s = \mathbb{E}[us^T]/T$ and $F_s = \mathbb{E}[ss^T]/T$. Projection in mean-zero score space gives

$$M_s = W_s^+ B_s, \qquad \Delta_s = F_s - B_s^T W_s^+ B_s \succcurlyeq 0. \qquad \text{(VII.35)}$$

Vanishing Δ_s is necessary and sufficient for the source scores to represent the field deformation at this finite-history or rate scope. This statistical map is not automatically the energy-domain embedding required by HMGBC's generator compression. For a real Gaussian family with mean derivatives e_a and covariance derivatives C_a,

$$F_{ab} = e_a^T C^{-1} e_b + \frac{1}{2}\mathrm{Tr}(C^{-1}C_a C^{-1} C_b). \qquad \text{(VII.36)}$$

Linear mean scores omit the second term. Gaussianity alone therefore does not permit discarding physical covariance variation; a pure coordinate-frame variation must also not be counted as new physical information. These results retain the frozen-chart scope of §IV.13. In unwhitened coordinates its exact identity is $J^T W_{\mathrm{core}} J = GP_G$, where $P_G = E_D J$ is the G-orthogonal projector. It becomes the corresponding projector matrix after raising an index or whitening. [A29, §8]

A separate covariance correction is useful for the six-mode event source of Full-Carrier Provenance. Set $u = \mathbf{1}/\sqrt{7}$, $W_M = M^{1/2}$ and $P = I - (W_M u)(W_M u)^T/(u^T M u)$. Since $PW_M\mathbf{1} = 0$, its transported common rank-one component vanishes. With $\upsilon > 0$,

$$\Sigma_Q = \upsilon PMP, \qquad \Sigma_Q^+ = \upsilon^{-1} W_M^{-1}(I - uu^T)W_M^{-1}. \qquad \text{(VII.37)}$$

For the consistently transported source $J_s = PW_M J_S$, the contraction is $J_s^T \Sigma_Q^+ J_s = \upsilon^{-1} J_S^T (I - uu^T) J_S$. Mass-transport factors cancel from this particular contraction. This corrects the source sentence suggesting survival of that common component; it does not eliminate anisotropy of PMP or identify this event covariance with the full weak/Y history covariance. [A29, §9; P32, Part IX]

VII.14 Coupled effective evolution and external calibration

The inherited leading electroweak action supplies an effective coupled field law once its kinetic coefficients are given. In source-connection coordinates $x = (gW_3, g'B)^T$, with $Q = T_3 + Y$, its transverse mode obeys

$$\mathcal{Z}\ddot{x} + (|\mathbf{k}|^2 \mathcal{Z} + \mathcal{M})x = j, \qquad \mathcal{Z} = \mathrm{diag}(Z_2, Z_Y), \qquad \text{(VII.38)}$$

$$\mathcal{M} = \frac{v^2}{4}\begin{pmatrix} 1 & -1 \\ -1 & 1 \end{pmatrix}, \qquad \mathsf{G}(Q) = (Q^2\mathcal{Z} + \mathcal{M})^{-1}. \qquad \text{(VII.39)}$$

Here $Q > 0$ in the response denotes spacelike momentum magnitude, rather than the charge operator in the preceding definition. The source calculation evaluates the photon/Z retarded solution and the spacelike inverse on the minimal leading branch, with no additional retained neutral vector. The mixed coefficient simplifies to

$$G_{3Y}(Q) = e^2\left[\frac{1}{Q^2} - \frac{1}{Q^2 + m_Z^2}\right]. \qquad \text{(VII.40)}$$

At this order the separate weak/hypercharge ratio cancels. The fixed chiral charges $(T_3, Y)_{\nu_L} = (1/2, -1/2)$, $(T_3, Y)_{e_L} = (-1/2, -1/2)$ and $(T_3, Y)_{e_R} = (0, -1)$ give $G_{3Y} = \mathcal{A}(e_L, e_R) - \mathcal{A}(\nu_L, e_R)$ for equally normalized transverse exchange coefficients. This is a source-amplitude identity; extracting it from cross sections requires the process-dependent analysis. [A29, §11; C26; P35–P36]

External calibration was executed using the frozen PDG listing inputs $\alpha(0)^{-1} = 137.035999084$, $M_W = 80.3692$ GeV and $M_Z = 91.1880$ GeV. These masses retain the listings' running-width convention. With $s_{\mathrm{OS}}^2 = 1 - M_W^2/M_Z^2$ and $e^2 = 4\pi\alpha(0)$,

$$Z_2^{\mathrm{OS}} = s_{\mathrm{OS}}^2/e^2, \qquad Z_Y^{\mathrm{OS}} = \left(1 - s_{\mathrm{OS}}^2\right)/e^2. \qquad \text{(VII.41)}$$

The numerical return is shown to enough digits to reproduce the calculation, not to assert that experimental precision.

Externally calibrated quantity	Value	Convention
Weak coefficient Z_2	2.43409468	On shell
Hypercharge coefficient Z_Y	8.47088364	On shell
Weak coupling g	0.64096050	On shell
Hypercharge coupling g'	0.34358614	On shell
v_{OS}	250.77739 GeV	Defined from the same mass inputs
$G_{3Y}(M_Z)$	$5.51403879 \times 10^{-6}$ GeV^{-2}	Leading spacelike response

These are measured-input effective parameters, not bare source predictions or modified-minimal-subtraction couplings. The independent muon-lifetime input $G_F = 1.1663785(6) \times 10^{-5}$ GeV^{-2} gives the calibrated left-projector current coefficient

$$C_\mu = 2\sqrt{2}G_F = (3.2990166 \pm 0.0000017) \times 10^{-5}\ \mathrm{GeV}^{-2}. \qquad \text{(VII.42)}$$

The leading on-shell coefficient is $3.18019131 \times 10^{-5}$ GeV^{-2}, so matching it to the muon result requires a 3.736 percent multiplicative total correction. This includes the required process matching and is not a measured propagator correction alone. The distinct Fermi-defined value is $v_{G_F} = 246.21967$ GeV. The archived response identities pass algebraic checks at approximately 8×10^{-15} relative error; no microscopic force coefficient was fitted to these measurements. [A29, §11; M8]

VII.15 The corrected weak and hypercharge ordering test

The source convention $q = 6Y$ implies $Z_Y = Z_q/36$. Therefore the hierarchy $g > g'$ is equivalent to $Z_q/Z_2 > 36$. RSMPC §77.3 compared the final coefficient ratio to 140, but that threshold belongs to MASD's internal norm convention. On the stated unit-wheel branch its factor $K_q/K_2 = 9/35$ converts 140 into 36. The internal norm statement is retained; its application to the final ratio is corrected. [A29, §12; C27; P4, §47B; P28, §77.3]

The unchanged current/score candidate consequently passes this ordering test:

$$Z_2 = 1.5807137020050954, \qquad Z_q = 184.70045096020377, \qquad \text{(VII.43)}$$

$$r = Z_Y/Z_2 = 3.2457288601470884, \qquad \sin^2\theta_W = 0.23553082001693254. \qquad \text{(VII.44)}$$

Removing the erroneous rejection does not establish the candidate's physical source. Its code combines a candidate current normalization with direct source-covector bath fractions; §VII.16 explains why those fractions cannot automatically be interpreted as the complete field response.

The leading coupled response offers a ratio-sensitive contrast complementary to (VII.40):

$$G_{33} - G_{YY} = \frac{e^2}{Q^2 + m_Z^2}\left(r - \frac{1}{r}\right). \qquad \text{(VII.45)}$$

The fixed-current combination is $\mathcal{A}_{\nu\nu} + \mathcal{A}_{LL} - 2\mathcal{A}_{\nu L} - \mathcal{A}_{RR}$. The candidate gives $r - 1/r = 2.9376316520658556$. This is a conditional contrast of that candidate, with no observed weak-angle input. Comparing its angle directly to an experimentally matched angle at another convention or scale would not complete the derivation.

VII.16 The source covector and the relaxed field response

The finite source archive constructs a defect covector $h = E_D^T u$, whereas a field variation produces the defect tangent $d = Ju$. On the checked retained columns, $J^T h = u$ in the declared Euclidean chart; hence $d = JJ^T h$. More generally, if $J^T h = G_X u$, then $d = JG_X^{-1} J^T h$. This identifies the archived map without selecting the physical metric G_X. [A29, §13; C28]

Applying that map changes the interpretation of the reported screening. All percentages below refer to the same inherited finite candidate and retain its colour, weak and integer-hypercharge ordering.

Response being contracted	Colour	Weak	Integer hypercharge
Source covector	2.649350%	2.725311%	2.274894%
Fixed field tangent	21.231278%	21.578365%	19.746059%
Field with common configuration relaxation	22.696965%	23.072975%	21.055148%

The final row uses the common full 226-coordinate parent and reproduces its previously archived retained diagonal, quoted in §IV.17. It is a grade N result. No source map equates this reduction to multiplication of the candidate current weights by the first row.

The same archive supplies a useful conditional bound. On its 183-dimensional core support, the maximum bath fraction is 0.2823009917016152. The bath annihilates the core nulls, so with $m = 0.7176990082983847$,

$$mW_{\text{core}} \preccurlyeq W_{\text{prim}} \preccurlyeq W_{\text{core}} \quad \Rightarrow \quad mZ_0 \preccurlyeq Z_1 \preccurlyeq Z_0. \qquad \text{(VII.46)}$$

The implication follows by minimizing the same quadratic parent over the same auxiliary space, provided its unchanged additional Hessian is nonnegative. It needs no source factorization. It is a finite static response bound; an extracted continuum kinetic coefficient requires its own justified comparison. The physical 50-dimensional representation and enlarged source cannot inherit this reduced archive's matrices by relabelling.

VII.17 Transport normalization and the limit of bath screening

The later candidate seat division is explicitly a constitutive rule in NFDMA-2. Treating it only as a coordinate change cannot alter a fixed physical source response: if $a = Lx$ and $K_x = L^T K_a L$, then $LK_x^{-1} L^T = K_a^{-1}$. A changed coefficient with an unchanged source vertex therefore specifies a different action, rather than deriving a new observable normalization. [A29, §14; C29]

The native joint field vertices use the same unit-face profile for all three weak directions and hypercharge. Their unweighted link Gram is diag($13/8$,$13/8$,$13/8$,$21/8$), while the face-circulation Gram gives the established representation traces. Neither is an energetic metric. In the fixed current convention, the undivided benchmark has $r_0 = 21/13$; the seat candidate has $r_0 = 42/13$. Counting active modes does not establish the extra relative factor of two.

Under the same-source bound (VII.46), any fixed-direction ratio satisfies

$$m \leq r_1/r_0 \leq 1/m = 1.393341760874007. \qquad \text{(VII.47)}$$

Thus this bath can enhance the ratio by at most 39.3342 percent. If the initial ratio were $21/13$, its allowed interval would be [1.159359936482,2.250782844489], excluding both the doubled ratio and (VII.44). This rules out simultaneously using that initial ratio, that inherited bound and the candidate final ratio. It does not establish a universal VERSF bound or show that the physical core must equal either benchmark. [A29, §15; C30]

VII.18 A sufficient internal trace attachment

The later H_CMR forward source yields a scalar-profile score Hessian after destination-function nuisance elimination. If F is the scalar source Fisher block, A the nuisance block and C_A the source–nuisance columns, it is $H_{\text{slot}} = F - C^T A^+ C$. Its archived implementation then attaches internal representation traces to its diagonal. The unchanged scalar family does not itself perform that attachment. [A29, §16; C31; P28, §§78–79]

A sufficient full quadratic parent can nevertheless be constructed explicitly. Choose internal source vectors with Gram $B_{AB} = \mathrm{Tr}(T_A T_B)$, and give the nuisance space the corresponding tensor pairing. Then

$$\hat{F}_{AB} = F_{AB} B_{AB}, \quad \hat{A} = A \otimes I, \quad \hat{C}_A = C_A \otimes v_A, \quad \hat{Z}_{AB} = H_{\mathrm{slot},AB} B_{AB}. \qquad \text{(VII.48)}$$

Orthogonal internal factors recover the reported diagonal exactly. This proves a sufficient attachment, not membership of the physical field source in that class. At an unbroken weak-symmetry reference, an invariant scalar-label law with no transforming internal mark or charged background has no nonzero equivariant linear map from the weak adjoint into a scalar bias. That observation does not forbid a quadratic gauge action, a charged background or operator-valued marks.

The physical calculation must therefore supply the actual joint address/internal field score, its nuisance pairing and any same-order coupled directions. The explicitly nontrivial native instrument response in §VI.11 supplies another operational object, but its coarser readout does not alone establish or disprove this full-parent attachment. The conditional trace construction, corrected screening results and empirical calibration each retain their separate roles.

VII.19 Exact event-to-gauge impulse on the common link

The source-grade event bridge uses the same compact link Ue in matter transport and in the closure action. A separate matter-vertex normalization is excluded at that construction level. For an oriented graph edge and its conjugate rotor momentum,

$$U_e = \exp(i\,\theta_e), \quad p_e = -i\,\partial/\partial\theta_e. \quad \text{(VII.49)}$$

Let γ be a signed path from a to b, so $B\gamma = \delta b - \delta a$. For one normalized charge-n channel the transport factor is

$$T(\gamma) = c(b)^\dagger \exp(i\,n\,\gamma\cdot\theta)\, c(a). \quad \text{(VII.50)}$$

The Gauss generators commute with this operation. The link factor raises the conjugate electric flux while the fermion factor transfers the same charge between the endpoints, giving the exact finite operator identity

$$\Delta p = n\gamma, \quad \Delta Q = n(\delta b - \delta a). \quad \text{(VII.51)}$$

Thus the event supplies a representation-normalized conjugate gauge impulse. The scalar count of a Fact is not being reused as a charge: n is the chosen physical U(1) charge coordinate. The event probability or branch amplitude remains separate, and the operation changes conjugate flux rather than instantly advancing the link angle. Subsequent link motion requires the gauge kinetic evolution. [P51]

VII.20 Conditional common-carrier U(1) normalization theorem

The geometric closure paper defines a U(1) holonomy on each cell and derives Chern-Weil integrality for the coarse closure surface. The local interface papers independently establish that primitive gauge-invariant observables are link-phase differences. The remaining bridge premise is therefore stated explicitly: suppose the geometric closure connection is induced by oriented products of the same compact links Ue used by the closure and matter/gauge transport. Then for an oriented face f,

$$Wf = \prod_{e\subset\partial f} Ue^{(\sigma fe)} = \exp(i\,\Theta f), \quad \Theta f = \Sigma_{e\subset\partial f}\, \sigma fe\, \theta e \pmod{2\pi}. \quad \text{(VII.52)}$$

Any continuous group homomorphism from this microscopic U(1) to a second U(1) has integer degree m, because $\exp[i\,m(\theta+2\pi)]$ must equal $\exp(i\,m\theta)$. Faithfulness requires $|m|=1$; choosing the same orientation fixes $m=+1$. Therefore, conditional on the common-carrier premise, there is no independent continuous embedding gain:

$$\exp(i\theta) \mapsto \exp(im\theta), \quad m\in\mathbb{Z}, \quad \text{faithful} + \text{orientation-preserving} \Rightarrow m=1 \Rightarrow \kappa emb=1. \quad \text{(VII.53)}$$

This theorem removes a generator/angle-rescaling ambiguity. It does not prove that the geometric phase fraction equals the physical Maxwell kinetic coupling. The geometric closure source itself distinguishes the Chern-Weil theorem from the additional electromagnetic bridge, so the coupling-response and RG questions remain separately typed. [P52; P54]

VII.21 Exact Wilson continuum normalization

The later interface audit closes a second apparent freedom. With the declared plaquette holonomy $Up = \exp(i\int p\, F)$, the standard Wilson action has

$$SW(F) = \beta(1 - \cos F) = (\beta/2)F^2 + O(F^4), \quad \beta = 1/g^2. \quad \text{(VII.54)}$$

The equality $\beta=1/g^2$ follows by expanding the same Wilson action and matching its quadratic coefficient to the declared continuum gauge action. Consequently the interface-to-continuum multiplier is cnorm=1 inside this convention; changing it requires changing the discretization, generator or field convention rather than tuning a physical correction. For electromagnetism,

$$\alpha EM = g^2/(4\pi), \quad \beta EM = 1/(4\pi\alpha EM). \quad (VII.55)$$

Sections VII.3–VII.4 therefore remain correctly typed as measured-alpha calibration of an effective electromagnetic mode. This paper does not replace that calibration by the K7 scalar admission number or by its saturated support trace. [P20; P21; P55]

VII.22 K7 admission–Wilson response non-equivalence and closure-projection rigidity

The K7 source branch supplies a scalar electromagnetic admission candidate. In its currently admitted leading form,

$$pEM = (1/128)(14/15) = 7/960. \quad (VII.56)$$

The later support-rank audit sharpens the typing of the 14/15 factor. On the strict closure-projection or polar-support branch, with thirteen transmitted polar directions, one transmitted record line and one annihilated global line, the positive gate effect is

$$Ecl = \Pi\dagger\Pi = PT + PR = \mathrm{diag}(I_{14}, 0). \quad (VII.57)$$

Hence the scalar support throughput is fixed by rank and trace while the saturation assumptions hold:

$$\eta gate(cl) = \mathrm{Tr}(Ecl)/15 = 14/15. \quad (VII.58)$$

A pure field rotation or basis change that preserves this saturated support does not alter the singular spectrum $1{\times}14, 0{\times}1$. Therefore the scalar closure-projection admission trace is locally field-rigid on that branch:

$$d\eta gate(cl)/dF = d^2\eta gate(cl)/dF^2 = 0 \quad \text{(fixed support and saturation)}. \quad (VII.59)$$

This is not a theorem that every full-refinement response is field-independent. In the full-refinement typing the coherent map may contain a positive attenuation/source-response factor in addition to its isometric support. Field dependence can live in those positive eigenvalues and, more generally, in the complete physical reduced Hessian. The scalar 7/960 therefore remains an admission probability and the reciprocal 960/7 cannot be promoted to a Wilson coefficient or to α^{-1}.

After the physical gauge Hessian is independently returned in the fixed generator and Wilson conventions, the photon coefficient is formed from the weak and hypercharge kinetic coefficients:

$$Z\gamma = Z_2 + Zq/36, \quad \alpha EM^{-1} = 4\pi\, Z\gamma. \quad (VII.60)$$

Only after that derivation may one compare $4\pi Z\gamma$ blindly with the structural number 960/7. Agreement would be a noncircular cross-check at the declared matching scale; disagreement would leave 7/960 as a structural electromagnetic-admission coefficient rather than the Maxwell fine-structure coupling. [P53–P56]

VII.23 Retyped electromagnetic P1 handoff

The scalar K7 curvature is therefore removed from the load-bearing electromagnetic programme. The event-to-flux impulse remains charge-normalized; the common-carrier embedding has no continuous faithful rescaling under its bridge premise; and the declared Wilson continuum map has cnorm=1. The remaining strength-bearing object is the complete positive/source response on the changing-link carrier, not the curvature of the saturated scalar support trace.

$$Wprim \to Gred(phys) \to (Z_3, Z_2, Zq) \to Z\gamma = Z_2 + Zq/36 \to \alpha EM^{-1} = 4\pi Z\gamma. \quad (VII.61)$$

This is the revised electromagnetic P1 route. The structural K7 number is retained only as a post-derivation comparator, $4\pi Z\gamma \mathrel{?}= 960/7$, never as an input. For the full Standard Model calculation the same physical parent must also determine the weak/hypercharge split and strong coefficient without factorwise rescaling. [P5; A2; P51–P56]

VII.24 Event-grain separation and the source-stopped D36 matter law

RCHS-25 corrects the earlier hard-versus-Dirichlet fork by separating the event grains. Finite endpoint relaxation belongs to the pre-completion trajectory; a hard completion relation, if eventually source-derived on the matter tangent, belongs to the completion operation. On the executed discrete-Fold record branch the persistent record clock is the first complete closed cover rather than an exponential surrogate. [P57]

$T_{rec} = T_{cover}, \quad E[T_{cover}] = 21.277682950918.$ (VII.62)

RCHS-26 then derives the source-even D36 stationary traffic. With $\alpha\star = 0.959001109719975$ and $Z = 19 + 12 \cosh \alpha\star$, the six spoke and six rim conductances are fixed by the same source law:

$c_{spoke} = 1/Z = 0.027060532986541, \quad c_{rim} = \cosh(\alpha\star)/Z = 0.040487489437977.$ (VII.63)

The rim/spoke ratio is therefore $\cosh \alpha\star = 1.496182261380952$, not a free heat-depth parameter. In mass-normalised coordinates the additive reversibilisation P_+ gives the exact source-stopped covariance handoff

$\bar{C}_{rec}^{-} = G_{cover}(\tilde{P}_+^{2}) \otimes I_{49}.$ (VII.64)

Conditional on the same-event attribution below, the stopped coherences are $\gamma_{spoke} = 0.999999027606$ and $\gamma_{rim} = 0.999998980024$. The near-common terminal state does not imply absence of current during the open trajectory; it motivates using accumulated pre-record current action rather than only the final pre-record current. The one remaining physical premise is explicit:

EPM1: one D36 pre-Fact Fold acts on the reconciled Ω⊥ matter endpoint tangent through its symmetric stationary traffic. (VII.65)

The newest configuration-update audits do not derive EPM1. They recover scalar closure dictionaries, restoring covectors, support-change constraints and receiving responses, but they still do not select the microscopic joint operation on the independent physical link/current carrier. EPM1 is therefore retained as CONDITIONAL, not silently promoted. [A34; P58]

VII.25 Source-stopped E_2 current occupation and the action/covariance firewall

RCHS-27 propagates the physical E_2 doublet through the D36 source-even Fold law and stops it on the actual first-cover record schedule. Conditional on EPM1 and the no-reinjection single-excitation branch, one Fold multiplies the E_2 amplitude and squared amplitude by

$\mu E_2 = -0.099388227586084, \quad qE_2 = \mu E_2^2 = 0.009878019782703, \quad H_{cover}(qE_2) = 1.009976568523946.$ (VII.66)

The source-even edge weighting gives $\beta E_2 = 3c_{rim}^2 + c_{spoke}^2 = 0.005649982848487$ and hence the two-quadrature stopped current occupation

$K_{J,occ} = \eta_J I_2, \quad \eta_J = \beta E_2\, H_{cover}(qE_2) = 0.005706350289534.$ (VII.67)

The exact C/W/Y factor overlap is HCWY = (1/49)[[36,18,36],[18,26,26],[36,26,47]]. The stopped occupation therefore has the factorised form

$G_{J,occ}(CWY\times E_2) = h_{phys}\, \eta_J\, H_{CWY} \otimes I_2.$ (VII.68)

The current corpus does not return h_{phys}. More importantly, the equality of this factor shape with the independently derived source-action current shape is a compatibility result, not an equality of scales. Current covariance, Fisher information and action stiffness remain separately typed; in particular $W_J \neq \Sigma_{J,occ}^{-1}$ by definition. [P59]

VII.26 Current-link reciprocity and the physical duality test

The finite EPMD current-link-record block contains a stronger action statement than a standalone current stiffness. After exact gauge/null quotienting, let W_J be the bare current metric, K_θ the current-relaxed link/connection metric and $\mathcal{K}$ the constitutive current-connection map. If they descend from the same quadratic parent, Schur elimination gives the exact matrix reciprocity identity [P18]:

$(\mathbb{K}_J(\text{relaxed}))^{-1} = W_J^{-1} + (1/2)\, \mathcal{K}\, K_\theta^{-1}\, \mathcal{K}^\dagger.$ (VII.69)

The physical release test is therefore

$\varepsilon_{dual} = \|(\mathbb{K}_J(\text{relaxed}))^{-1} - W_J^{-1} - (1/2)\mathcal{K}K_\theta^{-1}\mathcal{K}^\dagger\|.$ (VII.70)

A faithful same-parent execution requires ε_{dual} to vanish within the frozen numerical/regulator error model. On the unit diagnostic scalar branch the complementary reductions $K_\theta = 24/5$ and $K_J(\text{relaxed}) = 48/53$ satisfy the identity exactly, but those values remain diagnostic until W_{prim} and the physical factor/mode assignment are source-selected. The theorem fixes relative normalization inside one parent; it cannot fix the common overall action scale.

VII.27 Same-parent U(1) portal and the two-scalar reduction

At the present quadratic typing grade the only surviving scalar auxiliary portal on the physical E_2 factor carrier is the U(1) closure line. RCHS-6 shows that, if this line is exactly the U(1) member of the same current-link parent, its vector and denominator are not independent dials. On the magnitude-bearing same-grain branch write

$M = 4\Lambda\,\mathrm{HCWY}, \quad b = \beta\, eY, \quad eY = (0,0,1)^T.$ (VII.71)

Then the same-parent parent block forces

$gC = Mb, \quad aC = KY + b^T Mb, \quad Mshort = M - (Mb)(Mb)^T/(KY + b^T Mb).$ (VII.72)

Equivalently, $Mshort^{-1} = M^{-1} + bb^T/KY$. All finite portal freedom can therefore be represented by the dimensionless strength

$x = \beta^2(eY^T MeY)/KY \geq 0.$ (VII.73)

RCHS-7 supplies an exact finite-portal fingerprint:

$\det(Mshort)/\det(M) = (eY^T Mshort\, eY)/(eY^T MeY) = 1/(1+x).$ (VII.74)

Thus, conditional on the same-parent identification, the broad portal ambiguity collapses to an overall response scale Λ and one dimensionless portal strength x. A finite single-U(1) portal cannot erase the full C/W/Y metric; even the formal $x\to\infty$ limit leaves a positive two-dimensional C/W residual. Physical promotion still requires the source-coordinate identity, the absolute scale Λ and the finite x. [P61–P62]

VII.28 Exact identifiability boundary and the locked transverse source calculation

RCHS-28 proves an exact source-level non-identifiability statement at the stage before the same-parent reduction: the D36 propagator and stopped current covariance constrain current kinematics but do not select the operational action injection. Distinct positive action metrics can share the same current propagation, and the present source corpus does not by itself identify

MJJ(phys) = ιJ† Wop ιJ. (VII.75)

The RCHS-6/7 same-parent theorem narrows the Abelian part of that no-go but does not close it physically, because EPM1, the action injection, the U(1) same-parent identity, Λ and x remain unreturned. The 14–15 September configuration/receiver audits likewise do not supply a hidden joint field update or a discrete-record-to-continuous-phase assignment. No further Schur manipulation of the existing endpoint/current matrices can manufacture those missing source data. [A34; P60–P62]

The shortest next calculation is therefore the genuinely transverse, unnormalised changing-link source response, or an independently work-calibrated susceptibility of the same source:

$Kcurv(phys) = D\theta^2[-\log(d\mu raw/d\mu ref)]\theta{=}0$, cycle. (VII.76)

A successful return must be inserted into the complete same-source physical Hessian, pass the duality and single-U(1)-portal fingerprints where applicable, and only then be pulled back through the fixed rank-twelve generator columns to (Z_3,Z_2,Zq). The structural K7 scalar is excluded as an input to this step. The locked critical path is

physical changing-link source → Wprim/Gred(phys) → generator-differentiated gauge columns → (Z_3,Z_2,Zq) → canonical gauge fields and RG. (VII.77)

VII.29 Local closure coordinates and the physical alignment test

The same-parent condition in §VII.27 separates a geometric identification from an action identification. On the canonical wheel let B be the vertex–edge incidence, D the six oriented elementary-face rows and V an orthonormal E_2 face basis. The transverse link basis $R = D^T V/2$ obeys

$$BR = 0, \qquad R^T R = I_2, \qquad DR = 2V. \qquad \text{(VII.78)}$$

Thus a link variation $R\theta$ and its closure variation Vc are locally the same spatial deformation when $c = 2\theta$. A mixed coefficient scales by one half and its closure Hessian by one quarter under this coordinate change; the Schur correction is unchanged. On the later conditional chiral attachment, $A_\chi = S^3 - I - S = -S$ on E_2, so the corresponding map adds an orthogonal quadrature rotation and preserves this singular value on the compressed wheel. These facts do not prove the global common-carrier premise, transport an energetic metric through a hub refinement or select a physical portal strength. [A41; P18, §§39Q–39U]

The current probe must also remain the later CRTF radial tangent $\delta j_e = q_e P_A j_e$, rather than the older fixed gradient lift. For the declared diagonal current-square term with field-independent weights, at $U_e = I$ and $\delta U_e = iR_e Y$,

$$H^{J}_{\epsilon_A\theta} = -\sum_e w_{J,e}\,\kappa_e q_e R_e \operatorname{Im}\left(j_e^\dagger P_A Y \psi_{s(e)}\right). \qquad \text{(VII.79)}$$

Here q_e is the frozen spatial probe profile, not the integer generator $q = 6Y$. Equation (VII.79) is one contribution to the mixed Hessian. It is not the complete cross-defect or auxiliary-relaxed response. The actual radial tangent is background dependent; orthogonality of the older gradient lift to cycles therefore cannot establish a zero physical portal. [A41; P63]

For one real quadrature write the complete reduced current–closure parent as $H = \begin{pmatrix} M & -g \\ -g^T & a \end{pmatrix}$, with $M > 0$ and $a - g^T M^{-1} g > 0$. Its identification with the specific §VII.27 branch requires $M^{-1} g = \beta e_Y$. On $M = 4\Lambda H_{CWY}$ this is equivalent to

$$47 g_C - 36 g_Y = 0, \qquad 47 g_W - 26 g_Y = 0. \qquad \text{(VII.80)}$$

The zero vector is included. Completing the square in an arbitrary positive parent does not prove these physical-coordinate identities. Nor does the local conversion $c = 2\theta$ repair a failed alignment. [P61–P62; A41]

VII.30 Complete mixed response before a symmetry reduction

Use real coordinates for the six-defect vector d and its complete symmetric cross-metric W. Write $\Gamma = 1/2\, d^T W d + \Xi$, where Ξ retains the potential and any applicable fermion, effective-measure and orientation-source contributions, each counted once. For two physical probes i, j, direct differentiation gives

$$H_{ij} = d_i^T W d_j + d^T W d_{ij} + d_i^T W_j d + d_j^T W_i d + 1/2\, d^T W_{ij} d + \Xi_{ij}. \qquad \text{(VII.81)}$$

All current, continuity, closure, record, bond and completion cross blocks are included. At a common defect zero the residual-dependent terms vanish, recovering the MASD Jacobian pullback. An oriented displaced background need not be such a zero. Positivity or gauge covariance does not license replacing the full metric by its diagonal. [P4, Theorem 9A and §§12–20]

If z denotes the complete prescribed auxiliary space, stationary quadratic elimination gives

$$\widehat{H}_{ij} = H_{ij} - H_{iz} H_{zz}^{-1} H_{zj}, \qquad g_A = -\widehat{H}_{\epsilon_A\theta}. \qquad \text{(VII.82)}$$

Null directions require the same quotient and range conditions as the earlier Schur results. Statistical marginalization additionally retains its measure and determinant contributions. Equations (VII.81)–(VII.82) specify the complete contraction; the imaginary term in (VII.79) cannot be tested in isolation and promoted to the full result.

VII.31 Conjugate histories and fixed record symmetry

HCMR-P1 already supplies the retained-record conditional law. If $\mathcal{J}_h$ is the ordered composition of the coarse-grained CP operations for record h, its Fubini–Study averaged output is

$$\bar{\rho}_h = \frac{\mathcal{J}_h(I)}{\operatorname{Tr}\mathcal{J}_h(I)}. \qquad \text{(VII.83)}$$

Theorem 6 and Corollary 6.1 then give a covariance between conjugate branches and conjugate retained records. With $T = CK$ the declared antiunitary map,

$$T_* \mu_h^{(1)} = \mu_{\bar{h}}^{(6)}. \qquad \text{(VII.84)}$$

This does not state invariance of the posterior at one fixed retained record. The invariant prior is multiplied by a record-dependent likelihood. The output state, complete ensemble and comparison law transform covariantly, but the record cannot be discarded when applying that theorem. A new arbitrary preparation law is neither needed nor permitted at this conditional instrument level. [P14, §10A and §17]

An action statement requires covariance of the complete source, background and physical probe maps as well. Suppose that in transported linear fluctuation coordinates $H_{\bar{h}} = P^T H_h P$ and that P preserves the retained/relaxed split. Substitution into the Schur formula proves

$$\widehat{H}_{\bar{h}} = P_r^T \widehat{H}_h P_r. \qquad \text{(VII.85)}$$

For nonlinear coordinate changes this Hessian statement requires a stationary background or the appropriate covariant second variation. In a convention where the factor-radial probe is even and the closure probe is odd, (VII.85) specializes to

$$M_{\bar{h}} = M_h, \qquad a_{\bar{h}} = a_h, \qquad g_{\bar{h}} = -g_h. \qquad \text{(VII.86)}$$

This is a relation between histories. It forces a zero mixed block only when the relevant history/background or the specified response measure is itself invariant. Even the probe parity is a premise to check: CK sends $\exp(i\theta Y)$ to $\exp(-i\theta C Y^* C^{-1})$, and a spatial reflection also transports the E_2 quadratures. The current-cycle coordinate in the RCHS four-variable parent is not automatically the even radial amplitude used here. The established HCMR/PFHBA conjugate-pair results therefore do not, on their own, return a physical zero portal. [P18; P32; A41]

VII.32 Conjugation and the surviving stiffness correction

The response after the closure coordinate relaxes depends quadratically on the mixed coefficient:

$$Z_h = M_h - \Delta_h, \qquad \Delta_h = \frac{g_h g_h^T}{a_h} \succcurlyeq 0. \qquad \text{(VII.87)}$$

Under (VII.86), $\Delta_{\bar{h}} = \Delta_h$ exactly. More generally, a symmetry preserving the physical retained subspace transports this correction by the retained congruence. Choosing the sign of a conjugate branch is therefore unnecessary for this branch-even response once the complete action covariance and probe transport have been established. This conditional result does not establish those premises for the physical E_2 portal.

For a specified quenched ensemble with common M and finite moments,

$$\mathbb{E}[Z_h] = M - \mathbb{E}\left[\frac{g_h g_h^T}{a_h}\right]. \qquad \text{(VII.88)}$$

Consequently $\mathbb{E}[g_h] = 0$ does not imply zero screening. When $a_h = a$ and the signed mean vanishes, the correction is $\mathrm{Cov}(g_h)/a$. Since each correction is positive semidefinite, its average vanishes only if $g_h = 0$ almost surely. Opposite signs cannot erase this effect.

The averaging protocol remains physical input. For an annealed free energy with field-independent reference measure, the Hessian is $\mathbb{E}[\Gamma_{ij}] - \mathrm{Cov}(\Gamma_i, \Gamma_j)$; measure dependence must be included when present. An average action is a different operation. In the stationary Gaussian pair with mixed coefficients $\pm g$, integrating the responding closure separately in each branch gives the same quadratic stiffness $M - gg^T/a$, which their equal mixture retains. This verifies the distinction without selecting VERSF's operational grain. [A41; P63, D-RT10]

VII.33 An alignment test that survives history averaging

On the common-M branch set $e = e_Y$, $m_Y = e^T M e$ and $\overline{\Delta} = \mathbb{E}[g_h g_h^T / a_h]$. Define

$$\mathcal{A} = \mathrm{Tr}(M^{-1}\overline{\Delta}) - \frac{e^T \overline{\Delta} e}{m_Y}. \qquad \text{(VII.89)}$$

Completing the M^{-1} square gives the exact nonnegative identity

$$\mathcal{A} = \mathbb{E}\left[\frac{1}{a_h} r_h^T M^{-1} r_h\right] \geq 0, \qquad r_h = g_h - \frac{g_{Y,h}}{m_Y} M e. \qquad \text{(VII.90)}$$

Equality holds if and only if the mixed vectors align with Me_Y almost surely, including zero vectors. Thus the two equations (VII.80) must hold for every contributing history up to a null set; oppositely directed misalignments cannot cancel this witness. This supplies an ensemble test of the inherited RCHS-6 specialization without assuming its answer.

A mixture of rank-one corrections can acquire higher rank. The single-portal determinant identity (VII.74) must therefore not be applied directly to an averaged matrix without its rank and common-parent conditions.

If M_h varies, use the corresponding historywise nonnegative witness; the compressed common-M formula (VII.89) no longer applies. No physical value of $\mathcal{A}$ is returned here. [P61–P62; A41]

VII.34 The existing orientation source and the E2 response

PSAC already contains the odd source $-\sigma\alpha_\star\langle\omega_C, D_C\rangle$ on the gauge-typed Abelian closure line. Its declared centered Gaussian bath leaves this linear source unchanged. At fixed orientation it is therefore incorrect to assume an even closure action merely because the reference branch is reversal symmetric. Covariance can instead reverse the orientation label together with closure. The candidate master action and its no-double-counting rules remain at their published source grades. [P30, §§10I–10K and 10AA–10AF]

The spatial mode matters. PSAC §§10M–10O place the direct source in the uniform, rotation-invariant A_2 circulation. On the same canonical six-face wheel, the E_2 basis has zero column sums:

$$V^T\mathbf{1}_6 = 0. \qquad \text{(VII.91)}$$

Hence the existing uniform source has zero direct linear projection onto this E_2 mode. This does not exclude nonlinear effects on an E_2 Hessian about an oriented background. It does exclude inserting the A_2 affinity or canonical A_2 stiffness as the missing E_2 mixed vector or denominator. The orientation-to-internal-mode attachment in CRTF remains a separate source task. [P63, D-RT12–15]

The calculation therefore does not establish either zero or nonzero physical portal strength. Twenty-five exact checks of the local coordinate and conditional parent identities, followed by fifteen exact checks of the complete derivative, Schur covariance, branch-even correction, alignment witness and direct mode projection, support these statements. They are algebraic verification, not physical source selection. [A41]

The continuation of §VII.28 is now explicit: evaluate the history-conditioned complete E_2 mixed block and closure denominator with the native CRTF tangent, the already-defined retained-record instrument and the same changing-link action protocol. Form Δ_h and, at the specified ensemble grain, test (VII.89)–(VII.90). A vanishing signed mean is insufficient. The conditional probability law must not be relabelled an arbitrary missing phase law, and it must not be identified with an action Hessian without its source bridge. No physical Λ, x, weak or hypercharge coupling is selected by this update.

Part VIII Field configuration evolution from temporal holonomy

This part connects the source-selection question to an explicit operation between different field configurations. It first determines what a configuration-diagonal extension of the inherited commitment instrument can accomplish. It then derives a changing-configuration transfer from the previously supplied temporal Wilson action, retaining the map and physical-identification premises that control its application. The Wilson transfer method is standard lattice gauge theory; the VERSF question is whether the physical primitive source selects this action and its actual temporal channels. [A29, §§23–24]

VIII.1 What the commitment instrument changes

For a specified field configuration z, the complete instrument has Kraus operators $M_{r\alpha}(z)$, with the sum over all retained records and unobserved alternatives satisfying completeness. A declared extension to a joint configuration register uses

$$\mathsf{M}_{r\alpha} = \sum_z |z\rangle\langle z| \otimes M_{r\alpha}(z). \qquad \text{(VIII.1)}$$

This coherent register, its diagonal action and its alignment of Kraus amplitudes across different configurations are additional hypotheses. They are not returned merely by the fixed-field instrument. The conditioned state is the corresponding completely positive output divided by its trace. Completeness gives, for every configuration observable $F_f = \sum_z f\,(z)|z\rangle\langle z| \otimes I$,

$$\mathcal{E}^*(F_f) = F_f. \qquad \text{(VIII.2)}$$

Thus nonselective configuration populations are unchanged for every joint input state, while conditioned populations can change as information arrives. Repeated conditioned expectations are martingales under this diagonal extension. Field coherences can also change; the result is not a statement that quantum measurement has no disturbance.

There is a further reconstruction ambiguity. Multiplying every fixed-configuration Kraus operator by the same phase $e^{i\vartheta(z)}$ leaves that entire fixed-field instrument unchanged but conjugates the coherent configuration output by $\sum_z e^{i\vartheta(z)}\,|z\rangle\langle z|$. A gauge-invariant Wilson-character phase provides an admissible covariance example. This does not authorize alteration of an already specified global coherent source: it identifies information that the family of fixed-field completely positive maps does not supply. [A29, §23]

The archived finite execution uses three diagnostic weak/hypercharge configurations and the 50-dimensional internal carrier, hence a 150-dimensional joint state. It includes 595 retained outcomes in a complete opportunity instrument. Populations remain unchanged to 5.56×10^{-17}, while phase-related coherent outputs have trace distance 0.00691004136. An independent explicit-Kraus calculation verifies completeness and the population invariant. These are mechanism checks on the declared extension, not a physical transition law, a first-Fact process or a new coupling result.

VIII.2 Temporal transport around a swept boundary

The K = 7 Wilson Limit already writes spatial and temporal Wilson costs on the inherited holonomy carrier. Its locality, finite propagation scale, one-tick update and closure-covariance premises are source inputs to the present construction. The Closure Symmetry paper's bare spatial–temporal coefficient equality retains feature-matching and minimality conditions; its labelled chain-complex realization remains open in §10(L1). [P37–P38]

Use a finite spatial complex with edge-by-vertex gradient B, face-by-edge incidence D and $DB = 0$. Link phases form an edge torus, with gauge equivalence $\theta \sim \theta + B\alpha$. The spatial cost is

$$S_s(\theta) = \sum_p \beta_{s,p}\,[1 - \cos(D\theta)_p]. \qquad \text{(VIII.3)}$$

Assume a reflection-compatible temporal slab whose channels sweep oriented spatial chains. Let the integer matrix C_t record those chains and let ϕ be temporal vertex-link phases. Multiplication around the swept boundary gives

$$F_t = C_t(\theta' - \theta - B\phi) \pmod{2\pi}, \qquad S_t = \sum_r \beta_{t,r}\,[1 - \cos(F_t)_r]. \qquad \text{(VIII.4)}$$

Independent endpoint gauges are compensated by $\phi \mapsto \phi + \alpha' - \alpha$. The matrix C_t is a temporal incidence map, distinct from the bath couplings and covariance matrices used elsewhere in this paper. The swept-chain form itself must be established on the physical slab. A more general slab can require distinct top and bottom maps or additional variables. Fourteen channels do not by themselves determine those boundaries, and the twelve-edge/six-face diagnostic wheel is not assigned to them by counting.

VIII.3 The operation between configurations

Take the stated Wilson ensemble with product normalized Haar measure. Write $\delta = \theta' - \theta$ and

$$w_{C_t}(\delta) = \exp\left[\sum_r \beta_{t,r}\cos(C_t\delta)_r\right], \qquad c_0 = \int d\delta\, w_{C_t}(\delta). \qquad \text{(VIII.5)}$$

The field-independent temporal action constant has been removed. Integrating the temporal gauge variables yields

$$Q_{C_t}(\theta',\theta) = c_0^{-1}\int d\phi\, w_{C_t}(\theta' - \theta - B\phi). \qquad \text{(VIII.6)}$$

Translation invariance gives unit integral over θ'. Splitting each spatial slice action equally between its adjoining slabs then gives the transfer

$$T_{C_t}(\theta',\theta) = e^{-S_s(\theta')/2} Q_{C_t}(\theta',\theta) e^{-S_s(\theta)/2}. \qquad \text{(VIII.7)}$$

Multiplication and integration over intermediate slices reproduce one copy of every interior spatial action and one copy of every temporal action, with endpoint half-weights. This derives the operation directly from the declared history weight. For finite coefficients in this unmasked compact ensemble, its kernel is positive between distinct gauge configurations. Additional source admissibility restrictions, matter and records must be retained when present.

The operator acts on amplitudes by integration against T_{C_t}. The existing Perron/Doob normalization also represents its positive history law as a normalized chain, but that construction does not identify a slab with one completed Fact. This is initially Euclidean transfer. Its relation to the source's operational kinetic law, causal propagation and physical commitment clock remains part of the physical attachment.

VIII.4 The temporal map selects the electric flux spectrum

The character expansion $e^{\beta \cos u} = \sum_{m\in\mathbb{Z}} I_m(\beta) e^{imu}$ gives the exact Fourier coefficients

$$c_n = \sum_{m\in\mathbb{Z}^R:\, C_t^T m = n} \prod_r I_{m_r}(\beta_{t,r}). \qquad \text{(VIII.8)}$$

For strictly positive temporal coefficients, each Bessel factor is positive and the series is absolutely convergent. Gauge integration projects onto divergence-free integer electric fluxes. On the character $e^{in\cdot\theta}$,

$$q_n = (c_n/c_0)\, \mathbf{1}_{B^T n=0}. \qquad \text{(VIII.9)}$$

The kinetic operator is positive. On the full pure-field gauge-invariant Hilbert space it has no null vector precisely when

$$\ker(B^T) \cap \mathbb{Z}^E \;\subseteq\; C_t^T \mathbb{Z}^R. \qquad \text{(VIII.10)}$$

This integer-lattice condition is stronger than a real rank test. A positive pointwise kernel can still annihilate entire electric-flux characters if their indices are absent from that lattice. Multiplication by the bounded positive spatial half-weights preserves the presence or absence of an operator nullspace. [A29, §24.3; M10]

When (VIII.10) holds, the spectral logarithm defines the bare Hamiltonian, with its vacuum energy removed:

$$H_{C_t} = -a_t^{-1} \log\big(T_{C_t}/\lambda_0\big), \qquad U_{C_t}(t) = e^{-itH_{C_t}} \quad (\hbar = 1). \qquad \text{(VIII.11)}$$

This is a self-adjoint, possibly unbounded operator. If nulls remain, taking this logarithm on the whole original physical space is not justified. A source-selected support restriction would require its own argument. The standard positive-transfer construction supplies the mathematical reconstruction, not a proof that the resulting bare operator is the complete physical VERSF generator. [M9]

For the special realization $C_t = I$, the kinetic eigenvalues reduce to $\prod_e I_{n_e}(\beta_{t,e})/I_0(\beta_{t,e})$. This is a useful exact specialization, not a derivation of the fourteen-channel assignment. With nonconstant spatial cost, the logarithm of the full sandwich in (VIII.7) is generally not the sum of the kinetic logarithm and S_s/a_t at finite spacing.

VIII.5 The force from the same temporal action

A local classical force follows on a justified temporal-continuum or leading-derivative branch. Take $a_t\beta_{t,r} \to i_r > 0$ and $\beta_{s,p}/a_t \to \kappa_p$, or retain their corresponding finite-regulator leading coefficients with that restricted interpretation. Expanding the temporal holonomy about a smooth branch produces

$$\mathcal{I} = C_t^T \operatorname{diag}(i_r) C_t, \qquad V(\theta) = \sum_p \kappa_p \left[1 - \cos(D\theta)_p\right]. \qquad \text{(VIII.12)}$$

The inertia is therefore a pullback of the temporal action, rather than an independently assigned metric. The branch must have a nondegenerate physical kinetic form after its constraints are handled and no unresolved extra zero-cost compact sectors. On a branch admitting the transfer-to-real-time identification, the classical Lagrangian is

$$L = 1/2\,\big(\dot\theta - BA_0\big)^T \mathcal{I}\big(\dot\theta - BA_0\big) - V(\theta). \qquad \text{(VIII.13)}$$

Variation with respect to A_0 gives the Gauss constraint. In temporal gauge the force is

$$\Pi = \mathcal{I}\dot\theta, \qquad \dot\Pi = -D^T \operatorname{diag}(\kappa_p)\sin(D\theta), \qquad B^T\Pi = 0. \qquad \text{(VIII.14)}$$

The identity $DB = 0$ shows that this force preserves the constraint. Direct differentiation shows conservation of $1/2\,\dot\theta^T \mathcal{I}\dot\theta + V$. The flat-field stiffness $D^T\operatorname{diag}(\kappa_p)D$ is positive semidefinite; physical nulls are not assigned artificial restoring forces. Inverting $\mathcal{I}$ requires the actual constrained reduction, not a chosen Euclidean transverse projection.

For uniform coefficients and $C_t = I$, the leading equation is $\ddot{\theta} = -\beta_s D^T \sin(D\theta)/\left(\beta_t a_t^2\right)$. The Bessel asymptotic $\log[I_n(\beta)/I_0(\beta)] = -n^2/(2\beta) + O(\beta^{-2})$ independently recovers the same kinetic inertia at fixed electric-flux index. These are low-frequency or temporal-continuum statements. At the primitive finite tick, (VIII.7) and its admitted logarithm remain the specified operation. The Euclidean Euler–Lagrange potential sign must not be passed off as the real-time restoring sign. [A29, §24.4; M10]

VIII.6 Primitive normalization and the remaining physical attachment

The interface BCN result in §VII.5 is retained. If its source identification applies to the temporal channel,

$$\beta_t = \frac{\ln 2}{1 - \cos\left(2\pi/N_\phi\right)}, \qquad \frac{w\left(2\pi/N_\phi\right)}{w(0)} = \frac{1}{2}. \qquad \text{(VIII.15)}$$

This constrains the magnitude after that identification; it is not an arbitrary continuous coefficient once BCN and the phase resolution are supplied. The source distinguishes N_ϕ from $K = 7$ and the fourteen loop channels. Their connection is not supplied by replacing one count with another. A finite cyclic link realization replaces the integrals with finite sums, but finite face-record capacity alone does not select that link regulator. [P20]

The later fixed Wilson convention $\beta = 1/g^2$ is also preserved. The older Wilson-limit paper uses its β_{K7} both as a plaquette coefficient and as inverse fine-structure constant. Under the retained convention, the latter equals $4\pi\beta$. That older numerical symbol is therefore not inserted into this normalized operator without reconciliation. No generator rescaling or measured coupling is used to repair the source.

The construction returns a definite operation and force conditional on the source action, temporal incidence and physical clock attachment. It does not yet return the physical C_t, complete same-order matter/current/record contributions or their identification with the existing HMGBC operational heat. That identification must avoid double counting. The coordinate parameter and slab spacing here retain the inherited sequential-source meaning; the derivation does not supply an independent clock calibration or identify every reversible slab with an irreversible Fact. These specific dependencies remain open without invalidating the earlier conditional constructions or establishing programme-wide nonselection.

The construction returns an operation and force conditional on the temporal action, incidence and clock. Part IX supplies support and canonical-marginal comparisons: uniform independent edges pass uniquely within the diagonal edge class, while the physical marginal remains unselected. Part X gives source-listed propagation and commitment-progress operations with separate attachment obligations. The matter, current and record terms at the same order must be joined to HMGBC without double counting. A reversible slab is not automatically a completed Fact.

Part IX Temporal identification and the limits of reconstruction

The temporal comparison consists of explicit support, covariance, normalization and history tests. A unique independent-edge quadratic realization passes on the canonical marginal branch. That marginal and its clock remain physically unselected, and a complete one-tick Wilson law does not select a history law with unresolved memory. The following propositions retain these qualifications. The source audit and calculations are recorded in [A30–A35].

IX.1 Integer support and the sevenfold quotient

Fix the twelve-edge wheel, with edge-by-vertex incidence B and six triangle-cycle columns Z. Write $x = Z^T\theta$ and $C = Z^T$. Use $Se_i = e_{i+1}$ with indices modulo six. The chiral attachment is $A_{ch} = S^3 - I - S$ and the integer null vector below is h. The triangle cycles form a primitive integer basis of the cycle lattice. The exact invariants are

$$\mathrm{SNF}(Z) = (1,1,1,1,1,1), \qquad \mathrm{SNF}(A_{ch}) = (1,1,1,1,1,7). \qquad \text{(IX.1)}$$

For the candidate chiral temporal map $C_{ch} = A_{ch}^T Z^T$, the supported cycle-flux labels satisfy

$$k \in A_{ch}\mathbb{Z}^6 \quad \Leftrightarrow \quad h^T k = 0 \ (\mathrm{mod}\ 7), \qquad h = (5,4,6,2,3,1)^T. \qquad \text{(IX.2)}$$

Here $A_{ch}^T h = 0$ modulo seven. Thus the chiral kernel annihilates six charged coset spans. It cannot equal an injective heat transfer on the unrestricted physical torus, regardless of local Gaussian agreement. The quotient variables $y = A_{ch}^T x$ instead identify the seven equivalent peaks. For neutral k, the unique integer preimage $m = A_{ch}^{-1} k$ gives the exact eigenvalue

$$q_k = \prod_{j=1}^{6} \frac{I_{m_j}(\beta_{t,j})}{I_0(\beta_{t,j})}. \qquad \text{(IX.3)}$$

This is a six-rotor operation on the quotient. It is not yet a source-selected physical quotient. A different orientation convention transforms both the cycle coordinates and the charge vector; numerical charge labels must not be mixed across conventions.

For a spatial Wilson action with strictly positive face coefficients, preservation of this charge decomposition by the full sandwich requires every active spatial face to be neutral. In cycle coordinates c_p, the test is $h^T c_p = 0$ modulo seven. Chiral attached faces satisfy it; bare triangles do not. The physical observable algebra and other coupled operations must satisfy the corresponding requirement too. A charged spatial face destroys this particular decomposition, not every possible sector structure. Real-space admissibility, occupied-carrier support and integer Fourier support are different objects.

IX.2 The canonical covariance match and its rigidity

The full HMGBC kinetic operator includes resolved configuration directions; the endpoint matter operator alone does not classify it. The comparison therefore uses the operational link marginal, after all admitted coupled directions are handled. If P_x maps the resolved tangent to triangle holonomies, its per-tick covariance and precision are

$$\Sigma_x = a_t P_x G_{\mathrm{phys}}^{-1} P_x^T, \qquad K_x = \Sigma_x^{-1}. \qquad \text{(IX.4)}$$

Restricting the precision block before inversion gives a conditional law, not this marginal. At the explicit canonical choice $G_{\mathrm{op}} = I_{187}$, the wheel block reduces to $\Sigma_x = a_t G$, where

$$G = Z^T Z = 3I - S - S^T, \qquad \mathrm{spec}G = \{1,2,2,4,4,5\}. \qquad \text{(IX.5)}$$

The table compares quadratic precisions with the canonical target G^{-1}, with the common temporal coefficient omitted. The final row is normalized by its smallest ratio. These are Gaussian-order shape tests, not equality of finite-tick compact kernels with Gaussian laws.

Temporal construction	Generalized precision ratios	Canonical verdict
Independent triangle rotors	$1,2,2,4,4,5$	Fails shape

Temporal construction	Generalized precision ratios	Canonical verdict
Composite chiral cell rotors	$1,4,4,5,14,14$	Fails shape; also fails unrestricted injectivity
Uniform independent edges with Gauss reduction	$1,1,1,1,1,1$	Passes shape
Equal-weight additive chiral-cell incidences	$1,8/7,8/7,16/13,16/13,5/4$	Fails shape

Indeed, independent edge increments with positive diagonal precision W induce covariance $\beta_t^{-1} Z^T W^{-1} Z$. Uniform W gives the passing row. For equal cell weights, shared incidences give spoke weight four and rim weight three, so

$$Z^T W^{-1} Z = \frac{10I - 3S - 3S^T}{12}. \qquad \text{(IX.6)}$$

Diagonal rigidity proposition. If $Z^T \operatorname{diag}(u) Z = cZ^T Z$ on this wheel, then all twelve $u_e = c$. Adjacent off-diagonal entries determine each shared spoke weight as c. Each diagonal then determines the remaining rim weight as c. Uniform independent edges uniquely pass within the positive diagonal edge class. Whole-cell rescaling cannot repair the four-versus-three sharing imbalance; incidence-specific compensation would be an additional source choice.

Cyclic invariance alone permits fourteen real symmetric edge-covariance parameters. The map $\Sigma \mapsto Z^T \Sigma Z$ has rank four on that space. Fixing the canonical cycle marginal fixes those four observable parameters while leaving ten directions with $P_c \Delta\Sigma P_c = 0$, where P_c projects to cycle space. These are invisible to this Gaussian gauge-invariant marginal. They are not ten additional Gaussian field laws on the quotient. Neither result selects the physical marginal in (IX.4). [A31, §2]

IX.3 What the channel count and normalization do not select

The retrieved Wilson action displays a common temporal coefficient, without the incidence-specific compensation required by the additive cell reading. The earlier proposed identification of fourteen with twice a chiral heptagon length is therefore not established. A count of ten hinges plus four closure modes does not itself resolve orientation pairing or produce boundary words. The surviving canonical edge construction is a mathematical identification within its class; it is not an assignment of the source's fourteen channels. The boundary words and the update-register granularity remain source questions. [P37; A30, §8J.F]

Under the declared quadratic conventions, coefficient matching requires $v\beta_t = 1$, where v is the covariance scale per physical tick in those coordinates. If BCN also attaches to this temporal coefficient, then

$$v = \frac{1 - \cos(2\pi/N_\phi)}{\ln 2}, \qquad N(v) = \frac{2\pi}{\arccos(1 - v\ln 2)}. \qquad \text{(IX.7)}$$

The inverse applies for $0 < v \le 2/\ln 2$. An independently fixed v must yield an admitted integer $N_\phi \ge 2$ under this exact identification. For every such integer the numerator in (IX.7) is nonzero algebraic, while $\ln 2$ is transcendental; consequently v is transcendental. This is a conditional exact obstruction, not a rejection based on rounded values or approximate low-order agreement.

For illustration, $\beta(14) = 6.999285637540212 \ldots$ and $N(1/7) = 14.000726654890887 \ldots$. Neither equals the nearby integer. A finite Wilson variance is also not exactly $1/\beta_t$; the identity concerns the stated quadratic coefficient. The physical marginal, alphabet and clock-to-proposal attachment remain unselected.

IX.4 Character tests and their limits

For a controlled kinetic increment define $q_m = \langle e^{im\Delta x} \rangle$ and $D_m = \ln|q_m| - m^2 \ln|q_1|$. Wrapped Gaussian increments, including drift, give $D_m = 0$. For one independent Wilson edge,

$$q_m = \frac{I_{|m|}(\beta)}{I_0(\beta)}, \qquad D_2 = \ln\frac{I_2(\beta)}{I_0(\beta)} - 4\ln\frac{I_1(\beta)}{I_0(\beta)}. \qquad \text{(IX.8)}$$

The exact D_2 is positive and strictly decreasing from infinity to zero, so it identifies a unique parameter within the Wilson family. On a triangle with independent unit-incidence edges it is multiplied by three, and its large-β expansion is $3/(2\beta^3) + 9/(2\beta^4) + O(\beta^{-5})$. The terms proportional to m^2 at orders β^{-1} and β^{-2} cancel in the ladder. At $\beta(14)$ the exact triangle value is 0.00727841301150883 ...; the leading asymptotic alone is inadequate. A positive value by itself does not identify the Wilson family.

For a circle convolution semigroup with symmetric jump measure ν, after removing drift through character magnitudes,

$$D_2 = 2t\int (1-c)^2 d\nu, \quad D_3 = 4t\int (1-c)^2(2+c)d\nu, \quad c = \cos\theta. \qquad \text{(IX.9)}$$

The fourth-character kernel is

$$D_4 = 8t\int (1-c)^2(c^2+2c+2)\, d\nu, \qquad c = \cos\theta. \qquad \text{(IX.9a)}$$

Writing $r = D_3/D_2$ and $s = D_4/D_2$ when $D_2 > 0$ gives the necessary moment tests

$$2 \le r < 6, \qquad r^2 - 4r + 8 \le s \le 4r - 4. \qquad \text{(IX.10)}$$

The upper value six is a sharp supremum for a nonzero admissible jump measure. Passing these finite tests does not prove embedding; failing them excludes the specified memoryless embeddable class under the measurement controls. It does not establish a fundamental discrete clock. Four characters do not reconstruct an unrestricted jump measure, drift, cross-edge correlations or a joint field instrument. [A31, §§3–6]

Report both edge incidence and tick aggregation. Extensivity holds for independent identical edges and increments; shared backgrounds require the actual joint projection. Isolate the kinetic kick from spatial half-weights and matter terms, and condition on accessible background variables. A variance mixture can produce a positive ladder even though every conditioned increment is Gaussian.

IX.5 An explicit Wilson embedding and temporal nonuniqueness

The Hartman–Watson representation gives a positive variance law μ_β with

$$\int_0^\infty e^{-m^2 t/2}\,\mu_\beta(dt) = \frac{I_{|m|}(\beta)}{I_0(\beta)}. \qquad \text{(IX.11)}$$

Its infinite divisibility supplies the convolution embedding with characters $[I_m(\beta)/I_0(\beta)]^t$. On independent edges its generator acts on the torus character $\mathcal{E}_n(\theta) = e^{in\cdot\theta}$ as

$$\mathcal{L}_\beta \mathcal{E}_n = -\left[\sum_e \ln\frac{I_0(\beta)}{I_{n_e}(\beta)}\right]\mathcal{E}_n, \qquad B^{\mathsf{T}} n = 0. \qquad \text{(IX.12)}$$

This is an explicit mathematical evolution for the assumed Wilson law. At fixed finite β, its exponent grows as $m\ln m + O(m)$, so its Brownian coefficient is zero and its jump activity is infinite. The large-β Gaussian approximation does not identify a Brownian component at finite β. The Wilson tail is heavier than a Gaussian tail. Wilson itself is a particular wrapped Gaussian variance mixture; those two descriptions are not competing field-law classes. [A31, §5]

Finite-sector nonuniqueness theorem. The entire stationary one-tick Wilson law, conditional local precision and principal-angle variance can remain fixed while two-tick laws vary. The explicit construction [A32, §§4–6] uses positive densities $Q_{\pm,\epsilon} = \nu_\beta \pm \epsilon d$ with zero integral and zero second-moment perturbation, and $d''(0) = -\beta d(0)$. These conditions preserve the peak precision and variance. A two-state environment has transition matrix K with diagonal $1-p$ and off-diagonal p, where $0 < p < 1/2$; set $A = K^{1/2}$ and $u = (1,1)^T/\sqrt{2}$. Its Fourier blocks satisfy

$$T_{m,\epsilon} = A\mathrm{diag}(q_m + \epsilon h_m, q_m - \epsilon h_m)A,$$
$$u^T T_{m,\epsilon} u = q_m, \qquad \text{(IX.13)}$$
$$u^T T_{m,\epsilon}^2 u = q_m^2 + (1-2p)\epsilon^2 h_m^2. \qquad \text{(IX.14)}$$

The archive supplies explicit nonzero d and bounds ensuring pointwise and spectral positivity and injectivity. Independent edge copies respect the wheel symmetry, and gauge-invariant two-tick loop characters distinguish the models. This proves nonuniqueness under that finite-sector freeze. It does not prove that two complete models satisfy every VERSF primitive or that every fractional power is a physical Markov transfer. Even all single-tick characters cannot select unresolved temporal coupling.

IX.6 The corrected scope of the mechanism exclusions

Configuration-controlled maps are closed under composition, branch adaptation and convergent sums. They cannot transfer population between their fixed configuration blocks. Individual outcomes can still reweight populations by Bayesian conditioning; normalized conditioned populations are not generally invariant. A stopped sum such as $\mathcal{J}_r \sum_{n\geq 0} \mathcal{N}^n$ remains in the controlled class when well-defined. Neither this theorem nor §VIII.1 excludes physical interactions outside that class or history-dependent changes of the carrier. [A34]

The source semidirect composition is $(U_2, j_2)(U_1, j_1) = (U_2 U_1, j_2 + U_2 j_1)$. Compatible subdivision factorizes this operation and preserves inherited loop products; it does not itself deform a field. Writing a general update as left multiplication is algebraically always possible and selects a homogeneous kick law only with an additional configuration-independence premise. The closure-relaxation core $(I + S)^T (I + S)$ has an alternating zero mode and, on the zero-sum subspace, decay-rate pattern $\{0, r, r, 3r, 3r\}$. That deterministic transport alone cannot supply the positive-definite canonical fluctuation law. [A34]

For accumulation of iid elementary kicks with Fourier coefficients η_m and a stopping count independent of those kicks, $q_m = \mathbb{E}[\eta_m^N]$ and $N \geq 1$ imply $|q_m| \leq |\eta_m|$. That tail obstruction does not extend unchanged to field-correlated stopping. Finite positive reweighting cannot make an exactly absorbing set out of a strictly positive kernel. The executed sharp-arc and one-way-formation miniatures reject their specified implementations, not conditioning as a universal mechanism class. Sharp support in an append-only record ledger does not require a sharp boundary in the visible field increment density. [A34]

Finally, admissibility filters require operation-specific theorems. For normalized postselection $\rho \mapsto W\rho W / \mathrm{Tr}(W^2 \rho)$, preserving every probability of a POVM containing a nonscalar effect forces positive W to be scalar; commutation alone is insufficient. For an unread binary Lüders filter, preservation is equivalent to commutation with the effects. A general soft joint refinement can preserve the old terminal marginal without that restriction. The computed commutator gaps concern the frozen normalized effects, not universal physical stiffness or disturbance rates. [A33, §§7–9]

A resolved operation has polar form $K_a = V_a \sqrt{E_a}$, but coarse record outcomes generally require several Kraus operators. Their effect and conditional output are constrained parts of a CP instrument, not independently observable unrestricted dials. Subsequent field measurements can detect backaction after one event, while terminal-only histories may reveal it later. The character ladder depends on both branch weights and branch motion. These corrections prevent the earlier restricted exclusions from becoming a claim that the corpus contains no possible dynamics. [A33, §10]

Part X Commitment progress and the physical clock

The source places commitment at completed admissible closure. Commitment at completed admissible closure is explicitly primitive, and several propagation, receiving-interaction and renewal constructions are supplied. The task is to select and join those constructions on one physical carrier, with consistent units and an explicit independent-field output. The audit [A30] indexes 118 supplied PDFs, 113 distinct texts and 4,953 pages, with targeted reading and stated verification limits.

X.1 What commitment already means in the supplied primitives

Axiom FC states that completed admissible closure produces one persistent Fact. It supplies occurrence and persistence at the completed-record boundary; it does not independently fix the approach to that boundary, incident coupling, branch phase, numerical coefficient or field destination. It must not be strengthened into a biconditional without the separate pre-factual reversibility premises. The earlier demand for an extra coefficient that makes commitment itself occur is retired. [P39, Part LIX, §28; A30, §2]

On the supplied binary active plane, branch-preserving record write and renewal compose to

$$\mathcal{J}_a(\rho) = \mathrm{Tr}(P_a\rho)\, P_a \otimes |a\rangle\langle a|_L. \qquad \text{(X.1)}$$

Here the ledger records the allowed alternative and retains the past prefix. The probabilities are a valid stochastic law; no deterministic winner rule is required. This internal/ledger operation does not, by itself, assign the output of independent links and currents. The source also supplies constructions that change active support while preserving past records. Their source-dependent carrier maps and pullback tests must be checked at the stage where the support restriction acts. [A30, §§3, 8F]

The actual target is therefore a normalized joint operation on (z, κ, h), where z contains independent fields, κ denotes the commitment/support state in this paragraph, and h the retained history. This use of κ must not be confused with the continuum scalar below. The operation must state how an arrival changes progress or occurrence, how the completed record is retained, and where the fields go next.

X.2 Source-listed propagation and force

The scalar-action papers explicitly provide commitment-sourced causal dynamics. With metric signature $(-,+,+,+)$ and $\square_g = \nabla_\mu\nabla^\mu$,

$$S_\kappa = \int dV_g \left[-\frac{1}{2}(\nabla\kappa)^2 - \frac{1}{2}m_\kappa^2\kappa^2 + \kappa\rho\right],$$
$$\left(\square_g - m_\kappa^2\right)\kappa = -\rho. \qquad \text{(X.2)}$$

For $\mathcal{D} = -\square_g + m_\kappa^2$, a retarded inverse gives $\kappa = \kappa_{\mathrm{hom}} + G_{\mathrm{ret}} * \rho$. An event source increment $q_n\delta_g(x, x_n)$ produces $q_n G_{\mathrm{ret}}(x, x_n)$ once its source profile and continuum dictionary are supplied. On Fact-Momentum's canonical scalar branch, one Fact has unit source weight; Part XI executes the corresponding projection and response. The source relation $m_\kappa^2 = 4/(3\xi^2)$ retains its model assumptions. A finite front speed constrains causal propagation; a massive response generally also has support inside the light cone. It does not imply that every arrival completes a receiving Fold. [A30, §8A; P40]

Fact-Momentum independently returns a scalar force after correcting its action/equation sign convention. For static persistent sources Q_a, the supplied positive-kinetic scalar action gives

$$E_{\mathrm{int}} = -\sum_{a<b} \frac{Q_a Q_b e^{-m r_{ab}}}{4\pi r_{ab}},$$
$$\mathbf{F}_a = -\sum_{b\neq a} \frac{Q_a Q_b (1 + m r_{ab}) e^{-m r_{ab}}}{4\pi r_{ab}^2}\hat{\mathbf{r}}_{ab}. \qquad \text{(X.3)}$$

The unit vector points from b to a, so equal-sign static sources attract. This is a genuine conditional force-law return. Fact-Momentum's written normalization sets source weight equal to committed count. The mechanical response, source profile and map to microscopic Fold and gauge/current variables remain to be physically attached; see Part XI. A quadratic scalar action yields pair cross-terms, not an irreducible three-body potential. [P41; A30, §8C]

A separate interface model supplies $H = \sum_n p_n^2/(2\kappa) + J\sum_{\langle nm\rangle}[1 - \cos(\varphi_n - \varphi_m)]$ with its additional core terms. Its smooth phase force is $\dot{p}_n = -J\sum_{m\sim n}\sin(\varphi_n - \varphi_m)$. The constants and carrier are declared inputs. Endpoint phase differences alone define a pure-gauge link field and do not generate independent loop curvature; their attachment to the receiving increment remains separate. [P47; A30, §8J.D]

The oscillatory receiving model also has a valid conditional Volterra reduction. Its sine Green kernel and a derivative/cosine replacement are different operators; the latter cannot substitute without changing the equation and initial data. The audited primary small-coupling decay shift is positive on both sides of equal damping, so the proposed sign reversal does not follow. Amplitude, survival probability and normalized event hazard must remain distinct. [A30, §§8A–8D]

X.3 The occurrence rate and its receiving susceptibility

Theory of Fact Production lists the candidate rate

$$\lambda_F = r_{\mathrm{att}}c_{\mathrm{free}}e^{-b/\Phi},$$
$$D\ln\lambda_F = D\ln r_{\mathrm{att}} + D\ln c_{\mathrm{free}} - \frac{Db}{\Phi} + \frac{bD\Phi}{\Phi^2}. \qquad \text{(X.4)}$$

The attempt rate has inverse-time units; the remaining displayed factors are dimensionless in this convention. The environmental-entropy drive is $\Phi = (\Delta S_E/k_B)/\ln 2$. For a controlled deterministic interval exposure $\Lambda = \int \lambda_F dt$, the no-event probability is $e^{-\Lambda}$. If recorded types have fixed conditional probabilities q_a on that interval,

$$p_0 = e^{-\Lambda}, \qquad p_a = (1 - e^{-\Lambda})q_a. \qquad \text{(X.5)}$$

Thus unchanged relative outcome weights do not imply unchanged commitment occurrence. If type ratios vary during the interval, the type probabilities require their hazard-weighted time integrals. A random history-dependent intensity likewise requires its conditional survival construction rather than exponentiating an unconditional mean. [P42; A30, §§8C, 8I]

At a symmetric drive minimum with positive Φ_0, fixed b, attempt and capacity factors, the Hessian is $D^2\Lambda = \Lambda_0 bD^2\Phi/\Phi_0^2$. It can be compared with the source's quadratic occurrence witness on the same carrier and clock. In contrast, $\Phi = \alpha j^2$ with zero baseline gives $e^{-b/(\alpha j^2)}$, extended by zero at $j = 0$, whose derivatives all vanish there. It cannot supply a nonzero quadratic witness under those frozen premises. A strict eligibility threshold additionally requires an admissibility indicator; a smooth positive template below a forbidden threshold is not an allowed completed-event rate.

X.4 Effective ticks and recurrent events

TPB Reaction Rate supplies an effective nonnegative progress process: a tick contributes $X_i \geq 0$, accumulated progress is $S_n = \sum_{i=1}^n X_i$, and completion is first passage to one. The increment distribution is an explicit microscopic input. For iid increments with finite positive mean μ and overshoot $O = S_N - 1$,

$$N = \inf\{n : S_n \geq 1\}, \qquad \mathbb{E}N = \frac{1 + \mathbb{E}O}{\mu}. \qquad \text{(X.6)}$$

Independent Poisson opportunities of rate ν give $\mathbb{E}T = \mathbb{E}N/\nu$. The reciprocal mean is a long-run renewal rate under the renewal premises, not a general instantaneous hazard. The mean increment alone does not determine TPB: deterministic increments $2/5$ give $N = 3$, while Bernoulli unit increments of probability $2/5$ give mean $N = 5/2$. [P43; A30, §8J]

The later K7 renewal construction gives a normalized recurrent instrument with three stage-success probabilities and a record-preserving reset. At the explicitly benchmark choice $p = 1 - e^{-1}$ for all three stages, the mean is $3/p = 4.745930120607979$ opportunities and the reciprocal is 0.21070685294285256. These are model values, not a derived physical clock. [P44]

The archived first-entry mean 1.2346022499349605 and first closed-cover mean 21.27768295091855 belong to different stopping events. The receiving-phase audit reconstructs both and shows that internal-only evolution does not change the frozen scalar history-transition effects. The tested native phase commutes with the completion effects. This closes that particular timing route; an incident-dependent change of progress, history effects or support remains possible. [A30, §8H; A35]

X.5 A concrete incoming contact and its exact amplification

Paths to Folds supplies the pair interaction $U(\theta) = \exp(i\theta Z_S \otimes Z_E)$, with $\theta = \hbar^{-1} \int g(t)dt$. Combining it with the environmental-entropy definition of amplification gives a concrete contact-to-progress candidate. Treating the neighbouring Fold as the receiver's environmental pointer is an explicit cross-paper identification. Ordered Records and Realised Event States does not admit this interaction as a selected primitive phase source. The result below is therefore an exact conditional construction, not a primitive-uniqueness theorem. [P45, p. 13; P46, p. 13; A30, §8L]

Let the receiver be pure, with Z_S probabilities p and $1 - p$, initially uncorrelated with

$$\rho_E = 1/2\left(I + r_x X + r_y Y + r_z Z\right), \quad r = |\mathbf{r}| \leq 1, \quad r_\perp^2 = r_x^2 + r_y^2. \qquad \text{(X.7)}$$

The two conditional neighbour states are $\rho_{E,\pm} = e^{\pm i\theta Z} \rho_E e^{\mp i\theta Z}$. Their trace distance and the multiplier of the receiver's off-diagonal element are

$$D_E^2 = r_\perp^2 \sin^2(2\theta), \qquad \zeta = \cos(2\theta) + i r_z \sin(2\theta). \qquad \text{(X.8)}$$

Receiver orientation populations remain unchanged. The final averaged environmental Bloch radius is

$$r' = \sqrt{r^2 - 4p(1-p) r_\perp^2 \sin^2(2\theta)}. \qquad \text{(X.9)}$$

With natural binary entropy $h_2(x) = -x\ln x - (1-x)\ln(1-x)$, the source-defined amplification is exactly

$$a := \frac{\Delta S_E}{k_B} = h_2\left(\frac{1+r'}{2}\right) - h_2\left(\frac{1+r}{2}\right) \geq 0. \qquad \text{(X.10)}$$

Its physical dependence is on coupling and preparation, not a scalar ambient entropy alone. An incident field must supply the change in θ and in the relevant input state. In particular,

$$d\left(D_E^2\right) = \sin^2(2\theta) d\left(r_\perp^2\right) + 2 r_\perp^2 \sin(4\theta) d\theta. \qquad \text{(X.11)}$$

A local incoming Z phase leaves $r_\perp^2$ unchanged. It therefore does not change this pointer distinguishability merely by changing an unobserved phase convention.

There is a sharp distinction between dephasing and a readable record. At $p = 1/2$ and $\theta = \pi/8$, a pure transverse neighbour and a maximally mixed neighbour both give $\zeta = 1/\sqrt{2}$, hence $|\zeta|^2 = 1/2$. The pure neighbour gives $D_E^2 = 1/2$ and $a/\ln 2 = 0.6008760367$ bits. The maximally mixed neighbour gives $D_E = 0$ and $a = 0$. Identical receiver decoherence therefore does not establish identical environmental amplification. For a pure joint bipartite state, mutual information is twice the marginal entropy, so it cannot silently replace the source's entropy definition either.

X.6 Fresh neighbours give a derived progress rule

Now assume a fresh independent pure neighbour at every contact, the same receiver orientation observable, and no later interaction with earlier neighbours. Let z_j be the incoming neighbour's Z expectation and define

$$\epsilon_j = \left(1 - z_j^2\right)\sin^2(2\theta_j), \qquad L_n = \prod_{j=1}^{n}\left(1 - \epsilon_j\right), \quad R_n = 1 - L_n. \qquad \text{(X.12)}$$

Here L_n is the squared overlap of the two joint environmental branch states and R_n their squared trace distance. Direct multiplication of those branch overlaps proves

$$R_{n+1} = R_n + (1 - R_n)\epsilon_{n+1}. \qquad \text{(X.13)}$$

This is the contact-to-progress rule. For $\epsilon_j < 1$, an additive coordinate is

$$w_n = -\ln L_n, \qquad \Delta w_j = -\ln\left(1 - \epsilon_j\right) \geq 0. \qquad \text{(X.14)}$$

Given a specified environmental target $0 < D_* < 1$, choose $w_* = -\ln(1 - D_*^2)$ and $s_n = w_n / w_*$. Crossing $s = 1$ is exactly crossing that distinguishability target. This supplies the form of the positive TPB process in §X.4 conditional on identifying contacts with ticks and selecting the target on this environmental carrier. The source's worked criterion checks receiver branches instead and does not independently select this D_*. The first-passage formulas additionally require the stated increment-law and clock premises.

Equal contacts give equal increments of w but decreasing increments of R. Their corresponding threshold event is identical. Thus a numerical statement that ticks contribute unequally depends on the progress coordinate; physical comparisons must specify the measured quantity or completion criterion. No iid distribution is inferred from the deterministic overlap identity.

The total environmental amplification obeys

$$\frac{\Delta S_{E_{1:n}}}{k_B} = h_2\left(\frac{1 + \sqrt{1 - 4p(1-p)R_n}}{2}\right) \leq h_2(p) \leq \ln 2. \qquad \text{(X.15)}$$

This is information in the joint environment. Local accessibility, physical export and irreversible retention still require their own operation.

X.7 Reversible reuse and the one-bit threshold

If the same neighbour remains accessible and is reused coherently, the commuting phases add. For a balanced receiver and pure transverse neighbour,

$$R_n = \sin^2\left(2\sum_{j=1}^{n}\theta_j\right). \qquad \text{(X.16)}$$

Four diagnostic contacts with $\theta_j = \pi/8$ distinguish the two architectures without fitting a parameter.

Contacts	Fresh R_n	Reused R_n	Fresh amplification in bits	Reused amplification in bits
1	$1/2$	$1/2$	0.600876	0.600876
2	$3/4$	1	0.811278	1
3	$7/8$	$1/2$	0.907852	0.600876
4	$15/16$	0	0.954434	0

Opposite phases on the same accessible neighbour undo the unitary; opposite phases on different fresh neighbours do not erase their joint imprints. This concerns unfinished progress. If a persistent Fact was written at the second contact, continuing the reversible model without its retention operation would be invalid. No previously committed Fact is erased by this calculation.

The literal entropy threshold $\Delta S_E \geq k_B \ln 2$ also restricts the model. It is unreachable for $p \neq 1/2$. For $p = 1/2$, it requires $L_n = 0$, which no finite sequence with every $\epsilon_j < 1$ reaches. A perfect orthogonalizing contact, a justified tolerance or a different amplification definition is required for finite completion. Crossing a weaker distinguishability threshold alone does not satisfy all the source's commitment conditions.

Independent contacts need not produce independent averaged fragments. Two perfect copies of the same balanced bit have joint state $1/2\,|00\rangle\langle 00| + 1/2\,|11\rangle\langle 11|$: its joint entropy is one bit, while its marginal entropies sum to two. For n copies the corresponding values are one and n. The source's mode-count amplification must distinguish redundant copies from joint entropy. Increasing Φ proportionally to n already reduces b/Φ as $1/n$ at fixed b; additionally reducing b as $1/n$ requires a distinct premise and gives $1/n^2$ in that ratio. [P42, §5.7; A30, §8L.E]

Substituting (X.10) or (X.15) into $\Phi = a/\ln 2$ makes the proposed rate (X.4) state dependent on this branch. It does not select the exponential law, attempt rate, barrier, capacity factor, eligibility mask or clock. Nor does the controlled pair interaction move the independent U, j configurations.

X.8 Variable ticks and the horizon interpretation

The TPB sources permit fixed completed binary records with variable progress per opportunity. The interface account also distinguishes a proposed substrate tick density from distinguishability per tick. Counted opportunities, local proper time, an external clock and completed bits must therefore be kept separate. Variation of one ratio does not establish variation of an elementary proper-time unit. [P43, P47; A30, §8K]

On a static Schwarzschild exterior comparison, $d\tau = \alpha dt$ with $\alpha = \sqrt{1 - r_s/r}$. If the local bit rate is fixed at b_0 and an external reference counts opportunities at ν_0, then $dB/dn = b_0\alpha/\nu_0$ and the inferred external ticks per bit grow as $1/\alpha$. This is a conditional observer comparison. No massive static observer exists at the horizon, and this limit does not imply cessation of local change for an infaller.

The escalator analogy has a precise outward-propagation counterpart in the regular ingoing Painlevé–Gullstrand free-fall slicing of general relativity. With $w(r) = \sqrt{2GM/r}$,

$$ds^2 = -c^2 dt_{\mathrm{ff}}^2 + (dr + w\, dt_{\mathrm{ff}})^2, \qquad \frac{dr_{\mathrm{out}}}{dt_{\mathrm{ff}}} = c - w. \qquad \text{(X.17)}$$

Outgoing light has zero radial progress at the horizon and inward radial progress inside. A comoving infaller instead has $dr/dt_{\mathrm{ff}} = -w$ and $ds^2 = -c^2 dt_{\mathrm{ff}}^2$: local proper time continues. This is a GR comparison, not a derivation of the VERSF coupling or a literal flowing medium. The source horizon restrictions concern external accessibility and the admitted boundary. [A30, §8K; M11]

The proposed horizon normalization cannot yet calibrate (X.14). One binary bit per $4\ell_P^2$ gives $S/k_B = A\ln 2/\left(4\ell_P^2\right)$, whereas the standard area expression is $A/\left(4\ell_P^2\right)$. Matching them would require $4\ln 2\ \ell_P^2$ per binary bit, not an unchanged coefficient under unit conversion. The source's graph-distance condition also does not force quarter density: a square-lattice checkerboard has density one half and no adjacent selected sites. The gravity constitutive law requires an additional source relation, and its printed potential and force signs need reconciliation. These are separate repairs, not evidence that all TPB or horizon reasoning fails. [A30, §8K.D–F; P48]

X.9 Verification and the remaining physical selection

The contact formulas were checked by 64 seeded direct four-dimensional unitary evolutions and partial traces, including mixed incoming states. The maximum entropy residual was 4.11×10^{-15}; population, coherence, trace-distance and normalization residuals were below 4.45×10^{-16}. Independent explicit fresh-environment branch vectors verified the joint entropy to 2.78×10^{-16}. The fresh/reused sequence and redundant-copy counterexample were also evaluated directly. These checks are grade N. The executable and complete output are embedded in [A30, final appendix].

The next selection must fix incoming preparation and coupling, export or reuse of earlier contacts, the completed-closure criterion and joint record/current/link output. FC supplies commitment at the admitted boundary. Part XI fixes the scalar count normalization and executes the unit-event response on a stated K7 benchmark; its physical operator, profile and independent-field attachment remain to be selected.

The source-listed scalar dynamics and conditional progress operation are explicit. Their physical composition remains subject to the temporal and history gates of Part IX.

Part XI Unit Fact response on the K7 scalar branch

The source-count normalization is used to calculate a concrete field response. Fact-Momentum assigns one source unit to one committed Fact on its written canonical scalar branch. Exact projection then determines the impulse covector, and the full projected closure operator determines its later evolution. The calculation below reconstructs the published benchmark, with no fitted source gain. Physical selection of the benchmark operator and event profile remains a separate task. [P41; P49; A36–A40]

XI.1 Source count and emergent time

Fact-Momentum §12.6 identifies the source charge with the number of committed distinctions. Together with its scalar action and point-event source, this supplies the convention

$$q_e = N_{\text{committed},e}, \qquad q_e = 1 \quad \text{for one Fact.} \qquad \text{(XI.1)}$$

The scalar source weight is fixed by this count normalization. No additional adjustable gain is introduced on this already normalized branch. The identification is adopted at its source grade; the present calculation does not re-prove all the primitive uniqueness claims used to motivate it. The event distribution, spatial profile and microscopic coupling to independent links and currents remain distinct from the count normalization. [P41, §§12.5–12.10]

Physical time is not assumed as a primitive duration of one event. The action below uses the emergent continuum coordinate already supplied in Fact-Momentum. The operation at the event boundary is stated directly as a change between the states immediately before and after it. Subsequent propagation can be parametrized by an effective separation once that continuum description is admitted. Retention of an earlier Fact does not itself require repeated injection of its source on every later tick. [A36–A37]

XI.2 Exact projection and the K7 mass boundary

Let $Rx = \sum_a x_a \Psi_a$ synthesize the retained field from linearly independent, potentially overlapping modes. Their Gram matrix is $M = R^*R$. The expansion coefficients and unit-event covector are different objects:

$$x = M^{-1}R^*\varphi, \qquad b_e = R^* f_e, \qquad b_{e,a} = \Psi_a(s_e) \text{ for a point source.} \qquad \text{(XI.2)}$$

The coefficient formula is exact on the retained subspace and gives the orthogonal projection coefficients for a general field. It is the dual-basis construction of [P50], not the approximate replacement $M = I$. The point-source formula is understood distributionally against the smooth finite basis. It supplies a definite projected covector once the event location and profile are specified. [A39]

The preceding mass audit also prevents a numerical shortcut. The published derivation of the value $4/3$ requires a map from a six-dimensional space into four dimensions to satisfy $P^{\mathsf{T}}P = (2/3)I_6$. This is impossible because

$$\operatorname{rank}(P^{\mathsf{T}}P) \le 4 < 6 = \operatorname{rank}\big((2/3)I_6\big). \qquad \text{(XI.3)}$$

The valid Fano incidence identity does not repair that projection or select a replacement physical mass. Likewise the six-neighbour spatial wheel, the internal Fano carrier and the seven-site periodic scalar benchmark are not identified by their common count alone. Their variables, metrics and operators must be matched. In what follows, $m^2\xi^2 = 3/4$ reproduces [P49]'s printed benchmark; $4/3$ is a sensitivity comparison only. Both values are declared mass inputs. [A38–A39]

XI.3 The operation produced by a unit event

On the retained six-mode scalar sector define $D_{ab} = \langle \nabla\Psi_a, \nabla\Psi_b\rangle$ and $K_{ab} = \langle \Psi_a, K_{\mathrm{cl}}\Psi_b\rangle$. The complete projected stiffness is $L = D + K + m^2M$. The source action is

$$S_{\text{eff}} = \frac{1}{2}\int dt\,(\dot{x}^{\mathsf{T}}M\dot{x} - x^{\mathsf{T}}Lx) + b_e^{\mathsf{T}}x(t_e). \qquad \text{(XI.4)}$$

Varying the action and integrating its equation across the event gives

$$M\ddot{x} + Lx = b_e\delta(t - t_e), \qquad x^+ = x^-, \qquad p^+ = p^- + b_e, \quad p = M\dot{x}. \qquad \text{(XI.5)}$$

Thus a unit Fact gives a definite canonical momentum insertion. The configuration changes under the resulting scalar evolution. The variable p is the momentum conjugate to the modal coordinate x; it is not itself the spatial stress–energy density T_{0i} called fact-momentum in [P41]. That spatial quantity follows from the reconstructed field and its gradients. The action-consistent sign convention is $(\partial_t^2 - \nabla^2 + m^2)\varphi = S$, as in the sign repair controlling §X.2. [A36, A40]

For zero pre-event disturbance, set $A = M^{-1/2}LM^{-1/2}$, $c_e = M^{-1/2}b_e$ and $\tau = t - t_e > 0$. The retarded response is

$$x(\tau) = M^{-1/2}A^{-1/2}\sin(\sqrt{A}\,\tau)c_e, \qquad p(\tau) = M^{1/2}\cos(\sqrt{A}\,\tau)c_e. \qquad \text{(XI.6)}$$

It vanishes before the event. A pre-existing field disturbance contributes its homogeneous solution. Equation (XI.6) is exact for this finite-dimensional linear action, not a derivation of the full independent gauge-link/current operation.

XI.4 The mass dependence of the response

Use normalized units $\xi = c = 1$ and write $\mu = m^2\xi^2$. At fixed basis, closure kernel and event profile, $A(\mu) = A_0 + \mu I$. With $r = M^{1/2}x$,

$$r(\tau) = \tau c_e - \frac{\tau^3}{6}(A_0 + \mu I)c_e + O(\tau^5). \qquad \text{(XI.7)}$$

In particular,

$$r_{\mu_2}(\tau) - r_{\mu_1}(\tau) = -\frac{\mu_2 - \mu_1}{6}\tau^3 c_e + O(\tau^5). \qquad \text{(XI.8)}$$

The initial momentum insertion and displacement slope are independent of mass; the first mass-dependent displacement difference is cubic in effective separation. Starting from rest, the projected impulse energy is

$$E_6 = \frac{1}{2}b_e^{\mathsf{T}}M^{-1}b_e = \frac{1}{2}c_e^{\mathsf{T}}c_e. \qquad \text{(XI.9)}$$

This fixed-profile projected energy is not a universal energy per bit. A point source in the full continuum requires separate ultraviolet treatment. A self-consistently selected change of mass might also change the basis or kernel; equations (XI.7)–(XI.9) do not assume those additional changes away. [A40]

XI.5 Reconstructed response and graph

The reconstruction uses seven sites $s_j = j\xi, j = 0, \dots, 6$, on a circle of circumference $L_c = 7\xi$. The following formulas specify the implementation used for Table XI.1 and Figure XI.1, including the two different Gaussian width conventions. Let

$$g_j(s) = \sum_{n=-3}^{3} \exp\left[-\frac{(s - j\xi - nL_c)^2}{4\sigma^2}\right], \qquad \Psi_j(s) = \mathcal{N}_j g_j(s), \qquad \text{(XI.9a)}$$

$$\mathcal{N}_j^{-2} = \int_0^{L_c} g_j(s)^2\, ds, \qquad \sigma/\xi = 0.8.$$

The closure operator in this benchmark is multiplication by the positive function

$$V_{\text{cl}}(s) = +V_0 \sum_{j=0}^{6}\sum_{n=-3}^{3} \exp\left[-\frac{(s - j\xi - nL_c)^2}{2\ell^2}\right]. \qquad \text{(XI.9b)}$$

Here $\ell/\xi = 0.8$ and $V_0\xi^2 = 0.390625$. Thus each unperiodized basis Gaussian has standard deviation $\sqrt{2}\,\sigma$, whereas each potential bump has standard deviation ℓ. The coefficient V_0 is positive, and V_{cl} enters L with a plus sign. It is a sum of positive bumps at all seven sites; it is not a negative attractive well. Both sums use the displayed image truncation.

For this longitudinal benchmark, $M_{ab} = \int_0^{L_c} \Psi_a \Psi_b\, ds$, $D_{ab} = \int_0^{L_c} \Psi'_a \Psi'_b\, ds$ and $K_{ab} = \int_0^{L_c} \Psi_a V_{\text{cl}} \Psi_b\, ds$. The derivative used in D is the analytic derivative of (XI.9a). The event is a unit point source at $s_e = 0$, with $b_{e,a} = \Psi_a(0)$, and the transverse correction is zero. These matrices are then restricted to the six nonuniform Fourier coordinates. This declared event profile is not a derived three-dimensional Fold profile. [P49, §3 and Appendix A; A40]

The three nonuniform Fourier pairs give six real coordinates. The uniform mode is excluded from this six-mode output and recorded separately in the certificate; a point event also has a uniform component. The centered event is reflection-even and excites the cosine member of each pair. The contact response is

$$\varphi_6(0,\tau) = b_e^{\mathsf{T}} x(\tau) = \sum_{j=1}^{3} w_j \frac{\sin(\Omega_j \tau)}{\Omega_j}, \qquad w_j = \frac{2\left|\hat{b}_j\right|^2}{\widehat{M}_j}. \qquad \text{(XI.10)}$$

Here $\hat{b}$ uses the unitary Fourier transform and $\widehat{M}_j$ is a Gram eigenvalue. The w_j are contact-response residues, not probabilities or fractions of a Fact.

Table XI.1. Reconstructed pair frequencies in units of c/ξ and contact residues. The $3/4$ column reproduces the printed benchmark; $4/3$ is comparison only.

Fourier pair	Frequency at $\mu = 3/4$	Frequency at $\mu = 4/3$	Contact residue
1 and 6	1.529380047	1.709484326	0.285714294
2 and 5	2.180836837	2.310710420	0.285725617
3 and 4	2.964555291	3.061359405	0.301169583

The first residue is $w_1 = 0.285714294015\ldots$, differing from $2/7$ by approximately 8.30×10^{-9}. Its proximity to $2/7$ is numerical; no exact rational identity is asserted.

For both mass inputs, the initial contact slope and projected impulse energy obey the exact identity

$$\dot{\varphi}_6(0,0^+) = \sum_{j=1}^{3} w_j = b_e^{\mathsf{T}} M^{-1} b_e = 2E_6.$$

In the declared normalized units the common slope is 0.872609493954 and $E_6 = 0.436304746977$, rounded consistently to twelve significant figures. They are two presentations of one quadratic quantity, rather than independent checks. The highest-pair residue uses the full overlap matrix. The graph displays the subsequent responses to the same source insertion.

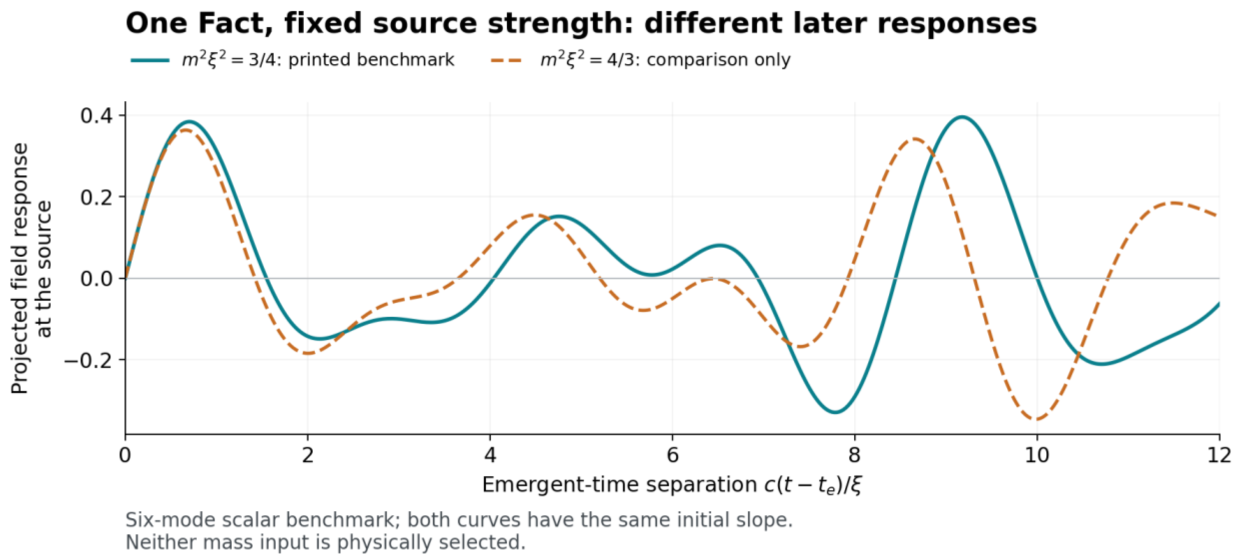

Figure XI.1. Response at the source to one Fact on the six-mode scalar benchmark. The solid curve uses the paper's mass input; the dashed curve uses the comparison input. Source strength, basis, kernel and event profile are identical. The horizontal axis is effective emergent-time separation, not a primitive tick duration. These finite-system recurrences do not establish a continuum decay tail or pointwise light cone. [A40]

XI.6 Verification and source corrections

Uniform-grid integration and independent adaptive quadrature agree on the reconstructed matrix entries to 5.6×10^{-16}. The pair frequencies reproduce every printed decimal of [P49] Table 2. A separately assembled canonical 12×12 matrix exponential agrees with (XI.6) to relative error 6.5×10^{-12}. The archived diagonalized propagation has maximum absolute energy drift 1.7×10^{-16} at the tested points. This last figure measures conservation within that numerical representation; it is not an error bound on all printed constants. The independently evaluated Fourier-residue sum and canonical quadratic form differ by 3.9×10^{-13} in the slope, or 1.95×10^{-13} in the energy. The consistently rounded values above respect their exact identity. The certificate also checks the cubic mass dependence. These checks are grade N; the source-selection conditions are collected in XI.7. [A40]

Two source corrections are material. First, [P49] §4.2 quotes a highest-pair Gram eigenvalue near 0.17. The explicit reconstruction in §XI.5 instead gives $\widehat{M}_3 = 0.0003737506918602834$, while the Table 2 frequencies reproduce. The printed roughly sixfold denominator estimate therefore does not describe this benchmark. All response calculations use the reconstructed Gram matrix.

Second, the continuum massive Bessel kernel displayed in Fact-Momentum §8.1 has an oscillatory envelope proportional to $\tau^{-3/2}$ at fixed spatial separation, not the τ^{-1} claimed in §8.3. This follows from $J_1(z) \sim \sqrt{2/(\pi z)}\cos(z - 3\pi/4)$ and the additional inverse-separation factor in the displayed kernel. The script verifies the asymptotic separately. It is a correction to the continuum statement, not a decay law for the finite graph in Figure XI.1. [P41; A40]

An independent numerical reconstruction reported during manuscript review corroborates Table XI.1, the contact residues, the Gram eigenvalue and the slope–energy identity. This provides corroboration beyond the archived internal checks; the separate reviewer implementation is not included in [A40].

XI.7 Physical selection task

The scalar branch has a fixed count normalization, an exact projected event-boundary operation and an executed response on the published benchmark. The missing question is not an additional unspecified source gain per Fact. It is which physical mass, closure kernel, spatial event profile and transverse contribution belong to the primitive commitment, and how this scalar operation attaches to the independent link/current and record outputs.

A retained record is also distinct from a source continuously applied after formation. The latter has the mass-normalized step response $A^{-1}\left[I - \cos\left(\sqrt{A}\tau\right)\right]c_e$, rather than the impulse response (XI.6). Its use requires a source-history premise. Selection of the event distribution and effective clock remains separate from the boundary law (XI.5). The temporal, source-map and same-action gates elsewhere in this manuscript continue to apply. [A37, A39–A40]

Part XII Master action phase selection and native momentum response

This part examines source selection for the recording phase. A complete source transfer, its real-time attachment and its physical record realization fix the joint marked operation. Fixed-field record probabilities alone do not fix it. The broader corpus already supplies conditional phase assignment, connection reconstruction and record-operation constructions; XII.7 corrects the earlier overly broad handoff and specifies how those results must enter. The exact pulse calculation also shows why the scalar trace of an interaction Hamiltonian cannot settle the phase. [A42–A43; P3; P4; P14; P32; P39; P64–P67]

XII.1 The source objects that must be fixed

MASD distinguishes the leading local rate expansion from an evaluated complete microscopic action. Its stated relation is

$$-\log\frac{d\mu_{\text{hist}}}{d\mu_0} = \Gamma_V + \frac{1}{2}\langle \mathbf{D}, W_{\text{prim}}\mathbf{D}\rangle + \Gamma_{\text{ferm}} + \Gamma_{\text{top}} + O(\parallel \mathbf{D} \parallel^3). \qquad \text{(XII.1)}$$

The operational metric, independent variables, complete cross blocks and common measure cannot be changed independently. This local relation does not by itself return every higher-order term or a marked coherent amplitude. PFHBA's bath coupling is explicitly to the linearized defect, and its amplitude-level descent requires source-supplied marks and projected amplitudes. Those qualifications remain active here. [P4, §§5, 9–10; P32, Parts XI–XII]

HMGBC supplies an existing full-carrier construction address, which must not be replaced by another invented generator:

$$T = M_{\exp(-a_t V^{\text{ref}}/2)} \exp(-a_t L^{\text{op}}) M_{\exp(-a_t V^{\text{ref}}/2)}, \qquad H = -a_t^{-1} \log T. \qquad \text{(XII.2)}$$

This is the finite split transfer, not automatically the exponential of the unsplit sum. The construction requires its actual operational generator, reference potential, carrier, measure and positivity certificate. Its terminal pushforward also consumes record transports and a frozen terminal map; its residuals do not prove that map unique. HMGBC §56A.11 explicitly retains these input and completeness conditions. No lack of numerical outputs alone prevents an otherwise fully specified blind execution, but an unreturned operator or realization cannot be supplied by choosing one of the desired phase candidates. [P3, §§56A.2, 56A.7, 56A.11; I.2]

The recent restricted endpoint construction preserves both U(1) Gauss constraints and the native finite-field C(U,ψ)U law. Its exact 650-dimensional unitary realization was reconstructed from those amplitudes. A single ZZ contact fails that native channel's rank test: at the tested backgrounds its rank bound is two, while the native current channel and each retained terminal map have rank thirteen. These are conditional current-pointer results; they are not a derivation of the complete permanent-Fact interaction. [A42]

XII.2 Selection once the complete source is returned

Proposition XII.1. On a finite admitted support, fix a positive-definite self-adjoint transfer T, its time scale, the physical realization and ready-state injection J, and the source-selected record projectors. Assume the admitted real-time operation is U(δ)=exp(−iδH), with H defined by (XII.2). Then its marked amplitudes and joint marked CP operation are fixed, up to basis changes that leave that complete operation invariant. A global rescaling of T changes only the common energy origin when this normalization is left unfixed.

Proof. The positive eigenvalues of T have unique real logarithms. Spectral calculus therefore fixes the self-adjoint H and hence U(δ). Projecting the fixed U(δ)J with the fixed record realization gives the amplitudes. Tracing the declared unresolved outputs gives a unique marked CP operation. A configuration-independent unitary change of unresolved environment basis leaves that operation unchanged. Multiplying T by a positive scalar adds a constant multiple of the identity to H, giving a global phase over the same fixed interval. No configuration-dependent phase follows from that energy-origin freedom. □

This is an application of the source's spectral reconstruction, not a claim that a positive stochastic matrix already supplies a physical marked dilation. Its premises include the full carrier and mark realization, not merely the unmarked Doob kernel. For a mixed ready state the equivalent fixed-channel statement applies. [P3; P32]

There is a useful admission test in a fixed positive configuration basis. If Dχ is diagonal and T has connected nonzero support, then

$$[T, D_\chi]_{ij} = T_{ij}\left(e^{i\chi_j} - e^{i\chi_i}\right). \qquad \text{(XII.3)}$$

Thus a diagonal phase preserves that same T only if it is constant on each connected component. Conjugating T preserves its spectrum and operator positivity but generally changes the kernel and its positive-basis realization. This test cannot be applied to an unspecified matrix-valued or fermionic source by assuming kernel positivity. It also does not forbid physical real-time phases produced by the fixed H. A simultaneous basis transformation of the entire theory, including states and readouts, is a different operation from changing the recording update alone.

XII.3 The tested phase changes a second derivative

Write the previously constructed dimensionless controlled-pulse generator as G(β), where β=θ+a−b is the restricted gauge-invariant relative angle. The two tested implementations obey

$$G_c = G - c(1 - \cos\beta)I, \qquad e^{-iG_c} = e^{ic(1-\cos\beta)} e^{-iG}. \qquad \text{(XII.4)}$$

Their fixed-field record maps agree, but their generator second derivatives differ:

$$\partial_\beta^2 (G_c - G)\big|_0 = -cI. \qquad \text{(XII.5)}$$

Consequently, if an independently derived complete source and the same pulse factorization fix this generator second jet, at most one member of this scalar family can match it. The tested c=1/4 variation is not invisible at that amplitude-generator grade. This does not identify G'' with an information Hessian or the Euclidean action Hessian without the corresponding source bridge. No value of that physical coefficient is assigned here.

A quadratic match would still not fix an arbitrary finite-field phase. For example,

$$\chi_2 = c(1 - \cos\beta)^2 = \frac{c}{4}\beta^4 + O(\beta^6), \quad \chi_2''(0) = 0, \quad \chi_2^{(4)}(0) = 6c. \qquad \text{(XII.6)}$$

More generally, c(1−cosβ)^m starts at order 2m. These functions demonstrate what a finite derivative test cannot determine. They are not asserted to be admissible additions to the complete VERSF action. MASD's leading quadratic expansion must not be promoted to a theorem fixing the whole phase tower. A symmetry, exact finite-field action or independently derived amplitude could impose further restrictions; none is manufactured by matching the quadratic form.

XII.4 Removing the identity coefficient does not select the phase

The previous interaction report exhibited a common scalar generator term as one realization of the ambiguity. That was not a proof that every realization has such a term. On its thirteen-state pointer let P0 denote the inactive state, including the fifty-dimensional internal identity, and Pe=I−P0. Define a preparatory pulse

$$R_\chi = \chi(\beta)\left(\frac{P_e}{12} - P_0\right), \qquad \mathrm{Tr}R_\chi = 0. \qquad \text{(XII.7)}$$

Since J injects the ready state into P0,

$$e^{-iR_\chi}J = e^{i\chi}J, \qquad e^{-iG}e^{-iR_\chi}J = e^{i\chi}e^{-iG}J. \qquad \text{(XII.8)}$$

Both G and Rχ are traceless, yet this implementation produces exactly the same phase-modified event column as (XII.4). Scaling the preparatory pulse to zero with the interaction strength preserves the inactive limit. Thus inspecting only the normalized trace of a full pointer Hamiltonian, or setting its explicit identity coefficient to zero, is insufficient. The energy relative to the prepared pointer state and the ordered interaction matter. This is a counterexample to that proposed selection shortcut, not a second source-admitted master action.

On the preceding two-configuration preparation, the literal and traceless-pulse implementations reproduce P(+Y)=0.505587370258 and 0.515323349688. The values are model predictions, not measurements or source targets. They verify that the correction is operationally consequential within the declared comparison.

XII.5 The precise remaining proof obligation

The joint marked operation must be obtained on the changing-field carrier by applying the existing source constructions, including their actual transfer, real-time attachment, preparation, retained projectors and unresolved outputs. The native instrument and conditional clock are already supplied inputs. PFHBA specifies amplitude and population-consistency stages; the holonomy and record-operation results consumed in XII.7 further constrain this handoff. The task is not to posit a new law merely because its joint realization has not been evaluated here. [P32; P39; P64–P67]

For a prescribed recording pulse, one may test its cross-configuration marked kernel against the native candidate. For a source that does not factor into that pulse and a later kinetic operation, compare the complete operation and its observable predictions directly. The phase of an isolated factor cannot be selected by changing the factorization: (K Dχ†)(Dχ V)=KV preserves the complete step. Conversely, modifying V while holding the independently fixed K and readout unchanged is a substantive change.

The pass condition is agreement with the independently returned joint amplitudes or joint marked CP map, including coherence between configurations, in the same physical realization and regulator limit. Agreement only with probabilities, a scalar rate, a Choi rank, a generator trace or a finite list of derivatives is not that pass. The consulted MASD/HMGBC/PFHBA chain supplies the construction and admission conditions but does not supply this completed physical return for the native event used here.

XII.6 Verification and verdict

The proof checks use exact rational Taylor coefficients, the inherited native interaction arrays and an independent matrix implementation of the traceless preparatory pulse. A separate three-state connected heat kernel verifies the phase-conjugation and Dirichlet-energy identities; it is an algebraic control, not a physical source or clock. The execution passes nine exact checks and sixteen numerical residual checks, with maximum residual below 6×10^{-14}. [A42]

The conditional selection proposition and the stated pulse identities are proved. Neither tested c is selected by this execution. The earlier two-candidate construction does not establish two theories satisfying the same complete master action or comparison data. The recovered corpus theorems in XII.7 govern the next compatibility calculation; no programme-wide absence claim follows from the restricted counterfamily. No gauge coupling is inferred.

XII.7 Corpus reconciliation and the comparison kernel

Audit note: the corpus supplies phase-assignment and record-operation constructions beyond the MASD/HMGBC/PFHBA chain reviewed above. Their hypotheses must be carried into the present calculation before a phase is classified as an independent physical input. No new physical coefficient is reported in this subsection. [A43]

Holonomy Assignment from Distinguishability proves, at its stated premise grade, that complete admissible comparison data D determine closed-loop holonomy and the co-terminal support kernel:

$$W_D(P,P') = h_D\left(P \circ P'^{-1}\right). \qquad \text{(XII.9)}$$

The histories share both preparation and registration endpoints. The constructive proof inherits composition and witnessability and explicitly retains comparison-realizability check C; the fallback uses Transport-Completeness and no-pre-individuation. D includes admissible transport-comparison invariants and is not merely a symmetric metric or the fixed-field record probabilities. Under those premises, two physically different phase assignments cannot share the same complete D. The later Route-M source-closure paper supplies explicit connection reconstruction from a complete loop assignment, up to gauge. Its Theorem 12 also closes the current physical off-shell integrability branch at the inherited holonomy grade. None of these results should be replaced by a new unconstrained phase law. [P64, §§4, 6–8; P65, Theorems 10–13A]

The record-operation side is also partly closed. PFDMI Theorem 51(a) supplies the native current-event strength family and its minimal-pointer semantics. PMS-EX58 supplies the first-cover trigger, the source-selected chiral binary basis, minimal completion maps and branch-preserving renewal, closing the Fold/R4 subchain relative to Axiom FC. P39 was already cited in this paper; its closure must survive the handoff to Part XII. Asking the pre-fact action to derive the occurrence of Facts again would reopen that declared primitive. The broader phase and history-to-active-dynamics obligations remain separately typed in the same theorem. PSAC also constructs a history-controlled active/discard isometry and an exact criterion for its continuation pullback; this is existing constructive machinery, although its physical history projector is not selected in full generality. [P15, Theorem 51; P39, §28 and Theorem 32.37; P66, §§28BM–28BQ]

There is a direct consequence for the earlier diagnostic. For field configurations x and x′, define the retained cross block from its native amplitudes and retained projector. A common event rephasing gives

$$\begin{aligned} \mathcal{B}_r^0(x,x')[X] &= \sum_\alpha Q_r\, L_\alpha(x) X L_\alpha(x')^\dagger Q_{r'}, \\ \mathcal{B}_r^\chi(x,x')[X] &= e^{i[\chi(x)-\chi(x')]}\mathcal{B}_r^0(x,x')[X]. \end{aligned} \qquad \text{(XII.10)}$$

Whenever the physical source fixes a nonzero block, preserving that block forces its phase factor to one. A connected graph of fixed nonzero comparison blocks therefore permits only a constant common phase. The archived x=0, x′=0.4 witness has a nonzero overlap, multiplied by exp[−i(1−cos0.4)/4] under the tested rephasing. Its two Y probabilities remain 0.505587370258 and 0.515323349688. If this comparison is admitted, the candidates change D; they cannot be used as two solutions over the same complete comparison data. If it is not admitted, these probabilities remain predictions of a diagnostic extension. [A43]

Equation (XII.10) is not an identification of an operator-valued record kernel with the scalar transport kernel in (XII.9). The physical comparison, its common endpoints, retained marks and unresolved outputs must be supplied by the source. The unchanged RCHS-29 route comparator has already been found insensitive to this common event rephasing; citing it again does not discharge the identification. The Maxwell connection's identity with substrate transport likewise fixes which transport is used under its inherited premise, without identifying every recording phase with that transport. [A42 and its predecessor phase_comparison/; P67, §4]

The corrected execution target is to apply the existing comparison kernel and full transfer to the existing event/commitment construction on one physically identified carrier. It is a compatibility and evaluation problem between returned constructions. The present review does not evaluate that joint physical kernel and hence selects neither tested c. It withdraws any reading of Part XII as a proof that the full corpus lacks phase-selection machinery or a record law. Existing first-cover, binary-basis, renewal, native-current and clock results remain consumed premises. [P15; P27; P39; P64–P67]

XII.8 Phase independent lower bounds on record backreaction

The joint comparison of XII.7 remains unevaluated at physical source grade. A separate consequence can nevertheless be obtained without selecting the disputed phase. Within the inherited configuration-diagonal native event, a field-sensitive record forces conjugate-flux disturbance. The calculation uses the supplied current amplitudes and retained projectors, with the existing neutral preparation and real incoming packet. It does not identify a current-pointer event with a completed Fact. [A44; P15; P39]

Let $|\Psi(\beta)\rangle$ be the normalized output purification, including unresolved current outputs and a fixed purification of the input state. Write $w = |f|^2$, with real periodic f, and use the dimensionless conjugate flux $p = -i\,\partial_\beta$. For fixed terminal projectors, define

$$\mu = -i\langle\Psi|\Psi'\rangle, \qquad g = \langle\Psi'|\Psi'\rangle - \mu^2, \qquad F_R = \sum_r \frac{(p_r{}')^2}{p_r}. \qquad \text{(XII.11)}$$

Primes denote derivatives with respect to the link coordinate. Smoothness, a fixed input preparation and positive retained probabilities are assumed on the tested support. Direct differentiation of the joint wave function gives

$$\mathrm{Var}_{\mathrm{out}}(p) = \mathrm{Var}_{\mathrm{in}}(p) + \langle g\rangle_w + \mathrm{Var}_w(\mu). \qquad \text{(XII.12)}$$

The replacement $\Psi \mapsto e^{i\chi}\Psi$ sends $\mu \mapsto \mu + \chi'$ and leaves g unchanged. Thus the common phase can alter the spatial variation of the mean impulse, but cannot remove the intrinsic contribution. On the circle, the periodic choice $\chi' = \bar{\mu} - \mu$, where $\bar{\mu}$ is the unweighted circle average, attains the minimum over smooth common phases. This minimizing phase is a mathematical control and is not selected as the physical operation.

For each retained outcome, write the normalized branch as Ψ_r, with corresponding μ_r and g_r. Orthogonality of the marks gives the exact decomposition

$$g = \frac{F_R}{4} + \sum_r p_r\, g_r + \sum_r p_r\,(\mu_r - \mu)^2 \;\geq\; \frac{F_R}{4}. \qquad \text{(XII.13)}$$

Equivalently, this inequality follows from Cauchy–Schwarz applied to the component of Ψ' orthogonal to Ψ. The probability-only consequence is

$$\mathrm{Var}_{\mathrm{out}}(p) - \mathrm{Var}_{\mathrm{in}}(p) \;\geq\; \frac{1}{4}\langle F_R\rangle_w. \qquad \text{(XII.14)}$$

This weaker bound survives any smooth configuration-diagonal isometric implementation with the same retained probabilities and the stated preparation. The stronger value $\langle g\rangle_w$ is invariant under common phases; it need not survive arbitrary field-dependent rotations of unresolved outputs.

For the inherited packet, the initial flux variance is 1.439999999926. The probability-only minimum increase is approximately 0.04544006. The native amplitude family's common-phase minimum increase is 0.249955331277, giving minimum outgoing variance 1.689955331203. The two previously tested operations give 1.690050219813 and 1.699388329797. Their difference therefore cannot eliminate the native family's intrinsic backreaction. The three nonnegative contributions in (XII.13), averaged over the packet, are approximately 0.04544006, 0.09857054 and 0.10594473.

The inherited charge-conditioned kinetic step is diagonal in flux, so it commutes with p and preserves its entire distribution. Equations (XII.12)–(XII.14) therefore remain valid after that step at any duration. This concerns flux variance: angle populations remain unchanged by the event alone, and a later angle-response law still requires the kinetic attachment. The physical source is not assumed to share this particular factorization or spectral choice.

The execution includes analytic derivatives, finite-difference controls, 96/192/384-point packet calculations and a field-dependent unresolved-output rotation that preserves the probability-only bound while changing g. The final Fisher integral changes by 3.03×10^{-10} between 192 and 384 points; 131 numerical identity and convergence checks pass. This is a conditional lower-bound theorem and native numerical evaluation. It selects no common phase, completed-Fact dynamics, absolute clock or physical gauge coupling. [A44]

XII.9 Completion and renewal preserve the field marginal on a fixed carrier

The completion question must consume PMS-EX58 rather than ask the pre-fact action to derive commitment again. The source already gives the R4 carrier, its chiral binary projectors, the minimal completion maps and branch-preserving renewal, relative to Axiom FC. The following consequence concerns those maps on a fixed product carrier. It does not identify the native fifty-dimensional current carrier with the two-dimensional R4 sector. [P15, Theorem 51; P39, §28 and Theorem 32.37; A45]

Let F be the field register and R the other degrees of freedom. Every field-independent trace-preserving channel $\Gamma: R \to R'$ obeys

$$\mathrm{Tr}_{R'}\big[(\mathrm{id}_F \otimes \Gamma)\big(\rho_{FR}\big)\big] = \mathrm{Tr}_R \rho_{FR}. \qquad \text{(XII.15)}$$

The proof is the adjoint identity $\Gamma^*(I) = I$, applied to every field observable. Thus the entire unselected field density operator and flux distribution survive, including the variance bound established before completion. For the source maps,

$$A_s = \big|C_s\rangle\langle\psi_s\big|, \qquad V|C_s\rangle = e^{i\chi_s}|\psi_s\rangle|s\rangle_{\mathrm{ledger}}, \quad s = \pm, \qquad \text{(XII.16)}$$

the sums $\sum_s A_s^\dagger A_s = I_{E2}$ and $V^\dagger V = I$ give (XII.15) when the chosen carrier and branch phases are field independent. The source's branch-preserving sech/tanh export also preserves this conclusion when its location amplitudes are field independent and all outputs are included. Fact occurrence and permanence retain their FC-relative grade; this is the Born ensemble of the source completion maps. [P39; A45]

An individual completed branch is conditioned on its outcome. Its variance need not equal the ensemble variance. With branch weights w_s,

$$\mathrm{Var}_{\mathrm{pre}}(p) = \sum_s w_s\, \mathrm{Var}_s(p) + \mathrm{Var}_{s\sim w}\big(\langle p\rangle_s\big). \qquad \text{(XII.17)}$$

The source-map test verifies the complete field density matrix through completion, renewal and export on a declared smooth R4 control input. Its flux variance remains 1.481285157590086, while the two conditional variances differ. These are control values, not first-cover predictions. A field-dependent branch phase preserves the binary probabilities but changes the field state, demonstrating the scope of the theorem.

The physical first-cover composition still requires the joint state arriving at commitment and the actual field dependence of its carrier attachment. A moving R4 embedding or field-controlled renewal need not be a channel on R alone. Consequently the numerical minima in XII.8 remain native one-link values; they are not multiplied by a mean cover time or transferred to every realized Fact. This preserves the existing clock and FC closures while identifying the precise additional composition to evaluate. [A45]

XII.10 Native response in all gauge directions and the coupling boundary

The same native amplitude family can be differentiated in every gauge direction. At background $U_0 = \exp(i\beta 6Y)$, vary $U(t) = \exp(itT_a)U_0$, retaining the original endpoint witness and neutral preparation. Differentiate the full current-dependent compensator, including its saturated strength and square root. For the normalized output purification define

$$\mu_a = -i\langle\Psi|\partial_a\Psi\rangle, \qquad G_{ab} = \mathrm{Re}\langle\partial_a\Psi|\,\partial_b\Psi\rangle - \mu_a\mu_b, \qquad \text{(XII.18)}$$

$$F_{ab} = \sum_r \frac{\partial_a p_r\ \partial_b p_r}{p_r}, \qquad G \succcurlyeq \frac{1}{4}F. \qquad \text{(XII.19)}$$

The matrix inequality follows from XII.8 along every real tangent. Both matrices are invariant under a common scalar phase. The intrinsic G retains the native unresolved-output implementation scope; F has the broader fixed-probability scope. The one-dimensional optimizing phase from XII.8 is not presumed to minimize all gauge directions simultaneously.

At the identity-link background, the mean intrinsic diagonal entries are 0.004519760345 for the eight colour directions, 0.004772806121 for the three weak directions, and 0.007037194013 for Y. Their mean probability-only lower bounds F/4 are 0.000121110111, 0.000061858235 and 0.001715006270. These are dimensionless local tangent coefficients. The native generator traces are 6, 13/2 and 21/2 respectively; replacing Y by q=6Y multiplies the last entries by 36 and reproduces the earlier local calculation. [A45]

At all three tested backgrounds, beta=0, 0.2 and 0.4, G is positive definite with rank twelve, while F has rank six, the maximum for seven normalized probabilities. Nonzero cross-factor blocks and colour anisotropy remain in the fixed endpoint witness. These matrices do not already form three physical scalar stiffnesses. A permanent binary readout also need not retain the seven-outcome score: its local Fisher matrix has rank at most one at a fixed preparation, although multiple records and histories can restore additional directions.

The coupling rule still requires the fully relaxed same-action plaquette-holonomy Hessian. No identity between that Hessian and the local noise geometry in (XII.18) has been derived here. The existing conditional coupling calculations retain their own premises, and the non-Abelian endpoint/environment Gauss completion is not supplied by this local tangent calculation. [P9; A45]

PMS-EX125/126 separately closes a tempting shortcut. The normalized current ray is radially invariant. If the incoming state and the completion channel are both independent of that radial parameter, their composition is independent too:

$$\begin{aligned} \rho_j &= \frac{jj^\dagger}{j^\dagger j}, \qquad \rho_{e^{\epsilon}j} = \rho_j, \\ \partial_\epsilon \Gamma\left(\rho_{\text{pre}}\right) &= 0 \quad \text{if } \partial_\epsilon \rho_{\text{pre}} = \partial_\epsilon \Gamma = 0. \end{aligned} \qquad \text{(XII.20)}$$

Field-independent completion cannot restore radial-current information already absent from its input. This also holds for a stopped history when every transition and its first-cover rule have no other dependence on that radial parameter. It is a corollary of the existing projective no-go, not a claim that the physical radial stiffness vanishes. The raw constitutive residual remains magnitude bearing before projectivization, and its physical mark-score attachment remains separately required. Gauge-angle response and radial-current response are distinct derivatives. [P39, §§111–112 and Theorem 32.84; A45]

XII.11 Native field momentum and the occurrence contribution

The earlier sections give preparation-dependent lower bounds and completion identities. We now calculate the momentum response of the existing native operation itself. The general operator identities below are consequences of completeness; their application and numerical evaluation on the archived VERSF family are the contribution of this execution. The operation is unchanged. [A46, §7]

Let $L_l(\theta)$ be smooth multiplication Kraus operators on the common field/internal carrier, with $\sum_l L_l^\dagger L_l = I$, and let $p = -i\,\partial_\theta$ on a common smooth domain. Define

$$\mathcal{A} = -i\sum_l L_l^\dagger L_l{}', \qquad \mathcal{B} = \sum_l (L_l{}')^\dagger L_l{}'. \qquad \text{(XII.21)}$$

Completeness makes $\mathcal{A}$ Hermitian. For the nonselective dual operation Φ^*, the Leibniz rule gives

$$\Phi^*(p) = p + \mathcal{A}, \qquad \Phi^*(p^2) - p^2 = \{\mathcal{A}, p\} + \mathcal{B}. \qquad \text{(XII.22)}$$

To verify the second identity, apply $pL = Lp - iL'$ twice and differentiate the completeness relation. Stacking the Kraus operators into an isometry V then gives

$$\mathcal{N} := \Phi^*(p^2) - \Phi^*(p)^2 = \mathcal{B} - \mathcal{A}^2 = V'^\dagger(I - VV^\dagger)V' \geqslant 0. \qquad \text{(XII.23)}$$

This is an operator measuring the extra second moment beyond the square of the transformed momentum. It is not the entire variance change for an arbitrary incoming field state. In particular, for a fixed pure internal preparation $|w\rangle$, the local purification geometry satisfies

$$g_w = \langle\mathcal{B}\rangle_w - \langle\mathcal{A}\rangle_w^2 = \langle\mathcal{N}\rangle_w + \mathrm{Var}_w(\mathcal{A}). \qquad \text{(XII.24)}$$

The preparation and operation must agree before this quantity is compared with (XII.18). Field-independent unitary changes of unresolved Kraus labels preserve (XII.21)–(XII.23); field-dependent changes can alter the coherent field operation even when pointwise record probabilities are unchanged.

The evaluated native family is $L_l(U) = C_l\big(\psi_4 - U\psi_0\big)U$ on archived edge 9, oriented $0 \to 4$, at identity background links. It retains the fifty-dimensional prime-chirp endpoint witness and maximal-current prescription, including the derivative of the normalized current, strength and fixed-rank square-root complement. The internal input is the pure source endpoint $w = \psi_0$. This differs from the neutral preparation used in XII.8–XII.10, so the numerical entries below are not substituted for their tensor G. Frozen endpoints also do not constitute a dynamical endpoint/Gauss completion.

Probe	$\langle\mathcal{B}\rangle_w$	$\langle\mathcal{N}\rangle_w$	$\langle\mathcal{N}_h\rangle_w$
Weak 1	0.0674173591	0.0399227519	0.00906993687
Weak 2	0.0670572684	0.0390849340	0.00900874580

Probe	$\langle \mathcal{B} \rangle_w$	$\langle \mathcal{N} \rangle_w$	$\langle \mathcal{N}_h \rangle_w$
Weak 3	0.0677324537	0.0398115974	0.00910625143
Hypercharge Y	0.1147401545	0.0570269488	0.01521363012

These are dimensionless local instrument coefficients in the declared generator coordinates. Their positivity gives a concrete nonzero momentum response in the tested directions. The witness is not weak-invariant, so its weak entries need not coincide. They are neither vacuum-averaged stiffnesses nor physical coupling values. Replacing Y by $q = 6Y$ multiplies the quadratic coefficients by 36, solely as a coordinate conversion.

For a declared kinetic term $H_g = \kappa p^2/2$, (XII.22) gives the exact work operator

$$\Phi^*\left(H_g\right) - H_g = \frac{\kappa}{2}\left(\{\mathcal{A}, p\} + \mathcal{B}\right). \qquad \text{(XII.25)}$$

The coefficient κ must come from an independently justified kinetic attachment. The formula does not identify a record Fisher metric or a local variance coefficient with energetic gauge curvature. The same differentiation applies direction by direction to invariant momentum derivatives; it does not treat non-Abelian finite impulses as commuting translations.

If this event occurs with field-independent probability h, while the complementary operation is field independent, completeness gives

$$\mathcal{A}_h = h\mathcal{A}, \qquad \mathcal{B}_h = h\mathcal{B}, \qquad \mathcal{N}_h = h\mathcal{N} + h(1-h)\mathcal{A}^2. \qquad \text{(XII.26)}$$

The last column uses the archived conditional selected-edge weight $h = H_{4,0} = 1/7$. It separates the operation's own additional variance from the contribution of uncertain occurrence. This is a single opportunity, not a stationary all-edge average or a completed first-cover Fact. A field-dependent gate requires its own derivative terms. Neither (XII.26) nor the native multiplication event supplies angle motion or a kinetic interval after idle opportunities.

The reconstructed generators and endpoints match the archive exactly, and the Kraus arrays agree within 1.23×10^{-15}. Completeness, derivative normalization, Hermiticity, positivity and the appropriate preparation-dependent readout-information bound were checked. Independent finite differences of the full nonlinear native family converge at second order, with final relative derivative errors below 6.5×10^{-9}. Archive A46 retains 33 exact local-work and scope checks together with these numerical controls. [A46, §7]

XII.12 Energetic matching and the scope of one bit normalization

The source in VII.19 fixes the common-link impulse without an adjustable gain. It also changes endpoint charge. Its energetic interpretation must therefore retain the joint balance

$$\Delta E_{\text{total}} = \Delta E_g + \Delta E_{\text{matter}} + \Delta E_{\text{record/bath}} + \cdots. \qquad \text{(XII.27)}$$

For a specified quadratic gauge energy, a finite commuting impulse v changes that term by $p^T G v + v^T G v/2$. The dependence on incoming flux prevents assigning the same strictly positive gauge work to every fixed kick without a justified averaging or compensation. The native operation's work is now explicit in (XII.25), but the complete physical energy operator and other sectors' contributions remain necessary inputs. Equal integrated flux through every closed boundary is insufficient to establish equality of local cost currents or their Hamiltonian generators; the local-work identification must be independently proved. [A46, §§6–7]

One common action normalization can affect relative relaxed responses when the substrate block does not scale with it. For the source-restricted parent with record blocks A, B, E and substrate block D, the Schur response is

$$K(C) = CA - C^2 B^T (D + CE)^{-1} B. \qquad \text{(XII.28)}$$

Only when the whole parent scales, or in an appropriate special case, must that scale cancel from ratios. The inherited-metric uniqueness theorem remains valid within its premises. A source-defined work budget could determine a surviving common scale and its scale-dependent ratios; the count of one bit is not already that physical work equation. [A46, §§6.5–7.6]

The prior BCN condition in VII.5 is likewise retained as a conditional calibration. The reviewed minimal-commitment proof imposes the reliability floor $\eta_B = 1/(1 + 2^B)$, then derives an upper bound on its likelihood ratio before selecting that upper bound as the minimum. This does not independently derive the normalization. In a specified symmetric binary experiment with posterior error $\epsilon(\Delta) = 1/(1 + e^{\Delta})$, the corrected attainable minimum is

$$\Delta_{\min} = \log\frac{1-\eta}{\eta}, \qquad 0 < \eta < \frac{1}{2}. \qquad \text{(XII.29)}$$

It equals $\ln 2$ only at the independently selected tolerance $\eta = 1/3$. This logistic error model is not a universal discrimination law. Finite alphabet size alone also does not make the Wilson coefficient unobservable: within the declared finite Wilson family its Fisher information is the positive variance of the phase cost, and even the binary vacuum-state frequency changes with the coefficient. Twenty exact checks of these normalization inferences are retained in A46, §8. The correction concerns this proof; it neither withdraws the source's binary primitive nor establishes nonuniqueness across all VERSF models.

Integrated result and physical handoff

Results of the combined calculation

Grade D results connect the admitted configuration generator to a kinetic reference, the calibrated source to an action Hessian, and the complete Gaussian history to its prescribed endpoint energy. The six-defect calculus supplies the full differential and moving-support correction. Ordered-holonomy refinement establishes its relative metric scaling under the inherited metric. These results retain the hypotheses stated in Parts I–V.

Grade N witnesses establish the ordered-record and completion-filing responses on their declared backgrounds. The source-stopped D36 current and current-link reciprocity calculations connect the matter and gauge constructions under the EPM1 and same-parent premises. Charge-normalized impulses, common-carrier normalization and Wilson matching remove the corresponding declared normalization freedoms. The E_2 alignment witness tests the complete mixed response; opposite mixed signs retain the same screening correction. [Parts VI–VII; A41]

The phase-source reconciliation in XII.7 carries existing holonomy, connection and record-operation results into the comparison test. Under their physical-identification premises (grade P), complete admissible comparison data constrain the diagnostic phases. The contact and unit-Fact calculations separately establish progress and scalar response within the specified interaction and operator. The finite-history exclusions retain their stated carrier and mechanism classes. [Parts VIII–XII; A42–A43]

The constructive endpoint combines grade D flux-moment and completion identities with grade N weak/Y coefficients for the native recording operation. The occurrence gate contributes at the selected-edge opportunity grain. The pure endpoint preparation in XII.11 is distinct from the neutral-preparation tensor in XII.10. Energetic matching must use the appropriate preparation and include matter, records and responding auxiliaries. The corrected one-bit normalization argument leaves that physical work balance as a grade P problem. [XII.8–XII.12; A44–A46]

Consolidated claim ledger

Claim	Grade	Established result	Physical matching requirement
Reconstruction and reduction	D / N	Generator, susceptibility and history reductions are complete in their declared classes.	Return physical rates or forcing, reference measure and the complete same-action carrier; Parts I–IV.
Support and refinement	D / N / P	Complete defect derivatives, corrected moving support and ordered-link geometry.	Identify the physical residual metric, completion geometry and interacting refinement; Parts III and V.
Record and source response	D / N / P	Ordered-record witnesses; source-stopped current shape; exact reciprocity and portal tests.	Identify preparation, retained records, event grain, same-parent attachment and responding auxiliaries; Parts VI–VII.
Impulse and normalization	D / P	Unit event impulses; common-carrier and Wilson normalization results; K7 retyping.	Match the normalized source to energetic response and operational units; VII.19–VII.28 and Part XI.
Temporal dynamics and commitment	D / N / P	Wilson transfer, finite-history tests and exact contact progress within their stated models.	Attach temporal incidence, physical clock, export and completion to the joint field operation; Parts VIII–X.
Native field momentum	D / N	Mean impulse, second moment, positive additional variance and occurrence term.	Use the specified operation, preparation and opportunity grain when forming the joint work balance; XII.8–XII.12.
Measured electroweak reference	E	Measured-alpha link coefficient and PDG-based effective response.	Maintain scale and radiative matching conventions; these are external calibrations; VII.3–VII.4 and VII.14.

Claim	Grade	Established result	Physical matching requirement
Physical transverse weight	P — open	No source-selected physical transverse weight is obtained.	Complete the same-action reduction with physical curvature embedding and all coupled sectors.
Endogenous gauge coefficients	P — open	No endogenous Standard Model gauge coefficients are issued.	Complete energetic/source-response matching, operational units and continuum/regulator matching. This is the next calculation, outside this paper.

The surviving transverse requirement

Ordered histories and filed records are tested separately. Three retained terminal observations preserve all 72 tested curvature directions under the declared normalized endpoint nuisance and provide much stronger information than two. Earliest-completion readouts show that final-outcome summaries can erase the response while a last-edge/ordered-pair record retains it. A different, action-side reduction also applies: conditional on EPM1, the D36 source-even Fold law fixes the pre-Fact matter generator, first-cover stopping functional and E_2 current occupation. The factor shape agrees exactly with the independent C/W/Y source-action shape, but the action scale remains separately typed. [A14–A20; P18; P57–P59]

The remaining physical operation must join an incoming influence to receiving-Fold progress or occurrence and to the joint current/link destination, while retaining earlier records. The latest configuration-update audits do not close that microscopic same-event attachment; EPM1 remains conditional. On the gauge side, the exact current-link reciprocity theorem and same-parent U(1) reduction mean the task is no longer to invent another strength mechanism. The source must return the physical operational metric and changing-link response, identify the surviving U(1) line with the same parent if that architecture is correct, and thereby determine the overall response scale and finite portal strength. The scalar K7 admission remains only a blind structural comparator. The outstanding inputs further include the physical scalar operator and event profile, actual temporal boundaries, export and completion criteria, effective clock attachment and the complete same-action weak/hypercharge contraction.

The immediate portal contraction is the history-conditioned complete E_2 mixed block and its closure denominator on the existing physical radial tangent. Its quadratic screening correction must be formed before any permitted history averaging. The conditional record law must be consumed at its retained CP-instrument grain; the complete action and its probe transport remain separate source requirements. The uniform A_2 orientation source is retained without using it as an E_2 strength. This narrows the executable target rather than selecting a numerical coupling. [VII.29–VII.34; A41]

The nonuniqueness theorem of §IX.5 applies to its explicit finite-sector freeze, even when the entire stationary one-tick Wilson law is fixed. It is not a theorem that two complete models satisfy every VERSF primitive. Likewise the earlier controlled-instrument, stopping, subdivision, finite-cost and sharp-conditioning results exclude their stated classes only. Axiom FC supplies commitment at completed closure; it does not by itself select the coupling, timing or independent-field response. The exclusions retain their stated carrier and mechanism scope.

Conclusion

The paper establishes a sequence of conditional constructions connecting configuration dynamics, retained records and field response. These include the generator and calibrated-action reconstructions, the six-defect differential, Gaussian history contractions, refinement geometry, ordered-record tests, the unit-Fact scalar response and the common-link charge-normalized impulse. The established source and normalization results retain their own premises; structural admission probabilities and current covariances are not assigned gauge-energy meanings by definition.

The constructive endpoint is the explicit momentum response of the specified native recording operation. Its derivatives determine the mean impulse, second moment and positive additional-variance operator. The archived weak and hypercharge probes give nonzero coefficients under the stated pure endpoint preparation. The occurrence law adds a separate Bernoulli variance term, while field-independent completion preserves the incoming field marginal at ensemble grade on a fixed carrier. These calculations specify how the admitted operation disturbs momentum without introducing an additional disturbance mechanism. [XII.8–XII.11; A44–A46]

There is one remaining physical matching problem for the coupling strengths: the source response must be matched to the complete energetic action, or to an independently work-calibrated susceptibility, on the same field and event carrier. This matching includes responding auxiliaries, matter and record sectors, physical preparation, event grain, operational scale and units, physical curvature embedding, and continuum/regulator matching. A common record-action normalization can change relative relaxed costs when the substrate block does not scale with it. Neither one-bit capacity nor the reviewed reliability argument independently supplies that normalization. The existing conditional coupling theorems remain available once their physical premises are met. [VII.5; XII.12; A46]

The result is a completed source-response calculation with explicit operator formulas, numerical coefficients and reproducible checks. It provides concrete data that a physical coupling derivation must reproduce under the same assumptions. Unique endogenous weak and hypercharge strengths have not been established, and no impossibility claim for the full VERSF programme follows. The paper closes with the calculable relation between the specified recording operation and its conjugate field-momentum response. Energetic/source-response matching is the starting point of the next calculation.

Technical supplement

The companion RCHS-35 Technical Supplement preserves the detailed scientific-status inventory (S1), source basis and coverage (S2), calculation-to-source map and archived verification (S3), detailed numerical executions (S4), the full objective ledger and synthesis (S5), and the common bibliography (S6). It is part of the evidence record for this paper.

References

Calculation archives incorporated

[A1] K. Taylor, *RCHS-35: Primitive Configuration Dynamics and the Gauge-Response Selection Test in VERSF*, working calculation R0, 8 September 2026. Original Markdown, Word manuscript and RCHS-35_Reproducibility_Package.zip. Source of Part I and its reported execution.

[A2] K. Taylor, *RCHS-35 Continuation: Calibrated Field Response and Quadratic Source Completion in VERSF*, RCHS-35C-R0, 8 September 2026. Original Markdown, Word manuscript and RCHS-35C_Reproducibility_Package.zip. Source of Part II and its reported execution.

[A3] K. Taylor, *RCHS-35D: Six-Defect Transverse Derivatives and the Common-Action Compatibility Test in VERSF*, R0, 8 September 2026. Original Markdown, Word manuscript and RCHS-35D_Reproducibility_Package.zip. Source of Part III, its explicit support correction and its reported execution.

[A4] K. Taylor, *RCHS-35E: History–Action Matching and the Transverse-Weight Selection Test in VERSF*, R0, 8 September 2026. Original Markdown, Word manuscript and RCHS-35E_Reproducibility_Package.zip. Source of Part IV and its reported execution.

[A5] K. Taylor, RCHS-36F: Ordered-Holonomy Refinement Metric and Karcher-Mean Regularity Test, working calculation, September 2026. Markdown calculation, numerical result manifest and RCHS-36F_Reproducibility_Package.zip. Source of Part V: exact binary ordered-holonomy metric scaling, minimal-fibre/basic-Haar result, link Laplacian intertwining, Karcher diagonal scaling and the constant-curvature midpoint obstruction. No physical W_prim, G_red or gauge coupling is issued.

[A6] Taylor, K. RCHS-36G: HCMR Six-Level Gauge No-Go (9 September 2026). Frozen comparison note and reproducibility archive.

[A7] Taylor, K. RCHS-36H: FB Irreversible Lift No-Go (9 September 2026). Conditional comparison note and reproducibility archive.

[A8] Taylor, K. RCHS-36I: D41 Gauge-Covariant Schur Capacity Bound, corrected revision 1 (9 September 2026). The corrected conditional bounds and covariance statement control this integration.

[A9] Taylor, K. RCHS-36J: Native Score Strength, Neutral-Record Capacity and Information Loss (9 September 2026). Calculation note, scripts, arrays and independent verifier.

[A10] Taylor, K. RCHS-36K: Gauge Identifiability With Free Endpoint Frames (9 September 2026). Calculation note and reproducibility archive.

[A11] Taylor, K. RCHS-36L: Sector Records and Relative Gauge Orientation (9 September 2026). Calculation note and reproducibility archive.

[A12] Taylor, K. RCHS-36M: Record-Conditioned Prediction and Curvature Response (9 September 2026). Innovation-space primary calculation, full-carrier check, ordered terminal and nonself results, and separate verification programs.

[A13] VERSF Corpus Audit for RCHS-36L (9 September 2026), with the subsequent source and preparation corrections documented in RCHS-36M. Inventory and focused-reading audit, not exhaustive proof verification.

[A14] K. Taylor, RCHS-36N: Ordered-Record Curvature Response with Free Normalized Endpoints. 9 September 2026. Calculation note and reproducibility package; full stated 693-coordinate endpoint extension.

[A15] K. Taylor, RCHS-36O: Three-Terminal Record Information Gain with Free Endpoints. 10 September 2026. Three-record likelihood, analytic derivatives, dense checks and efficient-information comparison.

[A16] K. Taylor, RCHS-36P: Earliest-Completion Record Retention Test. 10 September 2026. Closed-cover completion stratum and resolved final-outcome nuisance saturation.

[A17] K. Taylor, RCHS-36Q: A Retained Terminal Pair at Completion. 10 September 2026. Ordered-pair/last-edge witness and conditional stopped-record information bound.

[A18] K. Taylor, RCHS-36R: Record Export and Continuation Faithfulness. 10 September 2026. Record coarsening and carried-state continuation witnesses.

[A19] K. Taylor, RCHS-36S: Binary Fact Sequences and the Curvature-Response Bridge, corrected source scope. 10 September 2026. Restricted fixed-cycle rank theorem and native-channel attachment test.

[A20] K. Taylor, RCHS-36S: Corpus Reconciliation and Quadratic Fact Response, corrected successor handoff. 10 September 2026. Retains prior one-bit, memory, conditional-response and direct-action results.

[A21] K. Taylor, RCHS-36T: Representative Current/Link Response. 10 September 2026. Exact conditional scalar compliance, conjugate units, direct Hessian checks and source-grade boundary.

[A22] K. Taylor, RCHS-36U: Attempt to Select a Current/Link Amplitude Law. 10 September 2026. Marked-kernel moment reduction and conditional-likelihood tests; no physical amplitude law selected.

[A23] K. Taylor, RCHS-36V: Explicit Joint Update Hypothesis, corrected revision. 10 September 2026. Imposed-model calculations retained; physical promotion withdrawn following A24.

[A24] K. Taylor, RCHS-36W: Source Compatibility of the Proposed Record Feedback. 10 September 2026. Exact mixture-affinity identity, native counterexample and fixed-instrument compatibility criterion.

[A25] K. Taylor, VERSF: A Source-Derived Response Constraint and Its Refinement Test. 10 September 2026. Conditional generalized-spectrum test, converse and minimum effective refinement contribution.

[A26] K. Taylor, Electromagnetic Projection and Calibrated Record Response in VERSF. 10 September 2026. Native charge/flux map, measured-alpha reference, record-probability derivative and reproducibility archive.

[A27] K. Taylor, VERSF: Electroweak Source Selection after Electromagnetic Calibration, updated 11 September 2026, version 7 of the note and reproducibility package. §§7–12: joint FCHI retained-parent verification; duration-retaining return reduction; joint weak/Y and shared-link matter vertices; coupled Gaussian contraction; native operator test; recovery of prior Gaussian and quadratic innovation theorems. Conditional results are not physical coupling predictions.

[A28] K. Taylor, VERSF Corpus Review and Correction, with coverage package. 10 September 2026. Expanded representative-file screen and focused derivation/revision reading, with explicit coverage limits.

[A29] K. Taylor, VERSF Weight Selection Attempt, cumulative note and reproducibility package, updated 12 September 2026 through §24, version 21 before this manuscript integration. §§6–10: magnitude-bearing source response, score mapping and covariance corrections; §§11–16: calibrated effective evolution, corrected hierarchy, field attachment, normalization and bath tests; §§17–20: native internal evolution and endpoint-phase tests; §§21–22: autonomous-proposal and coupled-history tests; §§23–24: commitment lift and temporal-Wilson configuration operation. Original numerical inputs and analytic evidence remain in VERSF_Weight_Selection_Attempt.zip. Physical source outputs remain explicitly unreturned.

[A30] K. Taylor, VERSF: Commitment, Propagation and the Receiving-Fold Response, source audit updated 14 September 2026, version 9. VERSF_Commitment_and_Influence_Audit.md. Eight upload batches, 118 PDFs and 113 distinct extracted texts; §§8A–8L contain the propagation, support, receiving-phase, TPB, horizon and contact-to-progress results. The final appendix embeds verify_tick_progress.py and its complete output. Targeted source review, not exhaustive proof verification.

[A31] K. Taylor, VERSF: Convolution Embedding, Jump Moments and the Physical-Update Boundary, 2026 working calculation. VERSF_Levy_Embedding_and_Character_Gate.md and certificate.json. Exact circle moment gates, invariant covariance dimension, Hartman–Watson embedding and source-grade boundary. Primary mathematical sources and executable verification are listed in that archive.

[A32] K. Taylor, VERSF: Corrected Dynamics Freeze and Temporal Non-Uniqueness, 14 September 2026. VERSF_Dynamics_Freeze_and_Temporal_Nonuniqueness.md and certificate.json. Explicit positive finite-sector counterfamily preserving the complete stationary one-tick Wilson law, local precision and conditional variance; distinct two-tick laws. No full-primitive admissibility theorem is claimed.

[A33] K. Taylor, VERSF: History-Conditioned Sharp Selector Audit, with Soft Control and Commutator-Gap addendum, 2026 working calculation. VERSF_History_Conditioned_Sharp_Selector_Audit.md; soft_gap/addendum.md, gap_certificate.json and verifier. Normalized selective, unread Lüders and general soft joint operations are distinguished. Numerical gaps retain frozen-effect and outcome-normalization scope.

[A34] K. Taylor, VERSF configuration-update continuation audits, 2026 working calculations: Primitive Move Descent; Fold to MASD Bridge and Commitment Transport; One Edge Backreaction; Fact Stopped Field Update; SFVM Conditioning; Threshold Conditioning Miniature; One Way Formation; Commitment Write and Field Response. The corresponding notes, certificates and preregistered miniature specifications retain their separate carriers. Used here for scoped mechanism exclusions, not a theorem excluding all VERSF dynamics.

[A35] K. Taylor, VERSF Receiving Phase Attachment Checks, 14 September 2026. VERSF_Receiving_Phase_Attachment_Checks.zip; receiving_phase_attachment/README.md and certificate.json. Reconstructed wheel/chiral plane, native phase/effect test and hash-recorded EX2E/F2F inputs; first-entry and first closed-cover clocks are distinct.

[A36] K. Taylor, VERSF Fact Momentum Single Event Operation. Calculation note VERSF_Fact_Momentum_Single_Event_Operation.md, 14 September 2026. Effective scalar event impulse, action-sign repair and response verification; distinct from microscopic link/current selection.

[A37] K. Taylor, VERSF Commitment Update Without Assumed Duration. Calculation note VERSF_Commitment_Update_Without_Assumed_Duration.md, 14 September 2026. Ordered-event boundary operation and separate effective continuum clock attachment.

[A38] K. Taylor, K = 7 Operator Comparison and Correction to the Mass Projection. VERSF_K7_Operator_Comparison_and_Projection_Correction.md, 14 September 2026. Exact rank obstruction in the 4/3 derivation; distinct Fano, wheel and physical operator carriers.

[A39] K. Taylor, Corrected K7 Field Reduction. VERSF_Corrected_K7_Field_Reduction.md and verification archive, 14 September 2026. Exact Gram/dual projection and six-plane attachment scope. Part XI fixes its generic source gain to one on Fact-Momentum's written canonical branch.

[A40] K. Taylor, The Response to One Fact in the Projected K = 7 Scalar Model. VERSF_Unit_Fact_Response.md and VERSF_Unit_Fact_Response_Verification.zip, 15 September 2026. Reconstruction script, matrices, source covector, response table, graph and certificate; original source text and manifest retained. Source strength is exactly one; mass, kernel and profile remain declared inputs.

[A41] K. Taylor, U(1) Portal Identification and Complete Current–Closure Conjugation Audit, 17 September 2026. Appended execution in VERSF_Electroweak_Source_Selection_Result.md; VERSF_U1_Portal_Identification_Verification.zip. Exact local coordinate map, current-square derivative, conditional alignment criterion, complete derivative, Schur covariance, branch-even screening and ensemble alignment witness. Twenty-five plus fifteen exact checks; no physical coupling selected.

[A42] K. Taylor, Master Action Phase Selection and Native Recording Interaction Checks, 17 September 2026. Part XII proof and execution in the cumulative VERSF_Event_Compensator_and_Basis_Verification.zip, master_phase_proof/; predecessor joint_event/, phase_comparison/ and recording_interaction/ constructions retain their stated scopes. Nine exact Taylor checks and sixteen numerical residual checks. Conditional complete-source selection, traceless pointer-phase counterexample and finite-derivative limitation; no physical phase or gauge coupling selected.

[A43] K. Taylor, VERSF Phase and Record Law Corpus Reconciliation, 17 September 2026. VERSF_Full_Corpus_Phase_Reconciliation.md and full_corpus_phase_review/ in the cumulative event archive. Coverage manifest, source passages and six checks of the inherited comparison witness. Corrects the R11 handoff; no new physical phase selected.

[A44] K. Taylor, VERSF Phase Independent Record Backreaction Bound, 17 September 2026. VERSF_Phase_Independent_Record_Backreaction.md and invariant_backreaction/ in the cumulative event archive. Exact variance and retained-record decompositions; native packet evaluation; kinetic preservation; 131 numerical identity and convergence checks. The stronger native invariant and the probability-only bound have distinct implementation scopes.

[A45] K. Taylor, VERSF Completion Survival and Gauge Response, 18 September 2026. VERSF_Completion_and_Gauge_Response.md and completion_gauge_response/ in the cumulative event archive. Fixed-carrier completion theorem; source R4 channel tests; native twelve-generator derivatives; radial-current composition corollary; 74 numerical identity checks and independent derivative controls. No physical carrier attachment or gauge coupling is selected.

[A46] K. Taylor, Fact-Momentum and the Relative Gauge Costs: Attempted Uniqueness Derivation, updated 19 September 2026, version 4. VERSF_Fact_Momentum_Relative_Cost_Test.md and VERSF_Fact_Momentum_Relative_Cost_Evidence.zip. Sections 6–8 retain the scoped local-work and normalization proof corrections; §7 evaluates the native flux moments and occurrence contribution; §9 states the constructive stopping point. Exact-check scripts, native arrays, independent derivative controls and source excerpts are included. The operation and preparation are specified inputs; physical gauge strengths remain conditional.

VERSF sources consumed by those calculations

[P1] K. Taylor, *RCHS-29: Native Current Response, Hypercharge Visibility and Full-Configuration Source Reconstruction in VERSF*. Supplied integrated revision Pasted markdown(20260908-045004).md, September 2026; §§19A–19F, 20.3 and 21. Predecessor status and separation of response objects. The RCHS-29 manuscript remains a separate source.

[P2] K. Taylor, *RCHS-34: Full-Configuration Transfer Reconstruction and the Gauge-Link Source Test in VERSF*, September 2026; §§2–4 and 7–10. Known-reference split inverse and synthetic tests.

[P3] K. Taylor, *The VERSF History-Measure, Generation-Geometry and Branch-Closure Theorem* (HMGBC-1), supplied (10).pdf; §11A.1 and §§56A.1–56A.11. Continuous-update measure, operational transfer, full-carrier, action typing and admission requirements.

[P4] K. Taylor, *The VERSF Master Substrate Action and Constitutive-Descent Theorem* (MASD-1), supplied (10).pdf; §§9–10.1, 12–17, 20–24, 31, 47F and Appendix B. Common metric, six defects and physical action requirements. Appendix B's printed support derivative is explicitly corrected in §III.5 of this integrated manuscript, as documented by [A3]. Section 5 and §§9–10 distinguish the leading local rate expansion and its complete metric from an evaluated full microscopic action; used at XII.1.

[P5] K. Taylor, *RCHS-24: The Quadratic Gauge-Release Sufficiency and First-Fact Endpoint-Admission Reduction Theorem in VERSF*, controlling RCHS-24_latest_source.md snapshot in the calculation archives; §§3, 9I–9L and 14. Endpoint law, conditional gradient/Gibbs and susceptibility relations, current/link conventions, independent remainder and quadratic sufficiency.

[P6] K. Taylor, *Operational Curvature and Geodesic Structure in the VERSF Framework*, supplied (6)(2).pdf; §§4–5, PDF pp.11–14. Conditional refinement flows and operational geometry, not a supplied full-configuration drift.

[P7] K. Taylor, *Microscopic Origin of Refinement Transport in VERSF*, supplied (7)(2).pdf; §§13–14. Transport existence/composition and separate dynamical and normalization obligations.

[P8] K. Taylor, *The Universal Measure Principle*, supplied (3)(4).pdf; §7, PDF pp.27–28. Born probability on supplied operational states; not physical generator selection.

[P9] K. Taylor, *The Gauge-Response and Coupling-Evaluation Theorem in VERSF*, supplied (4)(1).pdf; §§8–12 and 34.2. Primitive-charge and coupling-conversion conventions, used without importing an experimental target.

[P10] K. Taylor, *Substrate Dynamics and the Higgs Ratio*, supplied (6)(2).pdf; §4 and §§5.9.10.1, 5.9.10.4. Declared gradient/quartic structure and conditional coefficient/microdynamics statements. The audited version is identified, not asserted to be the latest member of every manuscript family.

[P11] K. Taylor, *Independent link–record restoring law: explicit nonlinear covectors and the remaining source normalisation*, working calculation, 6 September 2026; §§3–10 and 12–14. Fixed-support force and polar derivatives, tests and physical-weight boundary.

[P12] K. Taylor, *Gradient–Gibbs Continuation: Fluctuation Covariance, Dynamic Schur Reduction and the Drift-to-Action Test*, working calculation, 5 September 2026; §§1–4. Conditional harmonic fluctuation balance and exact finite-time kernel. Its cited older substrate versions are inherited as audited in that note, not newly re-audited for this integration.

[P13] K. Taylor, *BTAC-1: BCB–TPB–Admissibility Deep Closure Attempt for the Remaining VERSF Standard Model Boundary*, 20 July 2026; §§2–4. Explicit budget/entropy constraints and the unresolved bath-adjacency result. Part IV's rate example neither imports its numerical branch outputs nor claims to rerun it.

[P14] K. Taylor, Ordered Records, Realised Event States, HCMR-P1, supplied (17).pdf; §10A/Theorem 3A and §17/Theorem 6, Corollaries 6.1–6.2. Retained CP-instrument conditional state and ensemble; covariance of conjugate branches and retained histories. Earlier RCHS-36L–M uses retain their stated source snapshots.

[P15] Taylor, K. The Primitive Field-Dependent Marked Instrument Programme in VERSF, complete version (113 pages), with PFDMI-EX2F and HCMR-XI-2 execution inputs. Native current instrument, representation census and archived endpoint/history data.

[P16] Taylor, K. Current-rigidity and RUDM sector sources, as identified in the RCHS-36L audit and reproduction package. The twelve innovation sectors and neutral-vector decomposition are distinct from the seven terminal blocks.

[P17] Taylor, K. RCHS-25–27, source versions identified in the RCHS-36M audit. Conditional first-cover clock, stationary-traffic generator and quadratic moments; not a complete nonlinear background-marginalized marked law.

[P18] K. Taylor, The Twelve-Sector Current-Rigidity, Source-Generated Rank-Six Current-Stiffness and Current-Link Schur Reciprocity Theorem in VERSF. §§13–14, 39A–39G, 40 and F7–F15. Positive conditional source response, direct continuum action route and factor-mode qualifications. The updated (1).pdf, §§34B–C and 39Q–39U, also supplies the actual radial-tangent reconciliation and conditional chiral wheel attachment used in VII.29.

[P19] K. Taylor, PFRA-1: Prior-Corpus Forward Physical-Return Attempt in VERSF. §§2–5. Conditional one-bit entropy normalization and no-fit gauge precursor, with whitened/factor-blind score limitation.

[P20] K. Taylor, Interface Matching and Coupling Normalization in Gauge Theories. §§3–5. Explicit bit-commitment normalization BCN and its fixed-phase-resolution consequences.

[P21] K. Taylor, GNC-EX2A: Generator-Normalisation Rank12 Embedding Closure. §§6–8. Fixed source-generator scale and Wilson continuum conversion; full physical source-response requirement.

[P22] K. Taylor, The Standard Model from Hexagonal Geometry. Appendix H, pp. 99–103. Conditional 3/13 weak-angle construction, H9 mode isotropy and stated failure conditions.

[P23] K. Taylor, GRCE-2-R3: Numerical Gauge Closure with Results. Numerical branch comparison and physical-direct qualification. The RRHF neutral-extended branch gives 45/194 under its score ledger; its source normalization is not inferred from numerical proximity.

[P24] K. Taylor, From Interface Structure to Physical Coupling. §§2–3 and open-status discussion. Interface scale and phase-resolution enumeration qualifications; no unstated placeholder value is supplied by this integration.

[P25] K. Taylor, Void Tensile Strength, supplied (4)(1).pdf. §2.2, §7.1 and Appendix H.4. Rigidity/Planck-pressure identification and electromagnetic response route; the microscopic alpha calculation remains explicitly separate there.

[P26] K. Taylor, The Twelve-Sector Commitment-Hazard Selector and Magnitude-Bearing Current-Mark Factor Theorem. §§8–10, Theorem 6 and corollaries. Coarse factor shape, refinement information and factor-blind splitting conditions.

[P27] K. Taylor, The Sequential Opportunity-to-Lorentzian Commitment-Time Attaching Map. §§24.23–24.25. Conditional factor geometry and single-portal response family.

[P28] K. Taylor, The Renormalised Standard Model Parameter Closure Theorem in VERSF, supplied (13).pdf; §64.4.1B–H, §§67 and 71, and final synthesis. Operational Gaussian proposal, exact core Fisher metric, canonical bath return and later correction to physical promotion of the whitened identity.

[P29] K. Taylor, Measure-Valued Continuous-Amplitude Proposal Kernel, PROPOSAL_KERNEL_THEOREM.md, source version consulted 11 September 2026. Complete short theorem and status statement. Read with the frozen-vacuum and quadratic-chart scope of [P28].

[P30] K. Taylor, The Primitive Selection, History-to-Curvature and Standard-Model Attaching-Map Closure Theorem in VERSF, supplied (8).pdf; §§10F–10O, especially Theorems 1B and 1C. Exact closure lift, inherited Gaussian proposal, bath protection and faithful-carrier scope. Sections 10Q–10T and 10AA–10AF supply stage-order triangularity, the candidate master action, its single odd source and no-double-counting conditions; §§10M–10O fix the uniform Abelian A_2 typing.

[P31] K. Taylor, VERSF Conditional Standard Model Derivation and Parameter-Closure Audit, supplied (4).pdf; SGPL-1 Gates 2–4, Theorem 12, and FCHI-1. Quadratic martingale innovation orthogonality, measure-valued kernel construction and the retained-parent scope.

[P32] K. Taylor, The Primitive Full-Carrier Provenance, supplied (14).pdf; Appendices E–F. Quadratic bath, retained local potential, positive transfer and Gaussian reference-path representation. Its branch-conjugacy results are also used in VII.31 without promoting the conditional source to physical admission. Parts XI–XII also specify the linearized-defect bath and source-amplitude/projector descent used in Part XII; an unmarked kernel does not supply that marked realization.

[P33] K. Taylor, The Finite Master-Action Fermion-Kernel Reconstruction and Source-Identity Gate in VERSF (MFKR), supplied (1).pdf, revision with Laplacian Square Rigidity and Quantitative Stability in its subtitle; §§3–7 and 20. Shared-link kinetic source, inherited infrared normalization and physical source-identification scope.

[P34] K. Taylor, The K7 Closure–Born–TPB Renewal Construction in VERSF, supplied (20).pdf; §§13–17, as identified in [A27, §8]. Finite-mean renewal identities only; this use does not supersede later physical-carrier revisions.

[P35] K. Taylor, The Electroweak Gauge-Curvature Dynamics in VERSF, supplied (3)(1).pdf; §§10–12 and 15. Leading electroweak action, kinetic convention and effective propagation, as consumed by [A29, §11].

[P36] K. Taylor, The Broken Electroweak Phase in VERSF, supplied (3)(1).pdf; §§8–11. Doublet mass matrix and chiral-current source normalization, as consumed by [A29, §11].

[P37] K. Taylor, The K = 7 Wilson Limit, supplied (5)(2).pdf; §§2–3. Inherited holonomy carrier, admissibility class and anisotropic spatial/temporal Wilson action. Its older coefficient notation is qualified in §VIII.6.

[P38] K. Taylor, The K = 7 Closure Symmetry, supplied (4)(2).pdf; §§6 and 10(L1). Conditional bare coefficient equality, feature matching and minimality; open labelled chain-complex realization. This source does not establish a complete coupled physical parent merely from the fourteen-channel count.

[P39] K. Taylor, Primitive Matter Selection in VERSF: Cumulative Executed Theorems on Fact Commitment, supplied (6).pdf, 276 pages; Part LIX, §28, pp. 71–73, and Part LX, §29, p. 74. PMS-1-R126P-INTEGRATED, Axiom FC, binary active plane and completed-closure scope. Exact upload S3 in [A30]. Its axiom-relative trigger, chiral basis, completion and renewal closure is explicitly consumed in XII.7; broader coherent-phase obligations remain separately graded.

[P40] K. Taylor, Unified Covariant Action for Emergent Commitment Geometry in VERSF, supplied (3)(2).pdf, §§6–7; and Effective Stress–Energy from Irreversible Commitment Flow in VERSF, supplied (10).pdf, §§2.3–2.9 and §5. Source-listed scalar action and retarded response. Exact uploads S25 and S27 in [A30]; mass and normalization assumptions retained.

[P41] K. Taylor, Fact-Momentum, supplied Fact-Momentum-1 (7)(20260914-052304).pdf. Corollary 4.5 and §§5–9, pp. 12–19: scalar action, point-event response and static force. §§12.5–12.10, pp. 29–31: q = N_committed and the remaining event-distribution question. The action/equation sign repair controls §§X.2 and XI.3; §XI.6 corrects the continuum tail asymptotic.

[P42] K. Taylor, The Theory of Fact Production, supplied (4)(20260914-052305).pdf, 49 pages. Eligibility, environmental-entropy drive and proposed intensity, pp. 13–23; mode-count discussion, p. 24; normalized jump construction, pp. 40–42; phenomenological status, pp. 46–47. Read with the entropy, threshold and redundancy corrections in [A30].

[P43] K. Taylor, TPB Reaction Rate, supplied (2)(20260914-163552).pdf, pp. 8–11. Nonnegative progress increments, first passage and distributional input. The overshoot and finite-mean conclusions are audited in [A30, §8J].

[P44] K. Taylor, The K7 Closure–Born–TPB Renewal Construction in VERSF, supplied (23).pdf, 20 pages. Three-stage recurrent instrument and ledger-preserving reset, especially p. 11. This later construction is distinguished from the version cited in [P34] and from the first closed-cover clock.

[P45] K. Taylor, Paths to Folds, supplied (6)(1).pdf, §§5.3–5.4, p. 13. Candidate controlled neighbouring interaction and reduced entropy. Its use as a physical primitive is not selected by the later event-state source [P46].

[P46] K. Taylor, Ordered Records and Realised Event States, supplied Ordered-Records-Realised-Event-States-(17).pdf, especially pp. 13 and 17. Physical phase-source obligations and completed-event scope. Exact upload S67 in [A30].

[P47] K. Taylor, Towards a Complete Information-Theoretic Physics: Closing the Remaining Gaps, supplied Towards-a-Complete-Information (2)(20260914-163602).pdf, pp. 25–27. Declared XY interface Hamiltonian, tick density and variable distinguishability. Exact upload S106 in [A30]; no pure-gauge endpoint phase is promoted to independent link curvature.

[P48] K. Taylor, horizon and entropy source batch supplied 14 September 2026: Redefining Entropy from First Principles; The Fallacy of Time as a Dimension; From Bit Conservation to Gravity; Hawking Radiation as a Constraint; Companion Note Bekenstein Hawkins; Deriving the Quarter. Exact uploads S113–S118, versions and page locators in [A30, §12]. The clock, area-unit, density and force-sign qualifications in [A30, §8K] control this integration.

[P49] K. Taylor, Full Projected Closure Operator and the Corrected Absolute Scale of the K = 7 Commitment-Threshold Spectrum. Full-Projected-Closure-Operator-(20260808-193828).pdf. §§2–3, pp. 7–9: full Gram/stiffness construction and printed benchmark. §4.2, p. 10: overlap statement corrected in XI.6. §12, p. 21: kernel-selection limit. Appendix A, pp. 23–24: reconstruction method.

[P50] K. Taylor, Exact Projection Coordinates and the Closure-Scale Derivation of the Commitment-Bath Cutoff in the VERSF Framework, consulted 14-page source. §§3–6, pp. 4–6: exact dual-basis and Galerkin coordinates. Part XI uses this projection theorem without promoting the separate conditional cutoff and mass claims.

[P51] K. Taylor, VERSF Fact-to-Gauge Event Bridge, source-graded finite calculation, 2026. Common-link fermion/gauge source, compact U(1) rotor, Gauss-preserving event factor and exact conjugate-flux update. Used in §VII.19; event amplitude and later kinetic evolution remain distinct.

[P52] K. Taylor, supplied U(1) geometric-closure / Chern–Weil calculation (internal source file), consulted 15 September 2026. Exact cell-holonomy sum, geometric phase-bookkeeping bridge and explicit separation between topological integrality and electromagnetic normalization. Used conditionally in §VII.20; no public-site title is asserted here.

[P53] K. Taylor, Finite Distinguishability and Local Capacity Competition: A Structural Basis for Per-Channel Interaction Dynamics, supplied PDF, consulted 15 September 2026. Per-channel second-order selection, inverse-participation structure and explicit statement that the theorem fixes form rather than physical magnitude.

[P54] K. Taylor, Completing the Interface Bridge: Phase Resolution, Symmetry Allocation, and Second-Order Selection in the VERSF Framework, supplied PDF, consulted 15 September 2026. Six equivalent interface channels, uniform allocation, link-variable observable algebra and the 1/6 local second-order coefficient.

[P55] K. Taylor, K7-ICN-1: Interface Continuum Normalization and Wilson-Convention Closure Audit, 2026 working audit. Exact cnorm=1 for the declared Wilson interface map; no-double-counting and integer-phase-resolution no-go; final physical alpha identification remains open.

[P56] K. Taylor, The Physical C/W/Y Radial-Current Tangent Field and Existing-Instrument Score Descent in VERSF, supplied revision, especially CRTF-EX2U–EX2W. Retypes the K7 electromagnetic source carrier to the primitive Fold boundary, separates the PFDMI 7+7 traversal descendant from Route-M 10+4 channels and forbids a same-carrier 14↔14 identification.

[P57] K. Taylor, RCHS-25: The Record-Clock Event-Grain Separation and Source-Stopped Endpoint Theorem in VERSF. September 2026. First-cover record clock, pre-fact/completion typing and the source-stopped covariance functional; physical matter-generator attribution retained as a separate gate.

[P58] K. Taylor, RCHS-26: The D36 Stationary-Traffic Matter-Endpoint Generator and Exact Per-Fold Continuity Theorem in VERSF. September 2026. Source-even D36 conductances, additive reversibilisation, tensor lift, exact per-Fold normalization and EPM1 boundary.

[P59] K. Taylor, RCHS-27: The Source-Stopped Pre-Record Current-Occupation, E_2 Isotropy and Quadratic Directing-Law Reduction Theorem in VERSF. September 2026. First-cover stopped E_2 current occupation, exact C/W/Y × E_2 shape and action/Fisher/current-covariance firewall.

[P60] K. Taylor, RCHS-28: Full Six-Defect E_2 Schur No-Go. September 2026. Exact non-identifiability of the physical Schur stiffness from the then-frozen endpoint/current source package and the requirement for new source information.

[P61] K. Taylor, RCHS-6: Abelian-Portal Schur Identification and Common-Axle Survival Theorem. September 2026. Rank-one same-parent U(1) specialization of current-link reciprocity, fixed portal direction and strict survival of nonzero factor response.

[P62] K. Taylor, RCHS-7: Finite U(1)-Portal Determinant Fingerprint and Maximal-Shorting Residual. September 2026. Exact determinant/Y-direction fingerprint, inverse-metric rank-one update, finite-rank survival and maximal-short residual geometry.

[P63] K. Taylor, The Physical CWY Radial Current Tangent Field and Existing Instrument Score Descent in VERSF, supplied 118-page PDF; §§2–7 and §26, especially D-RT10–15. Background-dependent radial probe, physical mixture grain, Abelian E_2 portal and distinct orientation-to-internal-mode attachment.

[P64] K. Taylor, Holonomy Assignment from Distinguishability, supplied (4)(1).pdf; §§4, 6–8. Conditional assignment uniqueness and co-terminal phase kernel; comparison-realizability check C and Transport-Completeness fallback retained.

[P65] K. Taylor, The Route-M Off-Shell Integrability Current Source Closure, supplied (1).pdf; Theorems 10–13A, §§12–14. Explicit face-to-edge map, current-source integrability and complete-loop connection reconstruction, with inherited assignment grade.

[P66] K. Taylor, The Primitive Selection, History-to-Curvature and Standard-Model Attaching-Map Closure Theorem in VERSF, supplied (9).pdf; §§28BM–28BQ. History-controlled active/discard isometry, hard-split pullback criterion and physical-selector boundary. Supplements the earlier source use at P30.

[P67] K. Taylor, The Structure Group of the Maxwell Connection, supplied (3)(2).pdf; §4. Identity of Maxwell and substrate transport under inherited M1; assignment-neutral scope, distinct from selection of a recording-operation phase.

Mathematical context cited in the archives

[M1] R. Chetrite and H. Touchette, “Nonequilibrium Markov processes conditioned on large deviations,” *Annales Henri Poincaré* **16**, 2005–2057 (2015), arXiv:1405.5157, DOI:10.1007/s00023-014-0375-8. Generalized Doob transforms, tilted path ensembles and driven processes.

[M2] L. Da Costa and G. A. Pavliotis, “The entropy production of stationary diffusions,” *Journal of Physics A: Mathematical and Theoretical* **56**, 365001 (2023), arXiv:2212.05125, DOI:10.1088/1751-8121/acdf98. Reversible/irreversible diffusion decomposition.

[M3] S. Boyd and L. Vandenberghe, *Convex Optimization*, Cambridge University Press, 2004, Appendix A.5.5. Schur complements and positive block matrices. The book is not redistributed in this release.

[M4] E. S. Gawlik and M. Leok, “Iterative Computation of the Fréchet Derivative of the Polar Decomposition,” *SIAM Journal on Matrix Analysis and Applications* **38** (2017), 1354–1379, arXiv:1608.04491, DOI:10.1137/16M108971X. Polar differential background.

[M5] N. J. Higham and S. D. Relton, “Higher Order Fréchet Derivatives of Matrix Functions and the Level-2 Condition Number,” *SIAM Journal on Matrix Analysis and Applications* **35** (2014), 1019–1037, DOI:10.1137/130945259. Matrix-function differential context.

[M6] L. Onsager and S. Machlup, "Fluctuations and Irreversible Processes," *Physical Review* **91**, 1505–1512 (1953), DOI:10.1103/PhysRev.91.1505. Gaussian fluctuation-history context. Archive [A4] consulted the official abstract; access to the full paywalled article is not claimed here.

[M7] NIST, 2022 CODATA Recommended Values of the Fundamental Physical Constants, SP 959, May 2024. Measured alpha and SI conversion inputs used by archive A26. https://physics.nist.gov/cuu/pdf/wallet_2022.pdf

[M8] Particle Data Group, 2025 Electroweak Model and Constraints on New Physics, revised November 2025, equations 10.19, 10.24 and 10.41a; 2025 W-boson and Z-boson listings, page 1. Frozen measurement inputs used in [A29, §11], retrieved 11 September 2026. https://pdg.lbl.gov/2025/reviews/rpp2025-rev-standard-model.pdf ; https://pdg.lbl.gov/2025/listings/rpp2025-list-w-boson.pdf ; https://pdg.lbl.gov/2025/listings/rpp2025-list-z-boson.pdf

[M9] M. Lüscher, Construction of a Selfadjoint, Strictly Positive Transfer Matrix for Euclidean Lattice Gauge Theories, Communications in Mathematical Physics 54 (1977), 283–292. DOI 10.1007/BF01614090. Original author preprint: https://bib-pubdb1.desy.de/record/396349/files/7611148.pdf . Mathematical transfer reconstruction, not VERSF physical source selection.

[M10] NIST Digital Library of Mathematical Functions, §10.32.3 and §10.40.1. Integer modified-Bessel Fourier coefficients and fixed-order large-argument asymptotics. https://dlmf.nist.gov/10.32 ; https://dlmf.nist.gov/10.40 . Used in the analytic temporal-transfer calculation of [A29, §24].

These mathematical references retain their source-archive role; no new literature-priority claim is made.

[M11] A. J. S. Hamilton and J. P. Lisle, The River Model of Black Holes, American Journal of Physics 76 (2008), 519–532; arXiv:gr-qc/0411060. Horizon-regular free-fall comparison only; not a VERSF primitive derivation.